



Politecnico di Torino

and

Universitat Politècnica de Catalunya

Department of Civil Engineering, DISEG

Barcelona school of Civil Engineering, ETSECCPB

Master Degree in Civil Engineering

Experimental investigation of wave loads on Pont del Petroli pier

Thesis Advisors

Dott. Corrado Altomare

Prof. Francesc Xavier Gironella I Cobos

Prof. Riccardo Vesipa

Candidate

Gianbattista Ambruoso

A.A. 2020 - 2021

“Non chi comincia ma quel che persevera”

Leonardo da Vinci

Ai miei genitori Salvatore e Marianna.

Abstract

On January 20, 2020, the storm Gloria causes the collapse of the final part of the walkway that connected it to the extremal platform of the Pont del Petroli pier to the beach of Badalona (Spain). A stretch of about 15 meters fell into the sea due to strong impacts caused by the wave actions. The present thesis focuses on the collection and analysis of data relation to the action of extreme waves and experimental related loads. Physical model tests at 1:10 model scale were carried out in the wave flume facility CIEM at Universitat Politècnica de Catalunya.

The forces acting on pier platform, both horizontally and vertically, and the horizontal force acting of the first (seawards) pile cap have been measured. Maximum horizontal forces larger than 2000 kN (in real scale) have been measured. The maximum recorded vertical force exceeded 1200 kN.

It has been evaluated how much these experimental results agree with the existing formulations proposed in the literature. In particular the two main analysis methods for evaluating extreme wave loads are Gaeta et al. (2012) and Cuomo et al. (2007). The aforementioned methods do not match the experimental data. Going into the matter, the method proposed by Cuomo et al. (2007) leads to high dispersion and the criteria for the evaluation of maximum forces proposed by Gaeta et al. (2012) underestimates some measurements of horizontal forces but it overestimates the maximum vertical forces for all the recorded vertical forces on the platform of the scaled model.

Finally, a visual comparison between the experimental modelling and the few information of the impacts observed during the Gloria storm has been carried out.

These differences are given for some relevant differences among our model setup and the model setup of the proposed literature. Further analysis are necessary to unravel the issues shown in this thesis work.

Estratto

Il 20 gennaio 2020 la tempesta Gloria provoca il crollo della parte finale della passerella che la univa alla piattaforma estrema del molo Pont del Petroli di Badalona (Spagna). Un tratto di circa 15 metri è precipitato in mare a causa di forti impatti dovuti dall'azione del moto ondoso. Il presente lavoro di tesi verte sulla raccolta di dati sperimentali e sull'analisi delle relazioni tra onde estreme e i loro relativi carichi. I test fisici sono stati condotti in un modello in scala ridotta 1:10 nel canale di investigazione CIEM presso l' Universitat Politècnica de Catalunya.

Sono state misurate le forze agenti sulla piattaforma del molo, sia orizzontali che verticali, e le forze orizzontali applicate al primo capitello più vicino alla piattaforma stessa. Sono stati misurati dei valori massimi delle forze orizzontali maggiori di 2000 kN (in scala reale) e i valori massimi registrati delle forze verticali superavano i 1200 kN.

A seguire sono stati confrontati i risultati sperimentali con alcune formulazioni esistenti in letteratura scientifica e quanto i risultati ottenuti fossero compatibili con le espressioni proposte. In particolare, i due studi impiegati maggiormente per l'individuazione dei carichi causati dall'azione di onde estreme sono Gaeta et al. (2012) e Cuomo et al. (2007). Ciò che emerge dalle comparazioni svolte è che le formulazioni succitate non conducono a un risultato adatto agli obiettivi della campagna sperimentale effettuata. Andando nel merito dei rispettivi metodi, la formulazione proposta da Cuomo et al. (2007) conduce a una dispersione rilevante dei valori di forze adimensionali. Per quanto concerne il criterio di valutazione delle forze massime proposto da Gaeta et al. (2012), questo sottostima in alcuni casi le forze orizzontali massime ma sovrastima le forze massime verticali per tutte le misure di forze verticali agenti sulla piattaforma in scala modello.

Infine è stata svolta una comparazione visiva tra i risultati ottenuti durante la modellazione sperimentale e le poche informazioni sugli impatti osservati durante la tempesta Gloria.

Queste differenze sono dovute ad alcune differenze tra le condizioni al contorno del caso in analisi e quelle degli studi citati. Pertanto si richiedono ulteriori indagini al fine di dipanare le questioni sollevate nel presente lavoro di tesi.

Table of contents

Abstract	2
Table of contents	4
List of figures	6
List of tables	9
1. Introduction.....	10
1.1 Objectives	11
1.2 Outline	12
1.3 Historical facts about Pont del Petroli	13
1.4 Case of study	14
2. Literature review.....	19
2.1 Loads on exposed jetties.....	19
2.2 Breaking criteria	23
2.3 Focused wave theory	25
3. Experimental setup	30
3.1 CIEM flume.....	30
3.2 Constant Froude number similitude	31
3.3 Evaluation of Reynolds number in the model and in the prototype	32
3.4 Model setup of Pont del Petroli	34
3.5 Number and type of used sensors, relative characteristics and relative position along the channel.....	36
3.6 Definition of time origin and instrument synchronization	40
4. Data post-processing.....	41
4.1 PPTs correction	41
4.2 LCs and PSs.....	41
4.3 Summation of LC results.....	42
4.4 Test program.....	43
5. Output files and preliminary considerations	44
5.1 Output files	44
5.2 Range of values of general details of the waves	50
5.3 Visual validation of the tests and their breaking shape	51
5.4 Analytical fitting of the tests	57

5.4.1 Preliminary evaluation of dependence of the loads from some basic characteristics.....	57
6. Final results and range of values of non-dimensional parameters.....	65
6.1 All-in-one group.....	66
6.2 Breaking waves impact	73
6.3 Non-breaking waves impact.....	76
6.4 New setting: η_{\max}/cl – Breaking waves	79
6.5 New setting: η_{\max}/cl – Non-breaking waves.....	83
7. Final discussion and conclusions.....	85
8. Bibliography	88
Appendices.....	90
Appendix 1 - Instruments characteristics	90
Appendix 2 - Organization and structure of data files	99
Appendix 3 – Further preliminar comparisons about the dependence of the loads from some basic characteristics	100
Breaking waves.....	100
Non-breaking waves	104

List of figures

Fig. 1 – Platform of Pont del Petroli in February 2017. Source: UPC database	13
Fig. 2 – Cross section of the platform of Pont del Petroli.	14
Fig. 3 – Longitudinal section of the Pont del Petroli.....	15
Fig. 4 - Cross section of the t-shaped concrete beam of Pont del Petroli.	16
Fig. 5 - Pont del Petroli of Badalona. Source: CCMA, 2020	17
Fig. 6 – Storm Gloria along the coast of Barcelona. Source: thelocal.es	17
Fig. 7- CIEM wave flume at UPC.....	30
Fig. 8 - Scaled model of Pont del Petroli	32
Fig. 9 - Sketch of the model of Pont del Petroli used in the tests.....	34
Fig. 10 - Representation of the scaled model of Pont del Petroli	34
Fig. 11 – Picture of the scaled model of Pont del Petroli.	35
Fig. 12 - Position of sensors along the CIEM (red circles = AWG, blue squares = PPT, black triangle = WG).....	38
Fig. 13 - 3D drawing of the Pont del Petroli model as built in the flume. (red = supporting piles; white = horizontal elements; green = LCs and PSs).	39
Fig. 14 - Raw data of vertical forces of sensors 1 and 3 for the test n°021220_6 FOC79	40
Fig. 15 - Sketch of the resulting final forces	41
Fig. 16 - Final result of filtered forces for test n°021220_6 FOC79	42
Fig. 17 - Picture of the impact occurred during test n°021220_6 FOC79.....	42
Fig. 18 - Measurement of forces of test 021220_6 FOC79.....	44
Fig. 19 - Measurement of forces of test 011220_8 - FOC73.....	45
Fig. 20 – Measurement of surface elevation distinguished by type of sensor.....	46
Fig. 21 – Maximum wave height and surface elevation.....	47
Fig. 22 – Free surface elevation at the peaks of horizontal and vertical forces on the structure.....	48
Fig. 23 – Target surface elevation vs measured surface elevation.	49
Fig. 24 – Summary of the visual validation of the tests and their breaking shape.	51
Fig. 25 - Position of point SIMAR 2111137. Source: Puertos del Estado	52
Fig. 26 - Visual validation of test 050221_9 - FOC282	53

Fig. 27 – Time series of significant wave height in SIMAR point 2111137. Time of occurrence: 15:30ca ; Hs = 5.7m Source: Puertos del Estado.....	54
Fig. 28 - Measured forces of the test 050221_9 - FOC282. Fx,platform = 1730 kN ; Fz,platform = 680 kN ; Fx,pilecap = 80 kN.....	54
Fig. 29 - Visual validation of test 050221_5 - FOC264.....	55
Fig. 30 - Time series of significant wave height in the SIMAR point 2111137. Time of occurrence: 10:00ca ; Hs = 5.3m. Source: Puertos del Estado.....	56
Fig. 31 - Measured forces of the test 050221_9 - FOC282. Fx,platform = 2150 kN ; Fz,platform = 600 kN ; Fx,pilecap = 70 kN.....	56
Fig. 32 – Dispersion of forces and maximum wave height for breaking waves (model scale).....	59
Fig. 33 – Breaking criteria according to Goda (2010) vs measured maximum wave height for breaking waves (model scale).....	61
Fig. 34 – Breaking condition of water depth (Rattanapitikon & Shibayama., 2006) vs water depth at the platform for breaking waves (model scale).	62
Fig. 35 - Dispersion of forces and maximum wave height for non-breaking waves (model scale).	63
Fig. 36 – Maximum horizontal forces and relative application of Cuomo et al. (2007).	68
Fig. 37 – Maximum vertical forces and relative application of Cuomo et al. (2007).	68
Fig. 38 – Maximum horizontal forces and relative application of Gaeta et al. (2012).....	70
Fig. 39 - Maximum vertical forces and relative application of Gaeta et al. (2012).....	71
Fig. 40 – Maximum horizontal forces and relative application of Cuomo et al. (2007) (breaking condition).	73
Fig. 41 – Maximum vertical forces and relative application of Cuomo et al. (2007) (breaking condition).	73
Fig. 42 – Maximum horizontal forces and relative application of Gaeta et al. (2012) (breaking condition).	75
Fig. 43 - Maximum vertical forces and relative application of Gaeta et al. (2012) (breaking condition).	75
Fig. 44 – Horizontal forces of non-breaking wave impacts according to Cuomo et al. (2007).....	76
Fig. 45 – Vertical forces of non-breaking wave impacts according to Cuomo et al. (2007).....	77
Fig. 46 – Non-dimensional horizontal forces of non-breaking wave impacts according to Gaeta et al. (2012).	78
Fig. 47 – Non-dimensional maximum vertical forces of non-breaking wave impacts according to Gaeta et al. (2012).	78
Fig. 48 – Application of Cuomo et al. (2007) to horizontal forces for breaking waves with the new setting.	80

Fig. 49 - Application of Cuomo et al. (2007) to vertical forces for breaking waves with the new setting. 80

Fig. 50 – Non-dimensional horizontal maximum forces according to Gaeta et al. (2012) for breaking waves with the new setting..... 81

Fig. 51 - Non-dimensional vertical maximum forces according to Gaeta et al. (2012) for breaking waves with the new setting..... 82

Fig. 52 - Application of Cuomo et al. (2007) to horizontal forces for non-breaking waves with the new setting. 83

Fig. 53 - Application of Cuomo et al. (2007) to vertical forces for non-breaking waves with the new setting. 83

Fig. 54 - Non-dimensional horizontal maximum forces according to Gaeta et al. (2012) for non-breaking waves with the new setting..... 84

Fig. 55 - Non-dimensional vertical maximum forces according to Gaeta et al. (2012) for non-breaking waves with the new setting..... 84

List of tables

Tab. 1 - Scale factor of the different physics element analyzed.....	33
Tab. 2 - Label and location of water surface elevation sensors.....	37
Tab. 3 - Z-coordinate of the pressure transducers and local water depth values. *It can vary slightly from test to test because of small changes in the beach profile.....	38
Tab. 4- Design of the focused wave used in the test 050221_9 - FOC282	53
Tab. 5 - Design of the focused wave used in the test 050221_5 - FOC264	56
Tab. 6 - Range of values of the analyzed parameters (measured values scaled to prototype scale).	66

1. Introduction

The aim of this thesis is to characterize the forces that led to the failure of the Pont del Petroli pier (Badalona, Catalonia) due to the storm Gloria happened in the night of the 20 January 2020. This thesis work is a part of previous further analysis led by the “Universitat Politècnica de Catalunya” (Barcelona, Spain), in particular with the Maritime Engineering Laboratory (LIM), within the EU-funded Horizon 2020 MSCA project DURCWAVE (Grant Agreement N. 792370).

During the storm, the closest buoy to the coastline of Badalona (the buoy Barcelona II) was dragged away from the measuring point and this compromised the practicability of the buoy. This caused a great lack of useful data in order to correctly evaluate the action of the waves on the coast of Badalona and their effects on the Pont del Petroli pier. For this reason, it has been started an experimental campaign at the UPC of Barcelona.

During the experimental campaign were made 221 tests that have been used to make considerations about the breaking condition of the waves and how much the breaking of the extreme waves affects the way they impact to the structure and the intensity of their relative loads. These extreme waves have been realized through the Focused Wave Group methodology, that is a method used in the DURCWAVE project. Anyway this will be used to create the extreme waves but the validation of this method is not the object of this thesis work.

The tests were carried out in the wave flume facility CIEM at Universitat Politècnica de Catalunya in a scaled model of Pont del Petroli with a 1:10 model scale.

Here are made considerations about a possible direct expression of the maximum forces, both vertical and horizontal, that were applied on the structure during the storm Gloria. The waves generated in the laboratory have been realized starting by few data available in the recordings of the database of the Spanish ports department.

In the present work are proposed some expressions that try to define a relationship between the maximum loads due to the impact of sea waves and their relative characteristics, such as the clearance (that is the distance between the mean sea level and the altitude of the platform of the pier), the surface elevation, the water depth at the toe of the structure and the maximum

wave height. Furthermore, are made some considerations about the breaking criteria of sea waves taking into account the hydraulic and geometric conditions (maximum wave height, longitude of the wave and water depth at the toe) using the formulation proposed by Goda (2010) and also Rattanapitikon and Shibayama (2006).

Then it has been evaluated how much the experimental results of horizontal and vertical forces, recorded in the tests made in the CIEM flume, match with the expressions proposed in the scientific literature. The principle methods used for evaluating extreme wave loads are Cuomo et al. (2007) and Gaeta et al. (2012). The first proposes a linear relationship between the non-dimensional loads due to waves impacts and its own parameter, in particular, the aforementioned essay set a linear regression for their recording of forces. The second method, proposed by Gaeta et al. (2012) set a line with a null independent constant parameter that wants to give a criterion to determine the maximum loads caused by wave impacts.

Finally, is presented a visual comparison between the experimental modelling and the few information of the impacts observed during the Gloria storm has been carried out. These are some pictures of the storm Gloria in the day before and the measurement of significant wave height of the buoy Barcelona I. The closest buoy Barcelona II was dragged away during the storm and so the buoy was not available to make considerations about the magnitude of the analyzed phenomenon. Further analysis are necessary to unravel the issues shown in this thesis work.

1.1 Objectives

The main objectives of this master thesis are:

- Search and collect images and information about the storm Gloria and the effect of the storm on the wave flow and their impact on the Pont del Petroli pier in Badalona;
- Collect experimental data of the horizontal and vertical forces applied to the model in reduced scale caused by the waves created in laboratory;
- Compare these results with scientific literature, evaluate how much the experimental results match with the proposed literature and make further considerations based on the available external data.

1.2 Outline

Chapter 2 – Literature review

The second chapter presents the general review of the literature used in this work about the topics of loads on exposed jetties, the focused wave theory and the breaking conditions for sea waves.

Chapter 3 – Experimental setup

In the fourth chapter are given detailed explanations concerning the measurements of forces and the use of sensors.

Chapter 4 – Data post-processing

The fifth chapter shows the correction and the filtering of the measurements before the production of the final results.

Chapter 5 – Output files and preliminary considerations

In the sixth chapter are presented the first products of this analysis work and are made some introductory considerations.

Chapter 6 – Final results

In this final part of the thesis work are made comparisons among the results of the physical campaign and the chosen scientific literature.

Chapter 7 – Final discussion and conclusions

Based on the preliminary considerations and the final discussions, there are summarized the most important results found in the present work.

Chapter 8 – Bibliography

In the last chapter are gathered all the references and the sources that have been used and presented along this master thesis work.

Appendices

Here are given the instrument characteristics, the structure of data files and also further preliminary comparisons that complete the results presented in the paragraph 5.4.

1.3 Historical facts about Pont del Petroli

The Oil Bridge was built in 1965 by the company CAMPSA and was used as a discharge pier until 1990. [Ajuntament de Badalona, 2012]

In 2003 it became the property of Badalona City Council and, after various stages of restoration, was opened to the public on June 13th 2009, enabled as a promenade and as a viewpoint of the city. [Martínez and Membrives, 2012] Three years later it was integrated with the rest of the promenade. The storm in early 2017 that affected the coast of Badalona, with waves of up to eight meters, destroyed much of the wooden beams that supported the pavement, severely damaged the stainless steel railing, and caused a lateral and longitudinal centimeter movement of some of the pieces. [Ajuntament de Badalona, 2017]



Fig. 1 – Platform of Pont del Petroli in February 2017. Source: UPC database

The repair was completed in October of the same year, which included improvements in the lighting, safety and accessibility of the bridge. In the night of the 20 January 2020, the Gloria storm wiped out the final section of the walkway, which connected it to the platform. Approximately a 15-meter stretch fell into the sea due to strong impacts caused by the wave action, which later appeared on the fragmented beach. [El punt avui, 2014]

1.4 Case of study

Pont del Petroli pier

The Pont del Petroli pier has a structural typology of a beam bridge. It has a total length of 235 m and a width of 3.20 m. The distance between pylons is 15 m. The bridge is supported by 16 groups of separate pylons every 15 m. The groups are double except for two consisting of four pylons. Three of the groups of pylons are in the sand of the beach and the rest in the water nailed 6 m in the sandy seabed. The platform has 20 more pylons with a maximum bathymetry of 12 m. All pylons have a diameter of 392 mm and a thickness of 12 mm. [Ajuntament de Badalona, 2012]

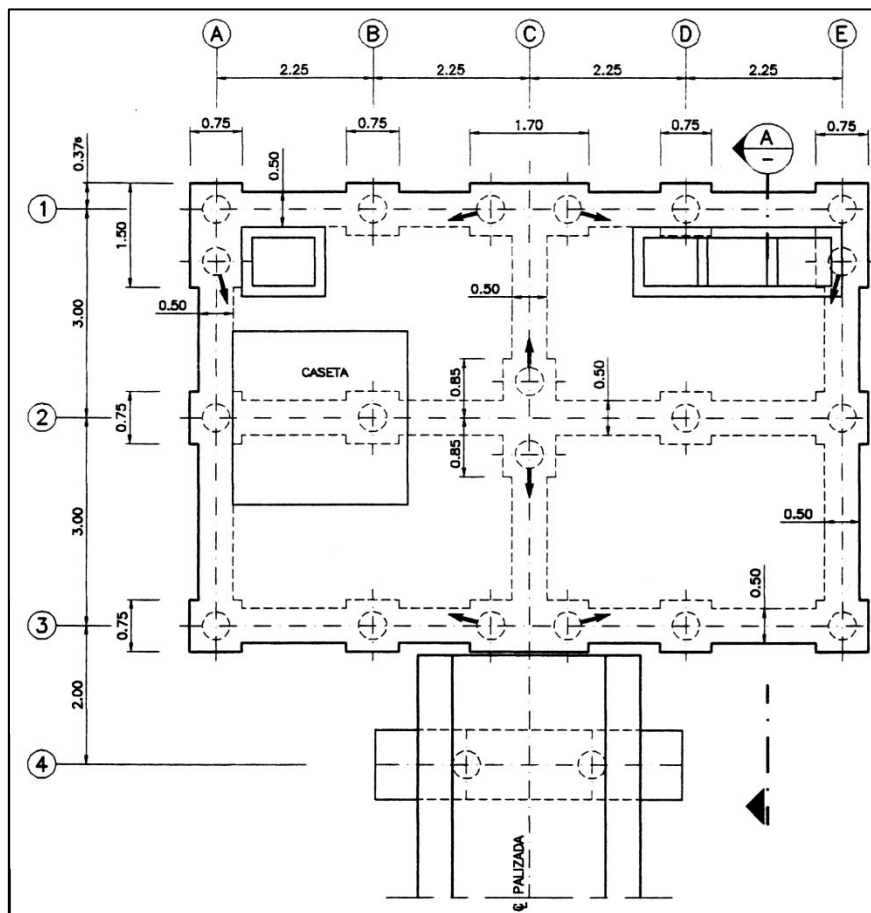


Fig. 2 – Cross section of the platform of Pont del Petroli.

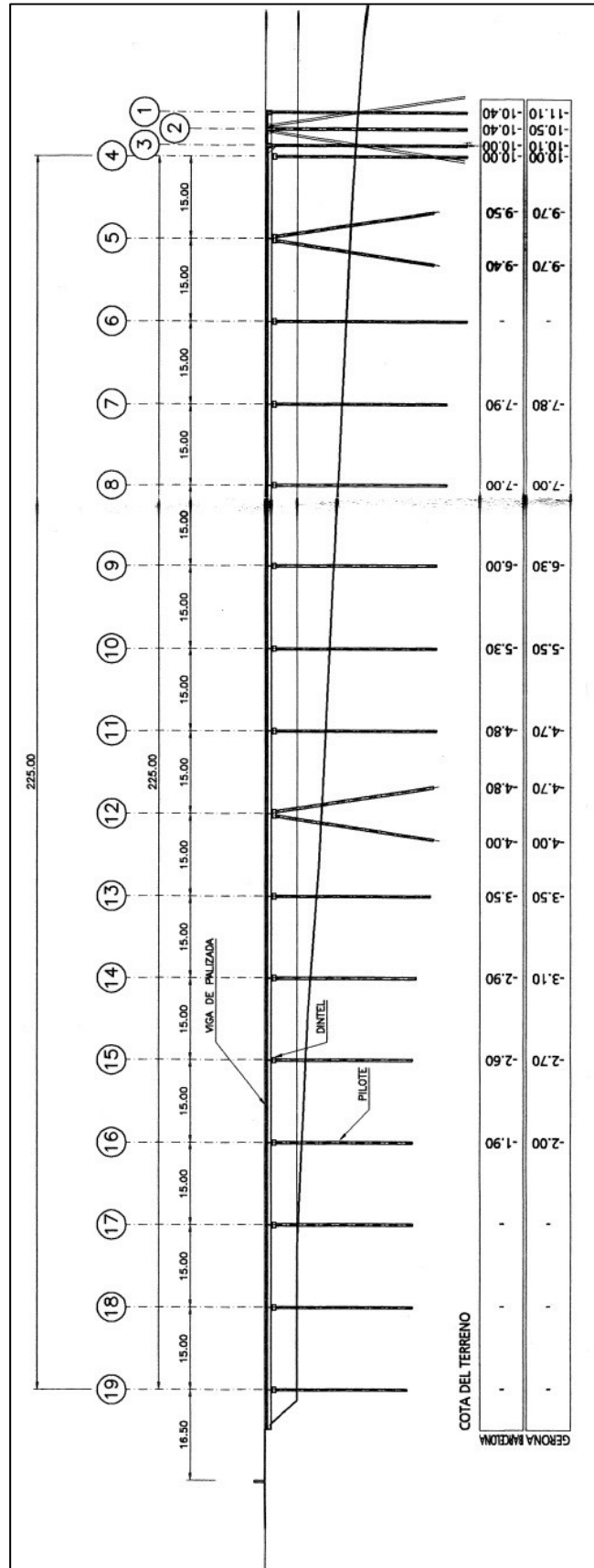


Fig. 3 – Longitudinal section of the Pont del Petroli.

The beams are supported by transverse load-bearing concrete heads that are much wider than the beams as the pipes through which the petroleum products circulated to the inside of the factory passed through this space. Each head is supported by two sloped metal pylons. Two of the 16 heads are supported by four pylons. The total number of pylons of the palisade is 36.

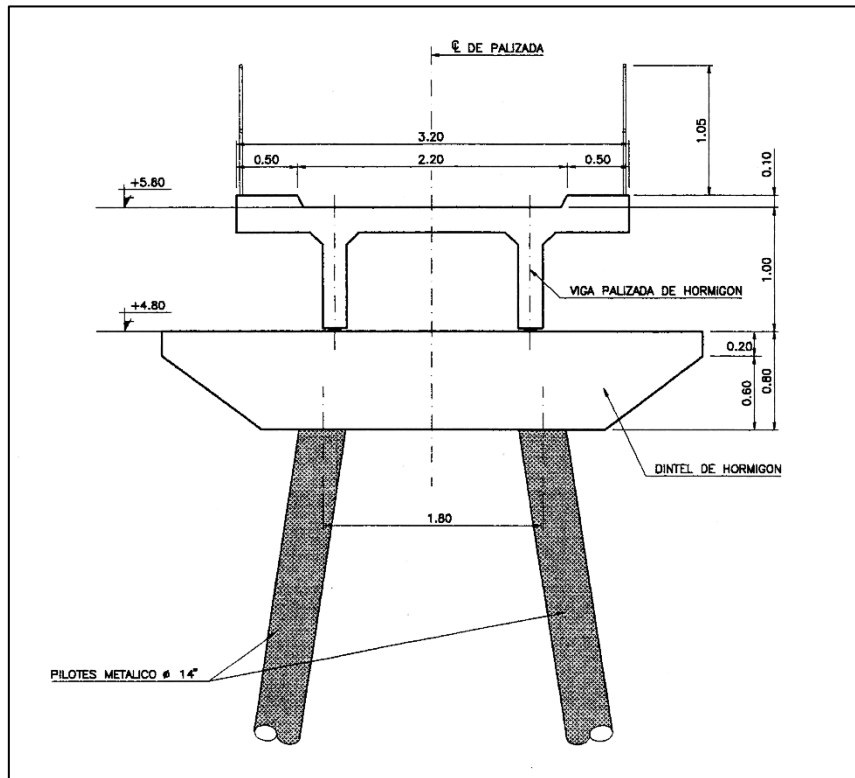


Fig. 4 - Cross section of the t-shaped concrete beam of Pont del Petroli.



Fig. 5 - Pont del Petroli of Badalona. Source: CCMA, 2020

Storm Gloria

After crossing northern Spain as a weak cyclone, the storm Gloria passed over the eastern coast passing through the Valencian region and Catalonia, that produced rainfalls of more than 400mm in Catalonia, snowfall and winds that reached 100 km/h [Servei Meteorològic de Catalunya, 19-23 January 2020].



Fig. 6 – Storm Gloria along the coast of Barcelona. Source: thelocal.es

Satellite images revealed the extent of the flooding as 320 square hectares of the delta of the Ebro river that disappeared under water. The biggest waves ever seen by Spain in the Mediterranean have been recorded during Storm Gloria on the Balearic Islands. Authorities said they had recorded waves of 14.8 meters in Menorca, beating the previous record of 13.6 off the island in 2001. Footage shows waves estimated to have reached the height of 14 meters in PortoColom in Mallorca. [Source: thelocal.es, *What's happening with deadly Storm Gloria in Spain*, 22 January 2020].

2. Literature review

2.1 Loads on exposed jetties

Cuomo et al. (2007) - Wave-in-deck loads on exposed jetties

In this paper were made tests on a model of a jetty with piles with model scale of 1/25. The jetty has load cells on the deck and there are pressure sensors on the seaward beam. The physical main characteristics of the model are the horizontal bottom, the loads on the deck are considered impulsive and quasi-static loads, on the seaward beam the horizontal loads are mainly quasi-static. It is different on the beams underneath the deck, where impulsive loads are noticed. Furthermore, the waves used in the tests are regular and they are not breaking.

This study includes extensive review on empirical formulas for horizontal and uplift forces and pressures and new parametric expressions for forces are derived. The analysis of the model is leaded with a combination of different characteristics of the waves such as three wave steepnesses of $s_m = 0.065 ; 0.040 ; 0.010$; two significant wave height of $H_{s,model} = 0.10m ; 0.22m$. So that in the prototype are obtained the following significant wave height: $H_s = 2.5m ; 5.5m$. Furthermore are analyzed two wave periods $T_m = 1s ; 3s$.

In the prototype correspond to $T = 5s ; 15s$ and four clearance heights $Cl = 0.01m ; 0.06m ; 0.11m ; 0.16m$. In the reality (prototype) they would correspond to $Cl = 0.25m ; 1.5m ; 2.75m ; 4m$. The clearance is the distance between the height of the jetty and the water depth. And two water depth conditions $d = 0.6m ; 0.75m$ are defined too. In the real case they would be equal to $d = 15m ; 18.75m$. The experimental linear expression is shown as follows:

$$F_{\frac{1}{250}}^* = \frac{F_{qs\frac{1}{250}}}{\rho_w * g * H_s * A[m^2]} = a * \left(\frac{\eta_{max} - c_l}{d} \right) + b$$

The previous non-dimensional force, that has been obtained by interpolation , is useful to determine the design force knowing the design heights of the clearance.

$$F_{\frac{1}{250}} = F_{\frac{1}{250}}^* * (\rho_w * g * H_s * A[m^2])$$

The standard error is determined as follows:

$$s_{\varepsilon} = \sqrt{\frac{\sum_{i=1}^N (y_i - \hat{y}_i)^2}{N - 2}}$$

Where y_i is the i -th measured load, \hat{y}_i represents the i -th predicted load and N is the total number of tests made.

$$F^*_{\max 1/250} = a * F^*_{qs+1/250}$$

Where the factor 'a' is the same calculated previously for the regression line of $F^*_{1/250}$.

Gaeta et al. (2012) - Uplift forces on wave exposed jetties: scale comparison and effect of venting

The model jetty consists essentially of a rectangular plate attached to a heavy reticular steel frame. The model scale is 1:4 with fixed bottom. The instruments used are: Pressure Aeration Units (PAU), 7 pressure sensors on the front face and accelerometers (to evaluate deck displacements).

The effect of wave irregularity is seen by the large pressures that are induced by the wave propagating under the deck are not synchronous. Impacts loads are found to be inherently a random process. The effect of venting is not so important. The presence of small venting does not significantly affect the loads for low Θ (i.e. clearance) values. The air venting seems to have a slight influence on the maximum forces at the bay deck for the higher values of the wave impact phase ($\Theta > 0.5$), when the wave impacts the soffit with increasing vertical velocity and the holes allow the mixture air-water to rapidly escape upwards. The experimental relationship between maximum forces and wave characteristics that has been proposed is:

$$F^*_{max} = \frac{F_{max}}{\rho g H_s A} = 5 * \theta = 5 * \frac{\eta_{max} - c}{\eta_{max}}$$

So the horizontal forces on the deck front are divided into quasi-static and impulsive loads.

These are defined as follows:

$$F_{QS} = \text{quasi - static horizontal force} = \rho g H_s * A * \theta$$

$$F_{max} = \text{maximum impulsive horizontal force} = 1.2 * \rho g H_s * A * \theta$$

The vertical impulsive loads on the bays are determined as:

$$F_{max} = 5 * \rho g H_s * A * \theta$$

where we define the water density $\rho = 1000 \text{ kg/m}^3$, the gravity acceleration $g = 9.81 \text{ m/s}^2$, the significant wave height H_s , the area on which is applied the load A and the non-dimensional parameter θ .

Fang et al. (2021) - Experimental investigation of focused wave action on coastal bridges with box girder

In this paper, the focused wave theory is used to represent extreme events and are highlighted the differences between slamming and quasi-static forces. Breaking and broken waves lead to complex and violent scenarios for elevated structures, due to non-linearity. Furthermore, trapped air is important for vertical uplifting forces: the model scale becomes important to avoid scale effects.

This paper evaluates failure of coastal bridges for lack of connection between superstructure and substructure through a model scale of 1:25 with horizontal bottom. They are considering a “New Wave” theory for focused waves where is made a comparison of time series and spectra with target conditions. Then is paid attention to only wave crest. The time domain LOESS smoother filter employed to divide quasi-static from slamming forces, with span equal to 0.6 s (other papers suggest 5% of the data)

Slamming forces are characterized by very high frequencies and the total horizontal force is proportional to the maximum focused wave amplitude (η_{\max}), then is found a quadratic relationship. The total vertical force is proportional to the maximum focused wave amplitude, in this case the relationship is linear. Furthermore is given a linear relationship between total and slamming vertical force. Then force is proportional to (η_{\max} - clearance/depth). It's given importance to wave steepness (wavelength is calculated based on regular waves).

2.2 Breaking criteria

Rattanapitikon and Shibayama (2006) - Breaking wave formulas for breaking depth and orbital to phase velocity ratio.

In this study h_b is the depth of the bottom of the sea that produce the breaking of the sea wave.

$$h_b = (3.86m^2 - 1.98m + 0.88)H_0 \left(\frac{H_0}{L_0}\right)^{-0.16}$$

Where m represents the bottom slope and in our case is equal to $m = 1/13 = 0.0769$, H_0 is the wave height in deep water, L_0 is the longitude of the wave in deep water.

The previous equation has been determined for 4 bottom slopes ($m = 0:01$, $m = 0:05$, $m = 0:10$, and $m = 0:20$). The computations of the breaker depth from this equation are carried out with 26 sources of collected data.

Furthermore, the use of this equation becomes questionable for the beaches having slope greater than 0.38 and for the deep-water wave steepness (H_0/L_0) greater than 0.112. Moreover, since the experimental data is not available for the range of $0,100 < H_0/L_0 < 0,104$, caution should be taken when using the equation for this narrow range. Because of the complexity of equation, unavailability of experimental data, and the narrow range of transition zone, the transition zone is not considered in this study.

Goda (2010) – Reanalysis of regular and random breaking wave statistics.

This study wants to define a manner to set a relationship between the regular wave height at breaking H_b depending on the longitude of waves in deep water L_0 , the water depth at breaking of regular waves h_b and the slope of the bottom $\tan(\theta) = 1/13 = 0.0769$. The formulation proposed by Goda (2010) is the following.

$$H_b = 0.17 * L_0 * \left\{ 1 - \exp\left(-1.5 * \frac{\pi h_b}{L_0} \left(1 + 15 * \tan(\theta)^{\frac{4}{3}}\right)\right) \right\}$$

By using the datasets available at the time, Goda (1970) prepared the diagrams of breaker index for four beach slopes of 1/10, 1/20, 1/30, and 1/100 by referring to the theoretical limiting wave heights on the horizontal bed calculated by Yamada and Shiotani (1968). The wave period T varies in the range 0.65 – 7.3s, the breaking depth h_b goes from 3.9cm to 125.0cm.

2.3 Focused wave theory

Whittaker et al. (2018), Extreme coastal responses using focused wave groups: Overtopping and horizontal forces exerted on an inclined seawall

The paper demonstrates the importance of the method of wave generation on overtopping. Focused wave groups provide insight into the relationship between incident wave properties and coastal responses.

Hughes and Thornton (2016) [Estimation of time-varying discharge and cumulative volume in individual overtopping waves] highlights the need to account for the properties of individual waves. A design approach involving short-duration focused wave group model tests could complement existing long-duration irregular wave method, yielding benefits such as:

- Increased repeatability;
- Assessment of model and scale effects;
- Possibility of enhanced measurement resolution for large wave interaction.

See **Whittaker et al. (2017)** for a detailed description of the NewWave for design purposes [Optimisation of focused wave group runup on a plane beach].

The NewWave focused wave group, based on a probabilistic analysis of the shape of a maximum in a linear, Gaussian process [Lindgren,1970], describes the most probable shape of a large wave in a given sea state [Boccotti, 1983]. Lindgren (1970) showed that the shape of a large event (wave) comprises both deterministic and random components with the deterministic component dominating for events large relative to the underlying process (sea state). This deterministic component is simply the scaled autocorrelation function (i.e. the Fourier transform of the energy density spectrum for the underlying sea state), and so the amplitude components are proportional to $S_{\eta\eta}(\omega)\cos(\omega t)\Delta\omega$ where $S_{\eta\eta}$ is the power spectral density, ω is angular frequency, t is time. Therefore, a NewWave-type focused wave group comprising N infinitesimal wave components is given by:

$$\eta(x, t) = \frac{A}{\sigma^2} \sum_{i=1}^N S_{\eta\eta}(\omega_i) \cos(k_i(x - x_f) - \omega_i(t - t_f) + \phi) \Delta\omega$$

Where σ is the standard deviation of the sea state (with an associated variance $\sigma^2 = \sum S_{\eta\eta}(\omega_i) \Delta\omega$ in this discretised form) and k_i is the wave number of the i -th wave component with angular frequency ω_i , which are related by the familiar linear dispersion relation $\omega^2 = gk * \tanh(kh)$ (where g is the acceleration due to gravity and h is the water depth), and x is the horizontal distance. All wave components come into phase at the focus location x_f and focus time t_f to yield large wave event with a linear focus (envelope) amplitude A . We allow the full range of focusing behaviours to occur by introducing the parameter ϕ referred to as the phase angle of the group at focus. For example, crest-focused wave correspond to a zero phase at focus $\phi = 0$ whereas trough-focused waves correspond to $\phi = \pi$.

Whittaker et al. (2016) [The average shape of large waves in coastal zones] demonstrated the validity of NewWave for pre-breaking waves in shallow water conditions, suggesting that extreme coastal response within a given sea state might be reproduced using a single incident wave group.

Focused wave groups are compact, so no absorption is needed. The authors also demonstrated that the range of validity of NewWave theory extends into shallow waters. This implies that linear frequency dispersion remains the dominant mechanism driving the statistics of wave elevation outside the main breaker line despite the increasing importance of nonlinear and local effects due to the bathymetry. A focused wave group represented by linear theory comprised wave components with specific frequencies, amplitudes and phases which coincide at a particular location in time.

The NewWave focused wave group describes the most probable shape of a large wave in a given sea state. The theoretical focus location controls dispersion of the wave group as it shoals and breaks during propagation. A focus location close to the structure means that the focus wave group energy reaches the structure in a compact, maximized, form.

The phase angle at focus provides a means to control the nature of the wave at focus (e.g. crest, trough) Otherwise, empirical formulas for overtopping discharge and volumes only

incorporates spectral parameters. However, this work shows the parametric dependence of the total overtopping on the focused location, amplitude and phase. In particular, phase can lead to changes in the overtopping of one order of magnitude.

The works show a correlation between maximum volumes and forces. Minimal reflection of the preceding waves seems very important to maximise both the volume and the forces.

Whittaker et al. (2017), Optimisation of focused wave group runup on a plane beach

Coastal communities rely on sea defence structures for protection against flood inundation. Worldwide, the populations of such communities are increasing, while much coastal defence infrastructure is ageing. Run-up, the maximum elevation attained by seawater above the still water shoreline, has a primary influence on surf zone sediment transport, beach levels and coastal erosion, wave overtopping of natural or artificial defence structures, and subsequent inland flooding. Storm-induced wave run-up and its consequences are particularly sensitive to sea level rise [J.W. Hall et al., 2006, P.B. Sayers, M.J. Walkden, M. Panzeri, Impacts of climate change on

coastal flood risk in England and Wales: 2030–2100; Sutherland and Gouldby, 2003, Vulnerability of coastal defences to climate change] and climate variability (Ruggiero, 2013) [Is the intensifying wave climate of the U.S. Pacific Northwest increasing flooding and erosion risk faster than sea-level rise?].

This study seeks to determine the effectiveness of a focused wave group as a predictor of extreme runup on a plane beach. Instead of representing the incident field as a parameter (such as the significant wave height or period), this approach generates a compact wave group representing an extreme event within the incident wave field.

Recent analysis of field data from wave buoys by Whittaker et al. (2016) [The average shape of large waves in coastal zones] has demonstrated that NewWave could represent the average shapes of large storm waves observed in shallow water of depth $kD < 0.5$. This is a powerful result, demonstrating that even in shallow water depths the average shape of the largest event is a property of all the waves in the sea state (i.e. the autocorrelation function).

The focusing event (x_f, t_f) is the spatial and temporal position/instant at which the wave group is in its most compact form according to Eq. (2), which applies the linear dispersion relation for a constant water depth D (allowing calculation of the required paddle signal to generate the focusing event). It is important at this point to clarify the difference between the phase of each Fourier component and the overall shape of the focused wave group. A single frequency component of an irregular sea state would have the form $\cos(k_i x - \omega_i t + \phi_i)$, where ϕ_i is the phase of each wave component randomly chosen from a uniform phase distribution on $(0, 2\pi)$. However, in formulating a focused wave group this phase is not random, and can be expressed in terms of the phase of the entire wave group in the form $\phi_i = -k_i x_f + \omega_i t_f + \phi$, where (x_f, t_f) is the focusing event and ϕ is the phase of the wave group at focus. Hence, the frequency-independent phase of all the wave components ϕ is distinct from the focusing of the group; this phase which determines the position of the individual waves within this group. The energy concentration within the group for any value of ϕ is independent of the value of ϕ , this is related to the envelope of the group which may conveniently be taken as that for the crest-focused case of $\phi = 0$. Thus, we can talk about crest-focused, trough-focused and up- and down-crossing events, all with the same envelope.

However, it should be noted that the creation of a perfectly focused wave group on a sloping beach is not the objective of the present work (particularly since breaking on the slope will prevent complete focusing of the large-amplitude waves of greatest interest). Instead, the wave group will be generated offshore with a given linear focus amplitude A and focus location x_f (i.e. where the Fourier components of the wave group come into phase ϕ), based on linear focusing in a constant water depth to that point. The wave group itself will evolve (nonlinearly) as it propagates up the slope, generating a maximum runup event.

Shaffer (1996) [Second-order wavemaker theory for irregular waves] is used to correct the wave generator signal for a proper second-order wave generation. Two factors contributed to the experimental-theoretical paddle signal discrepancy: the different transfer functions and the low frequency limit for the experimental paddle motion.

It is found that use of a linear paddle signal erroneously increased the maximum run-up elevations over the entire parameter space. The maximum run-up generated by a focused

wave group exhibited strong dependence on the linear wave group amplitude at focus location, and phase at focus of the wave group.

Orszaghova et al. (2014), Importance of second-order wave generation for focused wave group run-up and overtopping

The background of this paper is that focused wave groups offer a means for coastal engineers to determine extreme run-up and overtopping events.

The purpose of this work is to examine numerically the importance of second-order accurate laboratory wave generation for NewWave-type focused wave groups generated by a piston-type paddle generator, and interacting with a plane beach and a seawall in a wave basin.

The numerical wave tank is based on the Boussinesq equations for non-breaking waves, and the nonlinear shallow water equations for broken waves. During the model validation, good agreement is achieved between the numerical predictions and laboratory measurements of free surface elevation, run-up distances and overtopping volumes for the test cases driven by linear paddle signals. Errors in run-up distance and overtopping volume, arising from linear wave generation, are then assessed numerically by repeating the test cases using second-order accurate paddle signals.

Focused wave groups generated using first-order wave-maker theory are found to be substantially contaminated by a preceding long error wave, resulting in erroneously enhanced run-up distances and overtopping volumes.

Thus, the use of second-order wave-maker theory for wave group run-up and overtopping experiments is instead recommended.

3. Experimental setup

3.1 CIEM flume

The experiments were led in the CIEM (Canal d'Investigacio' I Experimentacio' Maritima) wave flume in the laboratory of maritime engineering of the UPC (Universitat Politecnica de Catalunya, Barcelona, Catalonia). The CIEM is an international research facility for controlled hydraulic experiments in coastal, harbor and oceanographic engineering.

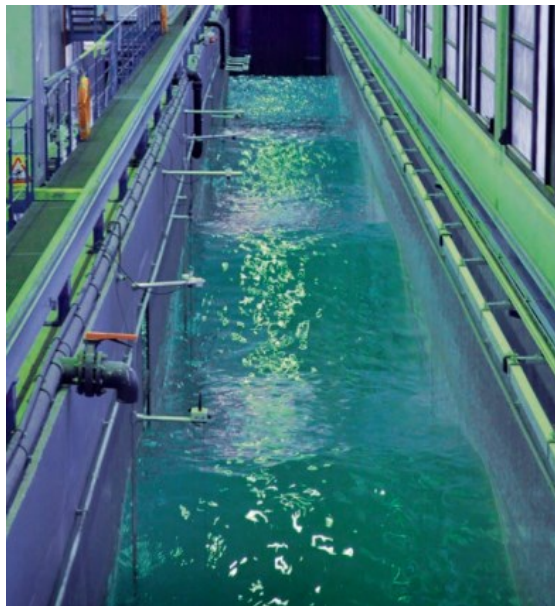


Fig. 7- CIEM wave flume at UPC

The CIEM wave flume is 100 m long, 3 m wide and up to 7 m deep inside the current generator's wells. This facility is used for scaled tests and studies under close-to-real conditions. Typical working scales are between 1/2 to 1/20. Waves and currents are generated by a wedge-type wave generator, the system is hydraulically actuated and PC-controlled. This is also capable to produce waves with heights up to 1.6 m. The control software allows regular and irregular waves generation.

3.2 Constant Froude number similitude

The geometrical scale of the model is 1/10. The scale method used is the constant number of Froude method. This means that the Froude's number in the model is the same of the real event. After having fixed the geometrical scale of the model it is possible to calculate the scale of the forces. The Froude number in the model is equal to the Froude number in the prototype, then for the scale of the velocities we obtain:

$$Fr_m = Fr_p; \frac{v_m}{\sqrt{g * L_m}} = \frac{v_p}{\sqrt{g * L_p}} \Rightarrow \frac{v_m}{v_p} = \sqrt{\frac{L_m}{L_p}} \Rightarrow \lambda_v = \lambda_L^{0.5}$$

For the time scale is given the following ratio:

$$v = \frac{L}{t}; \lambda_T = \frac{\lambda_L}{\lambda_v} = \frac{\lambda_L}{\lambda_L^{0.5}} = \lambda_L^{0.5}$$

The density of the water used in the model is approximately the same of the prototype. Then the scale of the forces (that is the ratio between the forces on the reduced pier and the forces on the real pier) will be equal to:

$$\lambda_F = \frac{F_m}{F_p} = \frac{\rho_m * L_m^3 * \frac{v_m}{t_m}}{\rho_p * L_p^3 * \frac{v_p}{t_p}} \Rightarrow \lambda_F = \lambda_L^3 * \frac{\lambda_v}{\lambda_T} = \lambda_L^3 * \frac{\lambda_L^{0.5}}{\lambda_L^{0.5}} = \lambda_L^3$$

So for a geometric scale of 1/10, the force scale is 1/1000.

The pressure scale for a model with a constant Froude number is equal to:

$$P = \frac{F}{A} = \frac{F}{L^2} \Rightarrow \lambda_P = \frac{\lambda_F}{\lambda_L^2} = \frac{\lambda_L^3}{\lambda_L^2} = \lambda_L$$



Fig. 8 - Scaled model of Pont del Petroli

3.3 Evaluation of Reynolds number in the model and in the prototype

An easy manner to evaluate the Reynolds number of this phenomenon is to use the wave Reynolds number. This formula consists in use the celerity of the wave (c [m/s]) as characteristic velocity of the problem and the water depth at the beginning of the platform (d [m]).

The celerity of the wave and the Reynolds number in the model are:

$$c_m = \sqrt{g * d_m}$$

$$Re_{w,m} = \frac{c_m * d_m}{\nu}$$

Where d_m is the aforementioned water depth at the beginning of the reduced platform, c_m is the wave celerity in the model and ν [m²/s] is the kinematic viscosity of the fluid. The considered fluid is water so the kinematic viscosity is equal to $\nu = 10^{-6}$ m²/s. The Reynolds number for the 221 tests in the model are in a range that goes from $2,30 * 10^6$ to $2,67 * 10^6$.

In the prototype the Reynolds number is deduced as follows:

$$Re_{w,p} = \frac{c_p * d_p}{\nu} = \frac{\left(\frac{c_m}{\lambda_p}\right) * \left(\frac{d_m}{\lambda_L}\right)}{\nu} = \frac{c_m * d_m}{\nu} * \frac{1}{\lambda_L^{0.5}} * \frac{1}{\lambda_L} = \frac{Re_{w,m}}{\lambda_L^{3/2}} = Re_{w,m} * 10^{3/2}$$

So for the prototype is obtained a range of the Reynolds number of $7,29*10^7 - 8,46*10^7$. These results agree with the type of hydraulic process that is analyzed because the physical phenomenon of breaking waves is very turbulent.

Measured element	Scale factor λ
Maximum wave crest – η [m]	1/10
Maximum wave height – Hmax [m]	1/10
Significant wave height – Hm0 [m]	1/10
Wave length of the focused wave – L [m]	1/10
Wave period – T [s]	$1/\sqrt{10}$
Phase of the focused wave – ϕ [°]	1
Forces – Fx, Fz [N]	1/1000
Pressures – P [Pa]	1/10
Celerity of the wave – c [m/s]	$1/\sqrt{10}$

Tab. 1 - Scale factor of the different physics element analyzed

3.4 Model setup of Pont del Petroli

The geometrical scale of the model is 1/10. Figure 2 and Figure 3 show the scaled model of the Pont del Petroli. The model is realized in steel, except for the plates forming the cover of the platform and footbridge, made in plywood. The platform starts at $x = 54$ m.

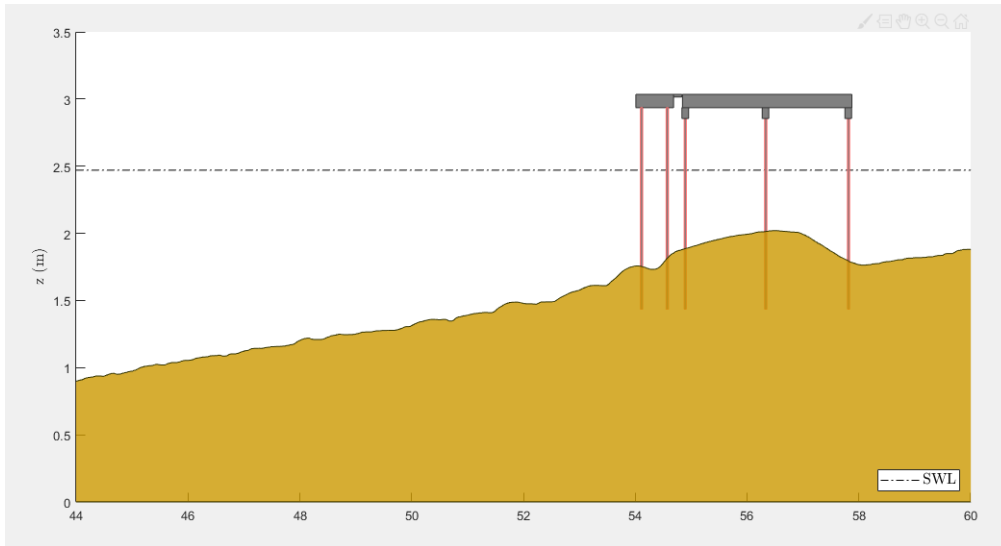


Fig. 9 - Sketch of the model of Pont del Petroli used in the tests

The foreshore, starting approx. at $x = 32$ m is made of sand. The sediment consisting of medium sand $d_{50} = 0.25$ mm, with a narrow grain size distribution ($d_{10} = 0.154$ mm and $d_{90} = 0.372$ mm) and a measured settling velocity (w_s) of 0.034 m/s. The sand used for this experiment is provided by Sibelco being the commercial name J5060S. The following figures show the scaled model of the Pont del Petroli which realization has been done only for the part closer to the platform.

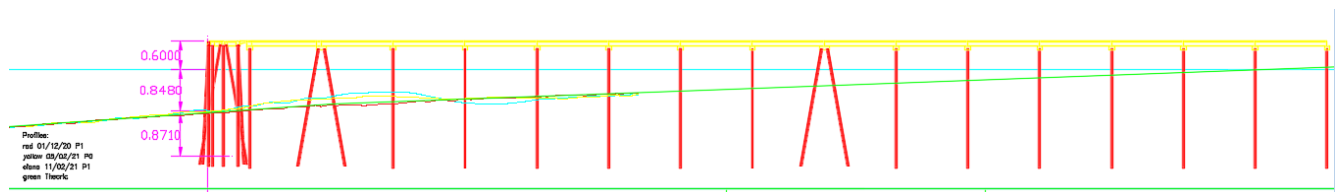


Fig. 10 - Representation of the scaled model of Pont del Petroli



Fig. 11 – Picture of the scaled model of Pont del Petroli.

3.5 Number and type of used sensors, relative characteristics and relative position along the channel

The characteristics of instruments used are described in the following.

1. Resistance Wave Gauges (WG)
2. Acoustic Wave Gauges (AWG)
3. Pore Pressure Sensors employed for surface elevation measurements (PPT)
4. Load cells (LC)
5. Pressure Sensors employed for measurements of exerted pressure on the footbridge (PS)
6. Echo Sounder

For water surface elevation were employed: 9 acoustic sensors AWG (Acoustic Wave Gauge), 10 resistive sensors RWG (Resistive Wave Gauge), 10 pore pressure transducers PPT (see Fig.12). Location of the sensors and corresponding channel in the output file of data acquisition are reported in Table 2. For the PPTs, the Z-coordinate of their placement and the corresponding local water depth values are reported in Table 3.

The sensor used for the measurement of forces on the platform of the pier are: 4 load cells for the measurement of vertical forces on the corners of the platform (LC1-LC4), 2 load cells for the measurement of horizontal forces on the front of the platform (LC5, LC6), 1 load cell for the measurement of horizontal forces on the first pile cap (LC7), 3 pressure sensors on the deck of the pier (PS1, PS7, PS8). A sketch representing the LCs and PSs placement is depicted in Fig.13. Sampling frequency of AWGs, WGs and PPTs is 40 Hz, meanwhile 2400 Hz is used for LCs and PSs.

Label	Channel in the acquisition output file	X (m)
WG0	3	11.86
WG13	4	11.86
AWG6	19	17.64
AWG0	13	19.44
AWG9	21	21.6

AWG5	18	23.6
AWG1	14	25.6
WG2	5	27.02
AWG2	15	27.6
WG3	6	28.57
AWG3	16	30.3
PPT0	22	34.41
WG7	7	35.96
PPT1	23	37.81
PPT2	24	41.96
WG11	8	44.13
PPT3	25	46.14
WG5	9	48.16
AWG4	17	50.24
WG6	10	52.12
WG8	11	53.55
AWG7	20	54
WG9	12	55.11
PPT5	26	57.83
PPT6	27	59.14
PPT8	29	60.41
PPT9	30	62.51
PPT11	31	64.73
PPT12	32	65.46
PPT13	33	67.11

Tab. 2 - Label and location of water surface elevation sensors

On 05/02/2021, from test 050221_37 on, the AWG7 has been moved to measure overtopping flows on the platform. The next position is: $x = 54.46\text{m}$, distance from the flume right wall= 1.49 m , distance from the platform $z = 0.61\text{ m}$.

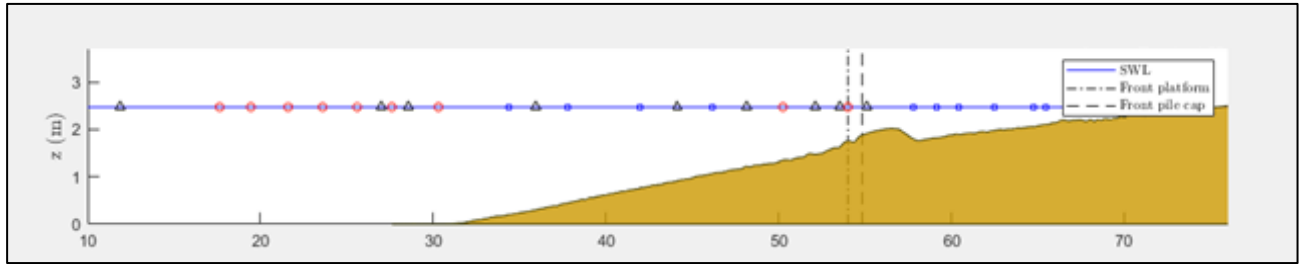


Fig. 12 - Position of sensors along the CIEM (red circles = AWG, blue squares = PPT, black triangle = WG).

Label	Z (m)	Local depth (m)*
PPT0	1.24	2.44
PPT1	1.41	2.20
PPT2	1.4	1.89
PPT3	1.37	1.60
PPT5	2.05	0.77
PPT6	2.04	0.72
PPT8	2.04	0.71
PPT9	2.04	0.64
PPT11	2.22	0.55
PPT12	2.21	0.53
PPT13	2.19	0.48

Tab. 3 - Z-coordinate of the pressure transducers and local water depth values. *It can vary slightly from test to test because of small changes in the beach profile.

The sensor used for the measurement of forces on the platform of the pier are: 4 sensors for the measurement of vertical forces on the corners of the platform, 2 sensors for the measurement of horizontal forces on the front of the platform, 1 sensor for the measurement of horizontal forces on the first pile cap, 3 pressure sensors on the deck of the pier.

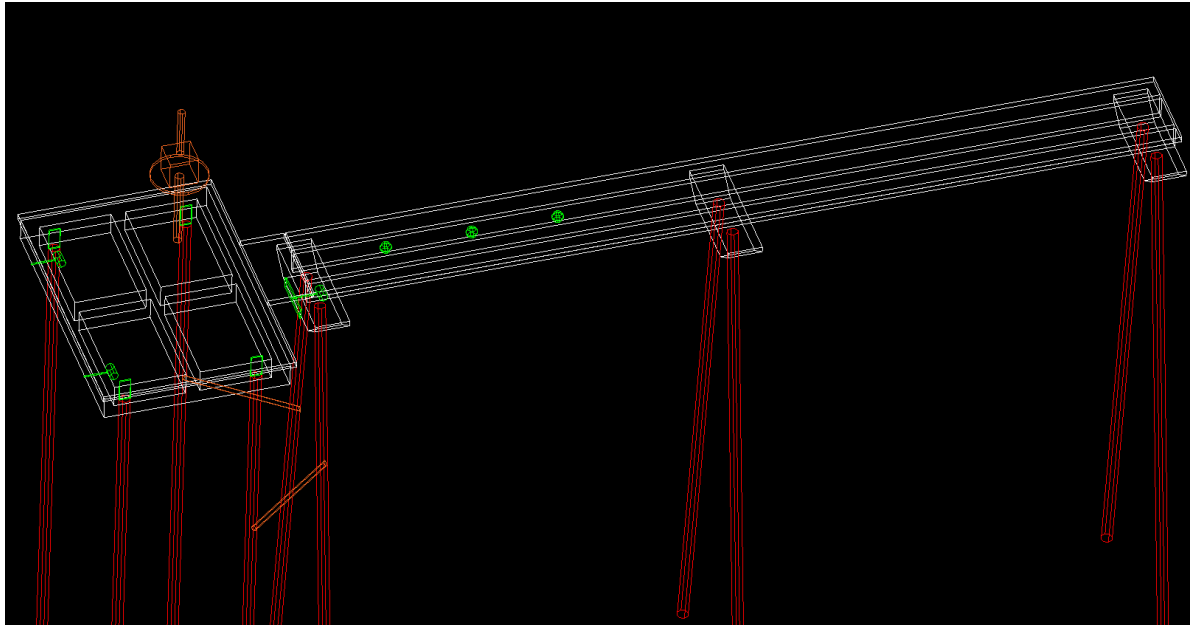


Fig. 13 - 3D drawing of the Pont del Petroli model as built in the flume. (red = supporting piles; white = horizontal elements; green = LCs and PSs).

The signals measured in the channel were “smoothed” with a filter and then the filtered signal has been used for the calculation of the forces acting on the model. In particular, at the beginning is made a ‘detrend’ of the measurement, i.e. if the signal has a certain drift it is calculated and eliminated in order to rectify it. After that, a low-pass filter is applied, a frequency filter that eliminates the highest frequencies (i.e. similar to the resonant frequencies of the structure, 50-80 Hz).

The forces acting on the platform are calculated as the average among the measured forces. Thus vertical forces are the average value of the four measurement of vertical forces applied on the platform and the final horizontal force is the average of the measurement of the two load cells placed behind the front of the platform.

3.6 Definition of time origin and instrument synchronization

The Wave generator Acquisition System (WAS) controls the time frame of the experiments. The WAS files start to record the equipment activities usually around 10-20 seconds before the wave paddle starts its movement (the wave generation). At the moment of starting waves there is a trigger signal sent to start other equipment and recorded on the WAS file. The WAS system controls the acquisition of all the CIEM equipment (WGs, AWGs, PPTs and synchronization signals of other equipment) at a frequency of 40 Hz.

The only equipment from the CIEM which is not recorded on the WAS files comprises both LCs and PSs which need to be recorded in an external computer in order to save the digital information. LCs and PSs are usually set to measure at 2400 Hz and they have their own time frame which is correlated with the WAS by mean of the TTL trigger signal that starts the LCs+PSs acquisition. The TTL signal generated at the wave generation is a trigger signal that goes from 0 to 5 V, stays at that voltage for 5 s, and then drops from 5 to 0 V.

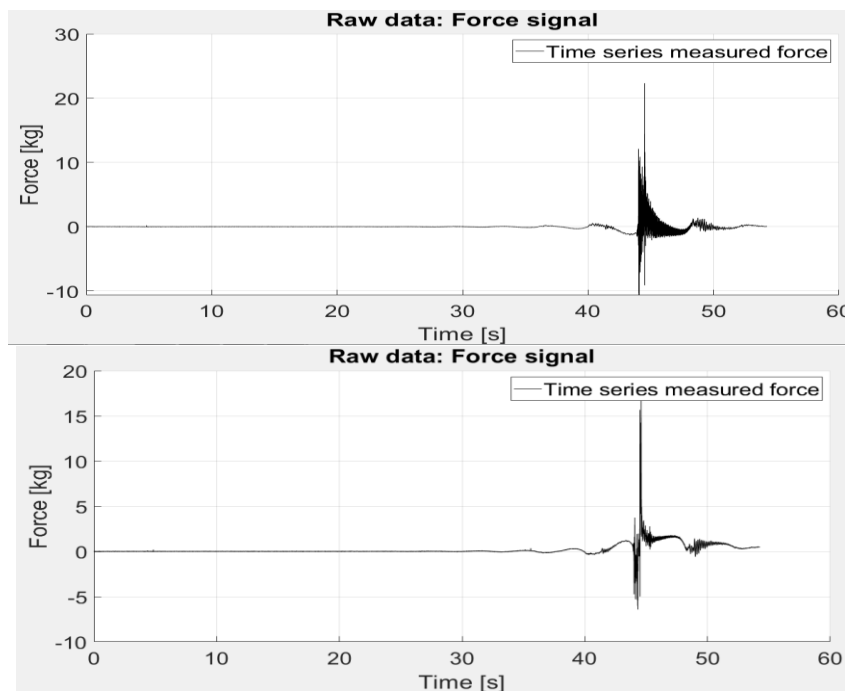


Fig. 14 - Raw data of vertical forces of sensors 1 and 3 for test n°021220_6 FOC79

4. Data post-processing

The raw signals from PPTs, LCs and PSs needed to be treated and corrected.

4.1 PPTs correction

A MatLab subroutine was employed to correct a detrended sea surface time series for depth attenuation. Frequency correction from 0.05 to 0.33 Hz. The subroutine was written by Urs Neumeier, 2003-2004 and modified from by T. Mason, SOC, January 1997.

4.2 LCs and PSs

A MatLab subroutine written by Maximilian Streicher (Ghent University) in 2017 and modified by Corrado Altomare in 2021 has been used for data filtering. First, any long duration drift was removed from the signal using the 'detrend' functionality. Besides, an offset correction was applied, by fitting a polynomial best-fit line to the lower values of the time-series (the noise band, not including the force peaks) and subtracting the polynomial best-fit line from the time-series.

The time-series was then transformed into frequency domain with FFT. In frequency domain the filters were set, to remove phenomena related to model effects (for example electronic current frequency, natural frequency of the measurement system) from the time series. A band-stop filter was used. For LCs, a low-pass filter was also employed to stay below the natural period of the measurement system. A Butterworth filter design of 4th order was used. Similar procedure is described in Kortenhaus et al. (2019).

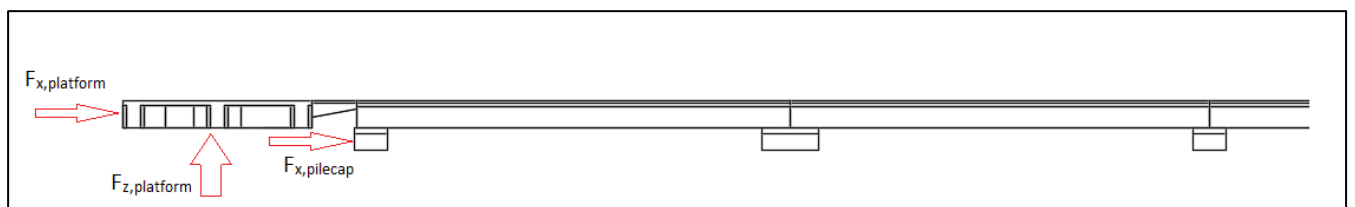


Fig. 15 - Sketch of the resulting final forces

4.3 Summation of LC results

The filtered time series from LCs 1 to 4 were summed to obtain the total vertical force acting on the pier platform. The filtered time series from LCs 5 and 6 were summed to obtain the total horizontal force acting on the pier platform.

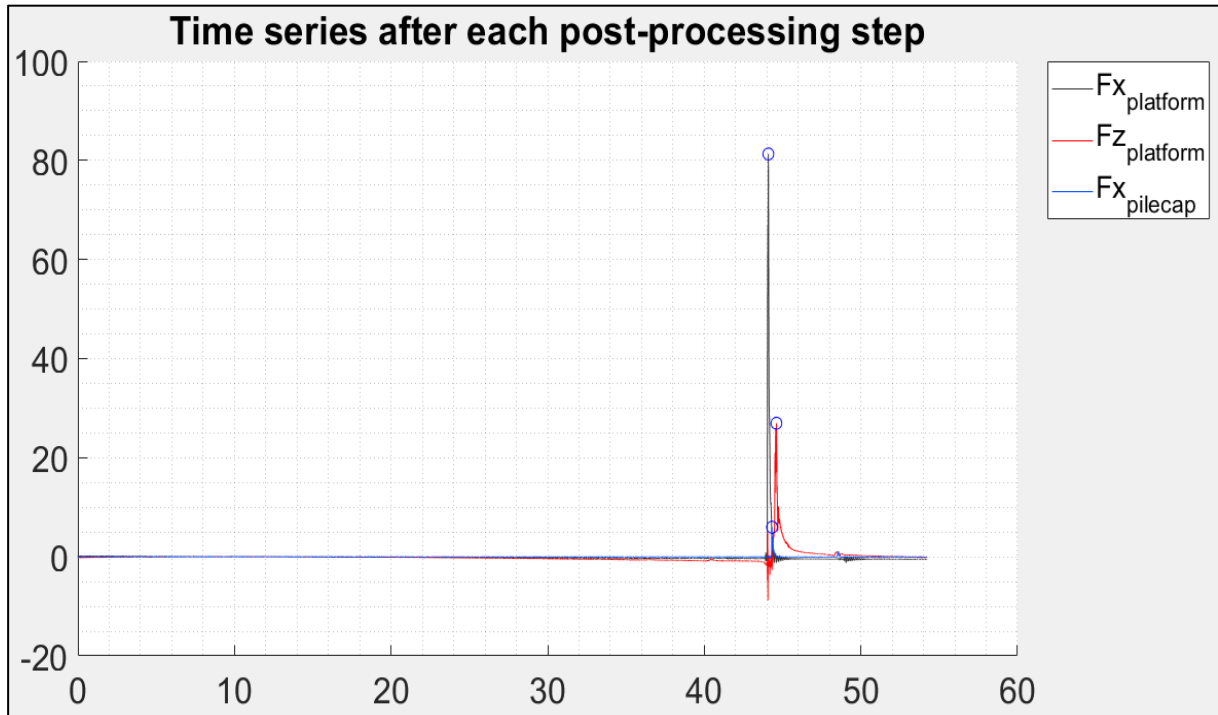


Fig. 16 - Final result of filtered forces for test n°021220_6 FOC79

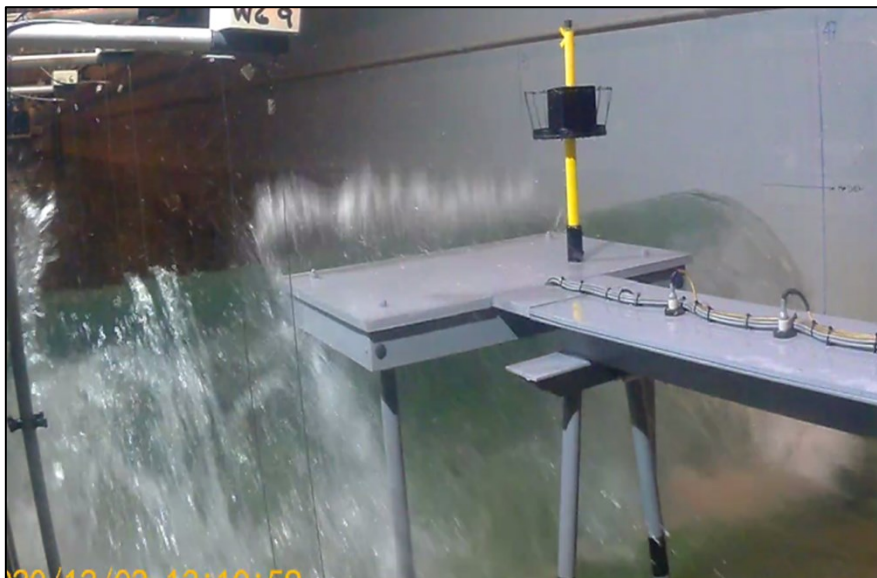


Fig. 17 - Picture of the impact occurred during test n°021220_6 FOC79

4.4 Test program

The number of tests carried out in the CIEM flume is 221. Focused wave groups were generated. Each focused wave group time series was created using the NewWave theory as described in Whittaker et al. (2017).

The range of target wave conditions is summarized as follows (expressed in model scale):

- maximum wave height at the focus location (H_{\max}): [0.65 – 1.11] m
- distance of the focused from the wave generator: [48.16 – 55.11] m
- phase of the focused: [0 – 270] °
- water depth at the wave generator: [2.435 – 2.520] m
- water depth at the pier toe: [0.815- 0.900] m
- pier clearance: [0.415-0.500] m

The range of measured wave conditions at the WG8 location are (expressed in model scale):

- maximum crest elevation (η_{\max}): [0.31 – 0.77] m
- maximum wave height (H_{\max}): [0.62 – 1.04] m
- wavelength at the toe associated to the highest wave: [8.36 – 11.57] m

5. Output files and preliminary considerations

In the present chapter are shown the final products obtained during the experimental campaign and then are made all the considerations and the comparisons with the scientific literature mentioned in the previous chapters.

5.1 Output files

In this paragraph are summarized the graphics that have been used to detect specific phenomena such as the breaking of the waves, the quantity and the magnitude of the horizontal and vertical impacts that affected the scaled model and eventual errors in the measurements of the load cells.

For each of the 221 tests were made measurements of vertical forces on the platform and horizontal forces on the platform and on the first pilecap. Then these measurements have been filtered giving as final result of forces a time series of loads as shown in Fig.18. Some of the tests recorded more than 1 impact (e.g. see Fig.19). This have happened because of the shape of the focused wave.

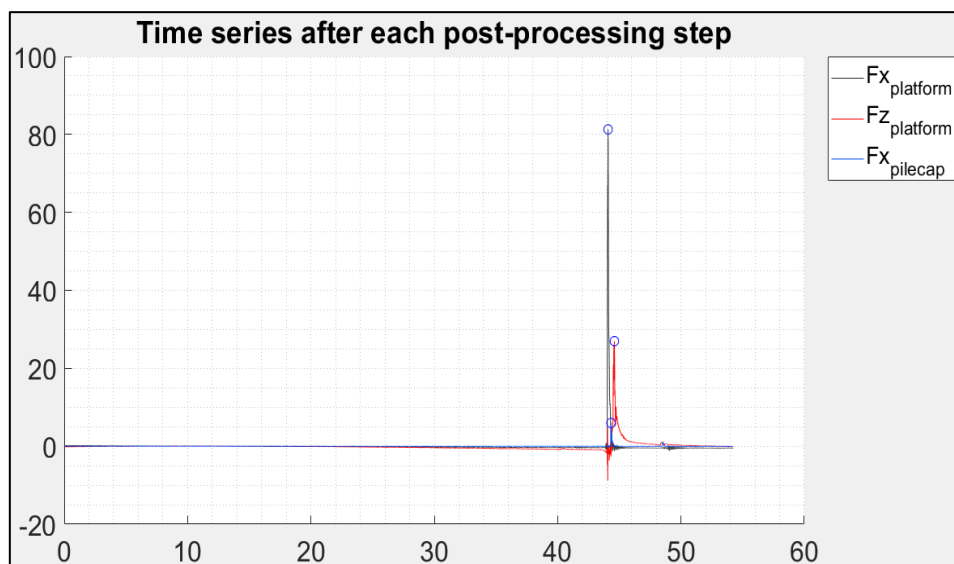


Fig. 18 - Measurement of forces of test 021220_6 FOC79

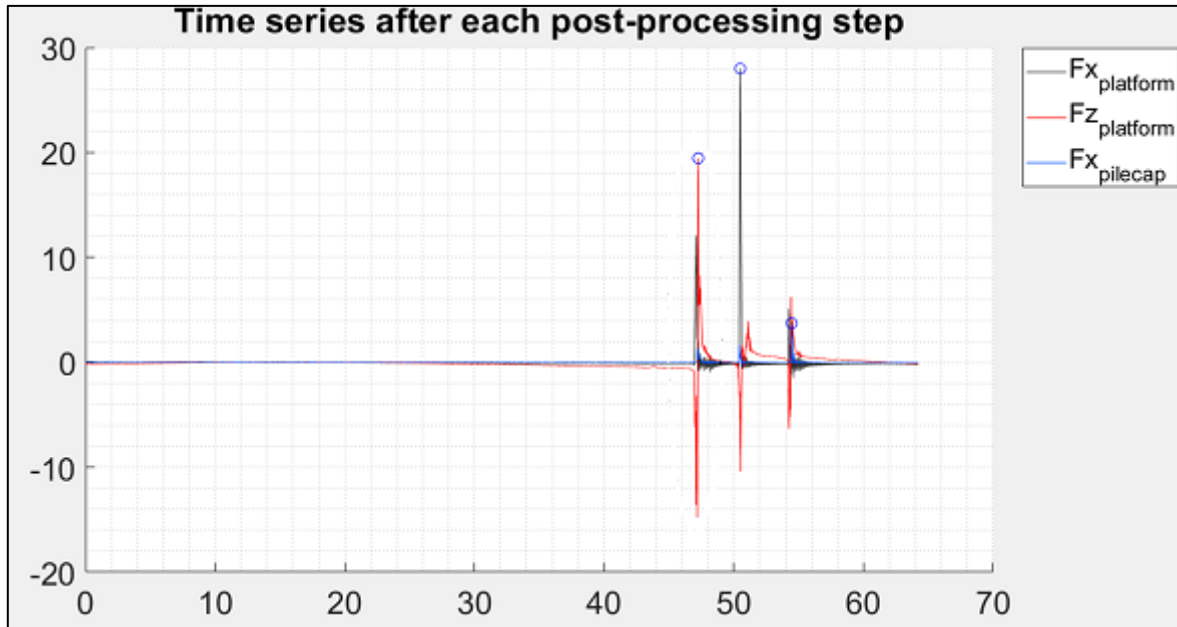


Fig. 19 - Measurement of forces of test 011220_8 - FOC73

With the measurement of dynamic elements such as the loads due to the wave impacts, then have been determined also the hydraulic elements of the wave. In the following figures we can see the magnitude of the measured maximum wave height and the surface elevation.

In Fig.20 are show the time series of each sensor that were measuring the surface elevation. On the y-axis are given the surface elevations $\eta(m)$ and on the x-axis the distance from the plate that generates the wave. These measurements are divided in three groups depending on the type of sensor:

- WG stands for the resistive sensor (first image starting from above);
- AWG represents the measurements made with the acoustic sensors (second graphic);
- PPT means that the measures of surface elevation were made with a pressure sensor (image on the bottom).

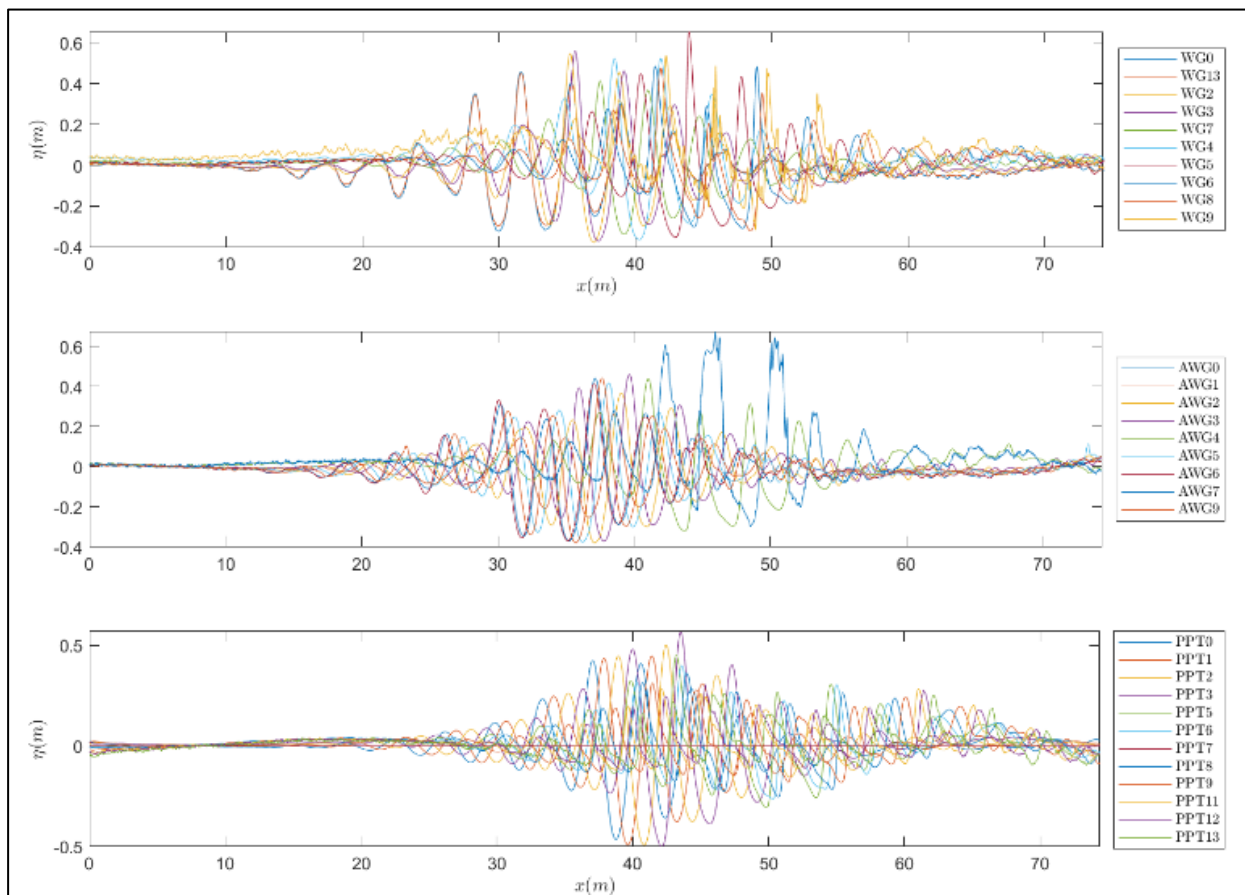


Fig. 20 – Time-series of measurements of surface elevation distinguished by type of sensor.

In Fig.21 are represented the values of maximum wave height $H_{max}(m)$, the surface elevation $\eta(m)$ and the setup of all the sensors used (first image). The sensors are represented differently depending of the type of the sensor. The black triangle stands for the resistive sensor (WG), the red circle represents the acoustic sensors (AWG) and the blue square are the pore pressure sensors (PPT).

The trend of these values let us understand if there is breaking of the sea wave. Usually the value of the maximum wave height H_{max} grows up due to the shoaling before the breaking. After the breaking the wave height decrease dramatically for the breaking of the wave that induces a strong dissipation.

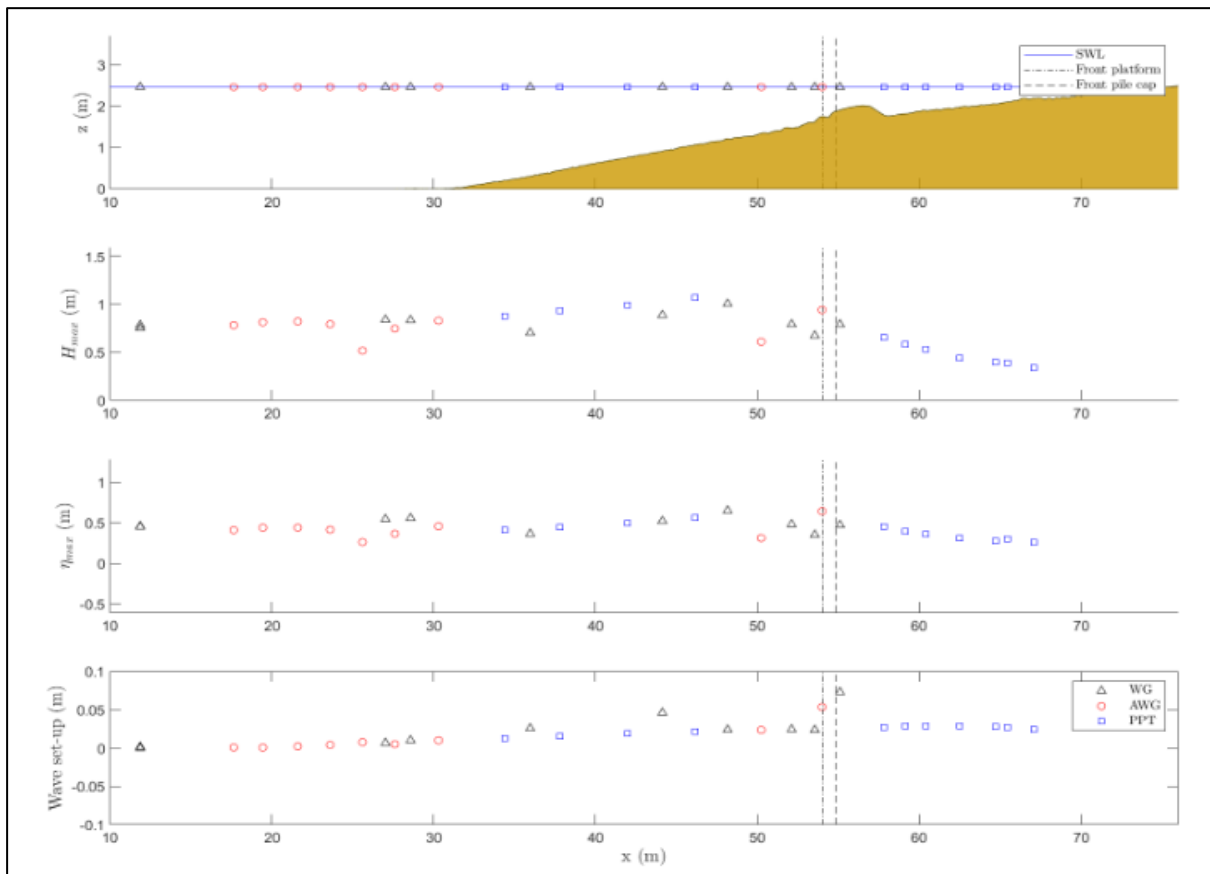


Fig. 21 – Maximum wave height and surface elevation

In Fig.22 is presented a simplified representation of the surface elevation profile in three different instants of time. These instants of time correspond to the instant when occur the three peaks of the horizontal forces on the platform (blue line), the peak of the vertical forces applied to the platform (red line) and the peak of the maximum horizontal force applied to the first pilecap (green line).

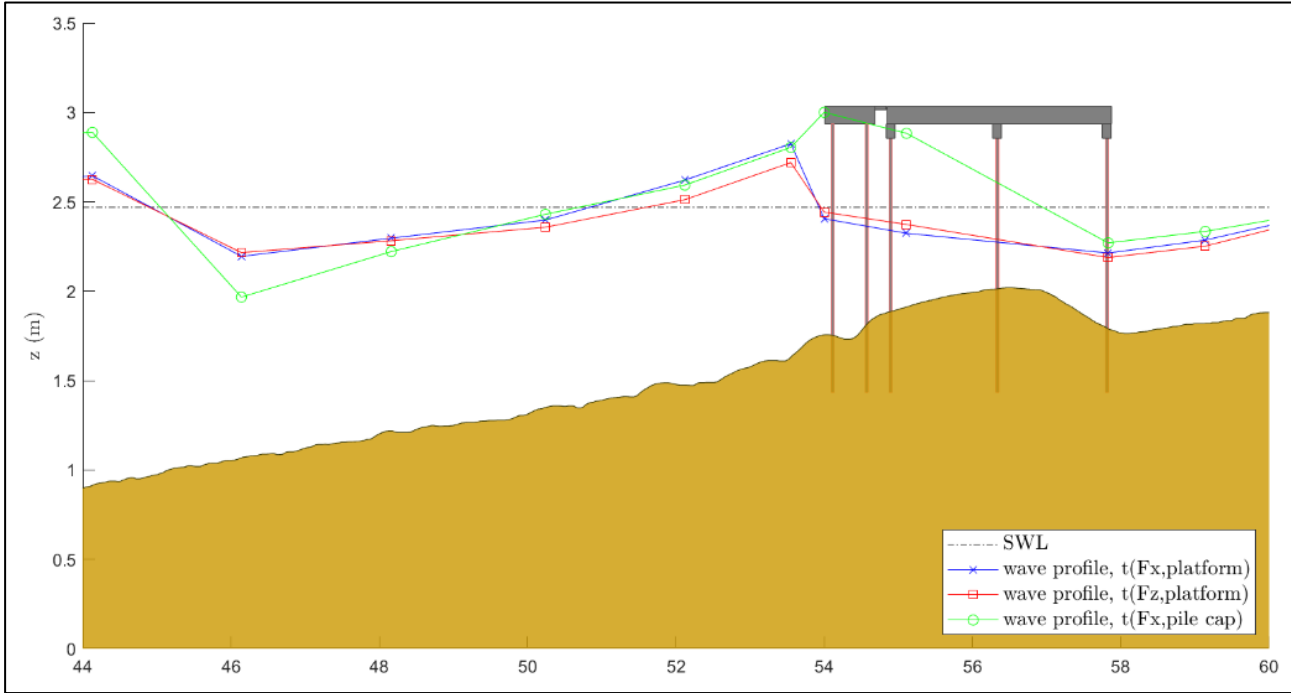


Fig. 22 – Free surface elevation at the peaks of horizontal and vertical forces on the structure.

The last figure proposed in the present paragraph is Fig.23. These graphics represent the surface elevation measured with four different sensors and the target value of the surface elevation $\eta(m)$. The surface elevation measured by the sensors is drawn in red, instead of the theoretical target value of surface elevation which is drawn with a black line.

This figure is useful in order to understand if the surface elevation that we are expected to realize through the focused wave theory is effectively reproduced in the channel during the test.

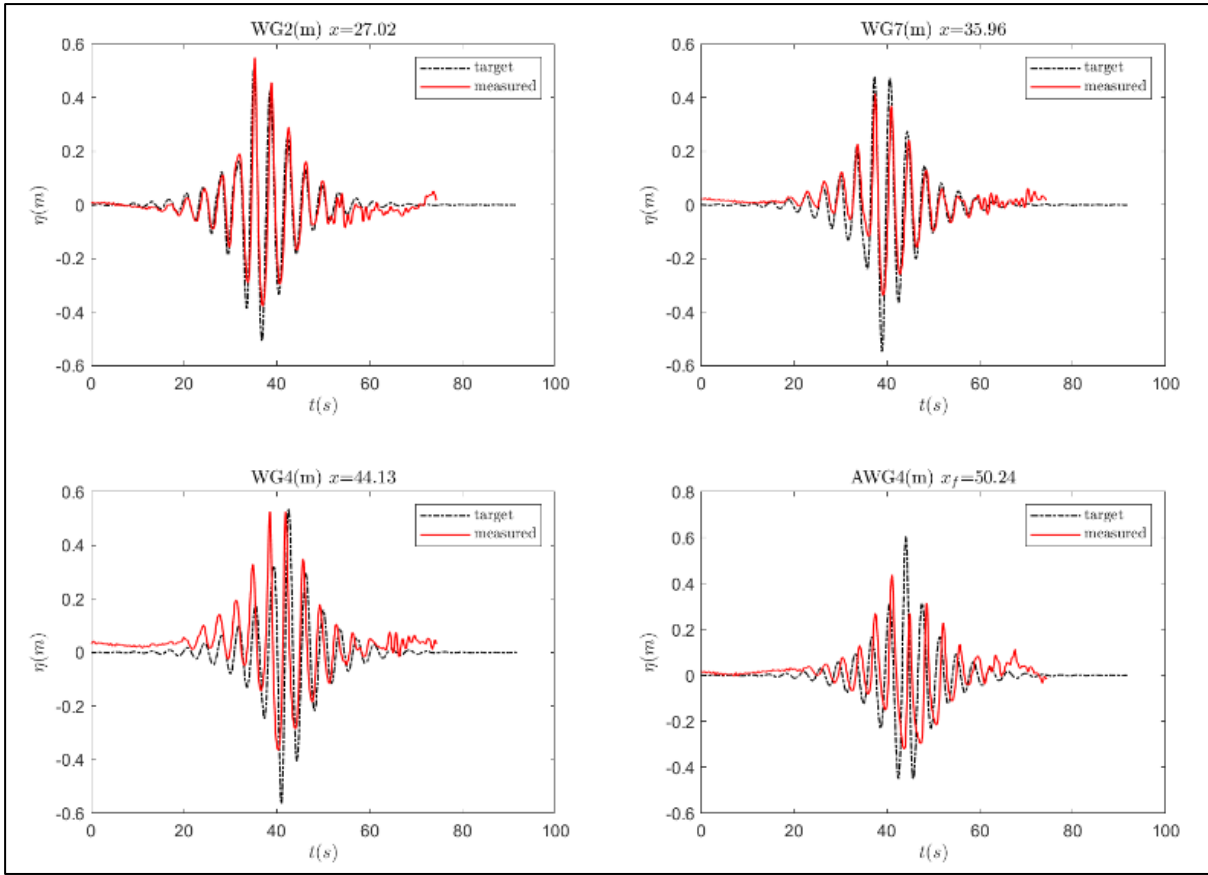


Fig. 23 – Target surface elevation vs measured surface elevation.

5.2 Range of values of general details of the waves

In this paragraph are summarized all the range of values of the target entities and the measured value of the physical elements.

Target elements

- maximum wave height of the focused wave (H_{\max}): [0.65 – 1.11] m
- wave period: [3.5 – 4.0]
- distance of the focused from the wave generator: [48.16 – 55.11] m
- phase of the focused: [0 – 270] °
- wave length of the focused: [14.89 – 17.78] m
- clearance: [0.415 - 0.500] m
- water depth to the generator plate: [2.435 – 2.520] m
- water depth to the toe: [0.815 - 0.9] m

Measured elements

- maximum surface elevation (η_{\max}): [0.28 – 0.6] m
- Reynolds number (in the model): [2.8*10⁶ - 3.49*10⁶]
- Maximum horizontal force to the platform (model scale): [0.53 – 215.95] kg
- Maximum vertical force to the platform (model scale): [0.70 - 121.29] kg
- Maximum horizontal force to the pilecap (model scale): [0.00 – 8.21] kg
- steepness of the wave: [0.04 - 0.07]
- water depth to the toe/ H_{\max} : [0.84 - 1.51]

5.3 Visual validation of the tests and their breaking shape

The aim of the visual analysis is to verify if the impact produced in laboratory has some kind of similarities with the impacts occurred during the storm Gloria. Some experiments were video-recorded and a part of them were compared with some pictures taken before the failure of the platform.

As shown in the following figures there are interesting affinities in the way of rupture of the waves in the model and the way of rupture of some waves in the reality of the event. In the following image is shown a comparison among a picture of an impact on the model, the measured forces on the model due to that impact, the maximum values of the measured horizontal forces on the platform, the maximum vertical force on the platform and the maximum horizontal force on the pilecap. Furthermore, have been added the main characteristics of the focused wave for the given impact model, a picture of an impact on the real structure due to the storm Gloria some hours before the failure of the structure that presents similarities with the breaking of the wave in the model test and the evolution of wave height during the storm Gloria where is possible to identify the hour and the wave height for that precise instant of capture of the real impact presented below.

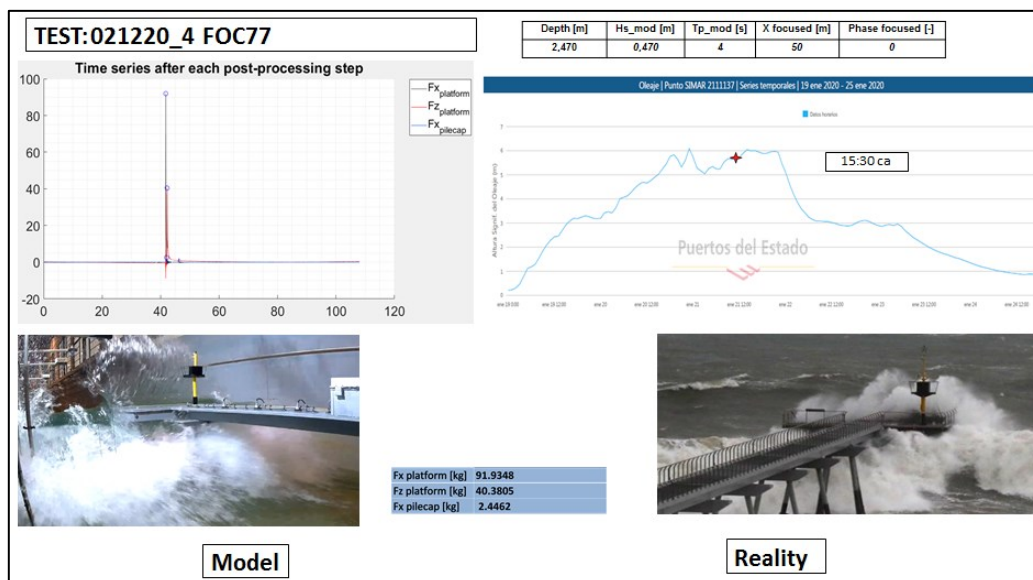


Fig. 24 – Summary of the visual validation of the tests and their breaking shape.

The value of the significant wave height was taken from the database of Puertos del Estado in the point SIMAR n°2111137 (Coordinates of the point: 2,25°E – 41,42°N) close to the Pont del Petroli.

The SIMAR dataset consists of time series of wind and wave parameters from numerical modeling. They are, simulated data and do not come from measurements direct from nature. The SIMAR series arise from the concatenation of the two large simulated data sets waves that the State Ports have traditionally counted on: SIMAR and WANA. The objective is to be able to offer more extensive time series in time and updated daily. [Source: Puertos del Estado]



Fig. 25 - Position of point SIMAR 2111137. Source: Puertos del Estado

In the next rows are collected some of the most relevant visual validation of two tests. The first is the test number 050221_9 (FOC282) that led to a value of horizontal load on the platform of 1730 kN (in the prototype scale); the second one is the test number 050221_5 (FOC264) which has led to a higher value of forces applied to the structure, in example a horizontal force of 2150 kN (prototype scale).

Test n°050221_9 – FOC282

We can see how this test gives results similar to what happened the day before the failure of the structure of Pont del Petroli. The way of breaking of the sea wave reproduced in laboratory is quite similar to the one shown in Fig.27b. Nevertheless, the model and the focused wave produced in the CIEM flume doesn't take into account the effect of three-dimensional effects such as a more precise modelling of the refraction due to a non-prismatic bathymetry of the bottom of the sea.

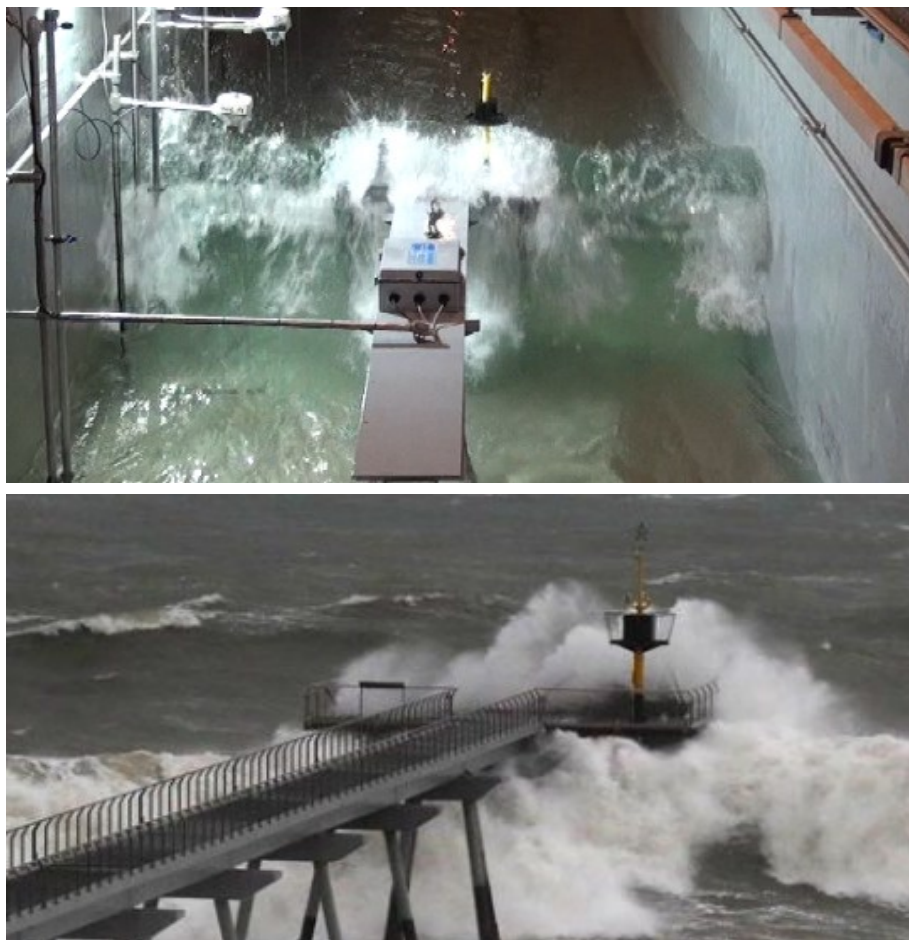


Fig. 26 - Visual validation of test 050221_9 - FOC282

Depth [m]	Hs_mod [m]	Tp_mod [s]	X focused [m]	Phase focused [-]
2,520	0,470	4	55,11	0

Tab. 4- Design of the focused wave used in the test 050221_9 - FOC282

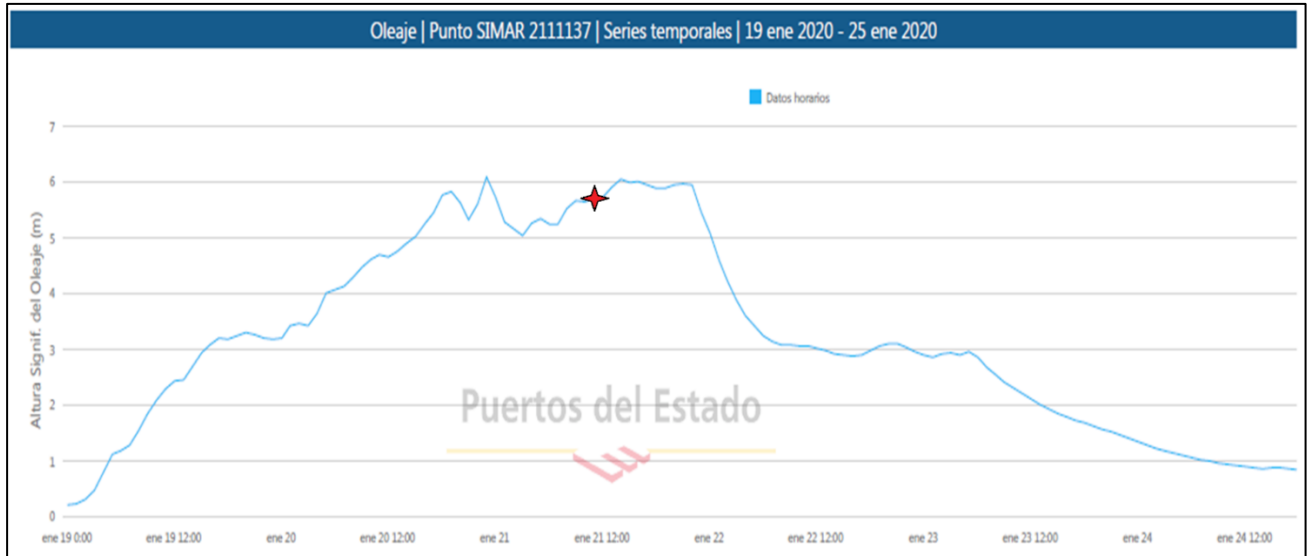


Fig. 27 – Time series of significant wave height in SIMAR point 2111137. Time of occurrence: 15:30ca ; $H_s = 5.7m$ Source: Puertos del Estado.

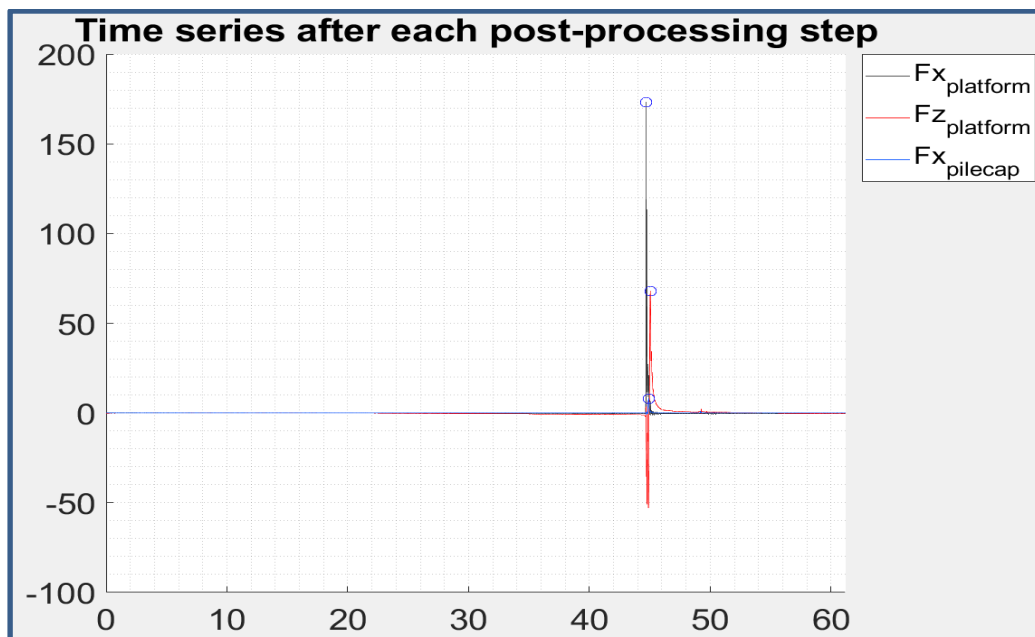


Fig. 28 - Measured forces of the test 050221_9 - FOC282. $F_{x,platform} = 1730$ kN ; $F_{z,platform} = 680$ kN ; $F_{x,pilecap} = 80$ kN

Test n°050221_5 – FOC264

In this case the similarities are present but are less evident than the previous test proposed. The way of breaking of the sea wave reproduced in laboratory is not represented properly in the test for the aforementioned effect of three-dimensional refraction due to a non-prismatic bathymetry of the bottom of the sea in the reality, contrarily to the bottom realized in the CIEM flume. Anyway, the way of approaching to the structure of the wave, the wave height reached and the point of application of the wave load are very similar to the one that is shown in Fig.29b.



Fig. 29 - Visual validation of test 050221_5 - FOC264

Depth [m]	Hs_mod [m]	Tp_mod [s]	X focused [m]	Phase focused [-]
2,520	0,470	4	53,55	270

Tab. 5 - Design of the focused wave used in the test 050221_5 - FOC264

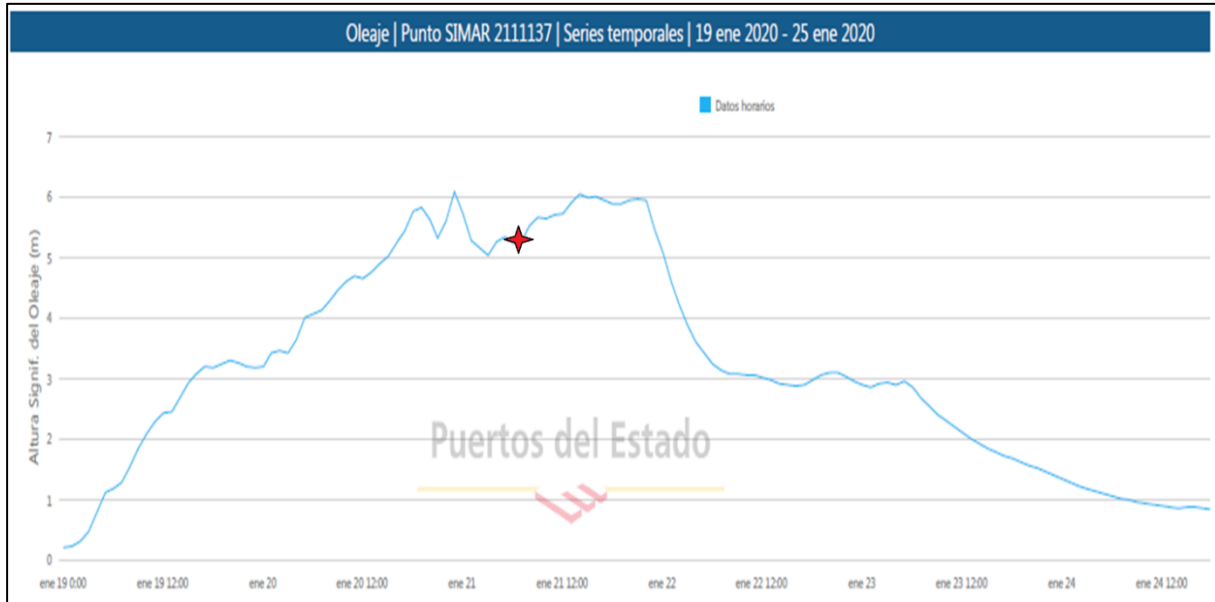


Fig. 30 - Time series of significant wave height in the SIMAR point 2111137. Time of occurrence: 10:00ca ; Hs = 5.3m. Source: Puertos del Estado.

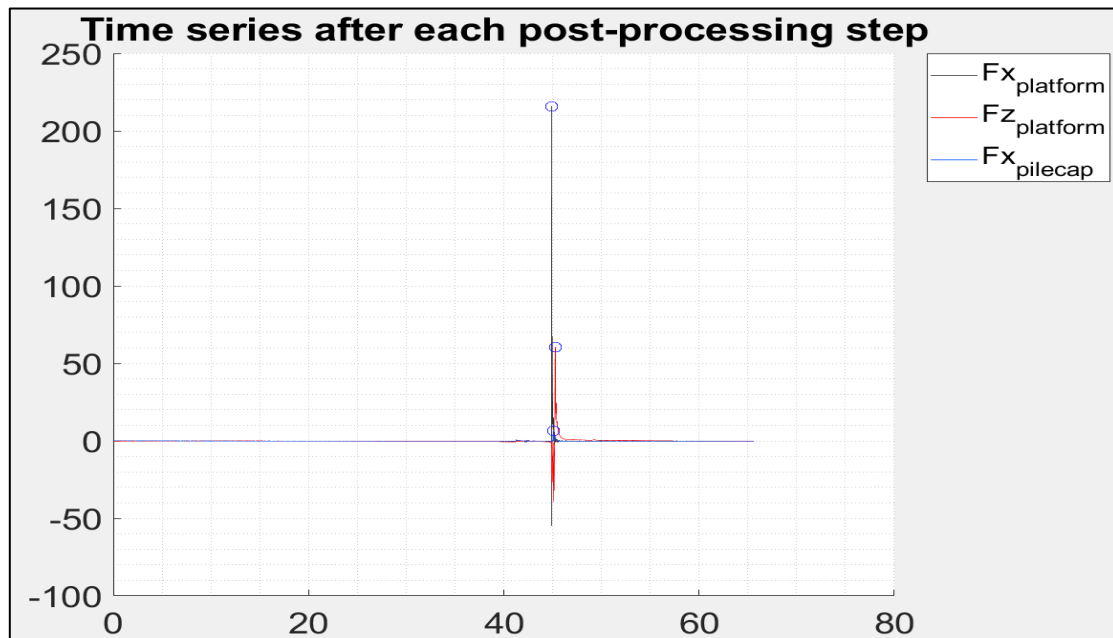


Fig. 31 - Measured forces of the test 050221_5 - FOC264. $F_{x,platform} = 2150$ kN ; $F_{z,platform} = 600$ kN ; $F_{x,pilecap} = 70$ kN

5.4 Analytical fitting of the tests

5.4.1 Preliminary evaluation of dependence of the loads from some basic characteristics

After an introductory visual validation of the tests using the recordings made in laboratory and some pictures about the storm Gloria impact on the Pont del Petroli, thus are made initial analytical evaluations between the loads from some basics hydraulic and geometric characteristics of the flow used along this essay (further examples are given in the Appendix 3). Furthermore, in the present chapter are made evaluations about the breaking criteria of the sea waves and it has been also introduced a new non-dimensional parameter that has been used trying to give a new point of view of the problem.

In particular, has been used as new breaking parameter, for this preliminary evaluation, the ratio between the maximum surface elevation η_{\max} (m) (referred to the mean sea level) and the clearance cl , that is the distance between the mean sea level and the altitude of the platform. Thus, the chosen parameter is η_{\max}/cl . This new parameter was chosen starting from some considerations made on the essay realized by Cuomo et al. (2007) that proposed as non-dimensional parameter the ratio of the difference between the maximum surface elevation and the clearance divided by the water depth at the toe of the structure. This is it: $\theta = (\eta_{\max} - cl)/d$

During the final analysis were detected several tests that leaded to negative values of the parameter theta proposed by Cuomo et al. (2007). Therefore, this has been modified giving back the advantage of having a non-dimensional parameter which is always positive. The condition $\eta_{\max} \geq cl$ implies the existence of a direct impact of the sea wave on the structure. Otherwise, for $\eta_{\max} < cl$ there shouldn't be an impact of the focused wave on the structure, and this happened the most of the time for waves that broke before the impact with the structure.

However, watching the recordings of the tests it's clear that this new parameter doesn't give precise information about the breaking of the wave and the relationship between its loads and the breaking conditions.

Therefore, the case history is here explained:

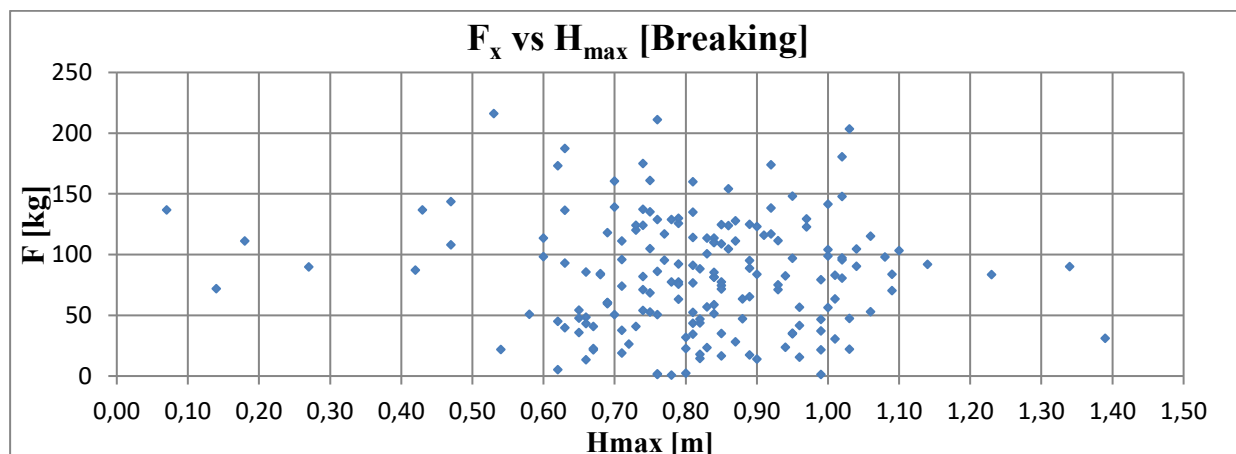
- the wave doesn't break but there is a direct impact on the structure: $\eta_{\max} \geq cl$ + Direct impact
- the wave could break on the top of the platform: $\eta_{\max} \geq cl$ + Breaking wave
- the wave surface elevation is smaller than the clearance: $\eta_{\max} < cl$ + No impact
- the wave surface elevation is smaller than the clearance caused by a previous breaking phenomenon. Then the breaking wave rebound on itself hitting the platform from below: $\eta_{\max} < cl$ + Vertical impact

This analysis was made in order to find a new setting that could explain the dependence of the direction and the magnitude of the impacts with the conditions of breaking of the waves. Anyway, for the considerations made here above, this new setting should be used with caution and further analysis should be made so as to achieve this aim.

Breaking waves

In this sub-paragraph are made preliminary considerations on those tests that belong to the group of waves with surface elevation that is lower than the clearance ($\eta_{\max} < cl$).

Relationship between loads on the structure and maximum wave height



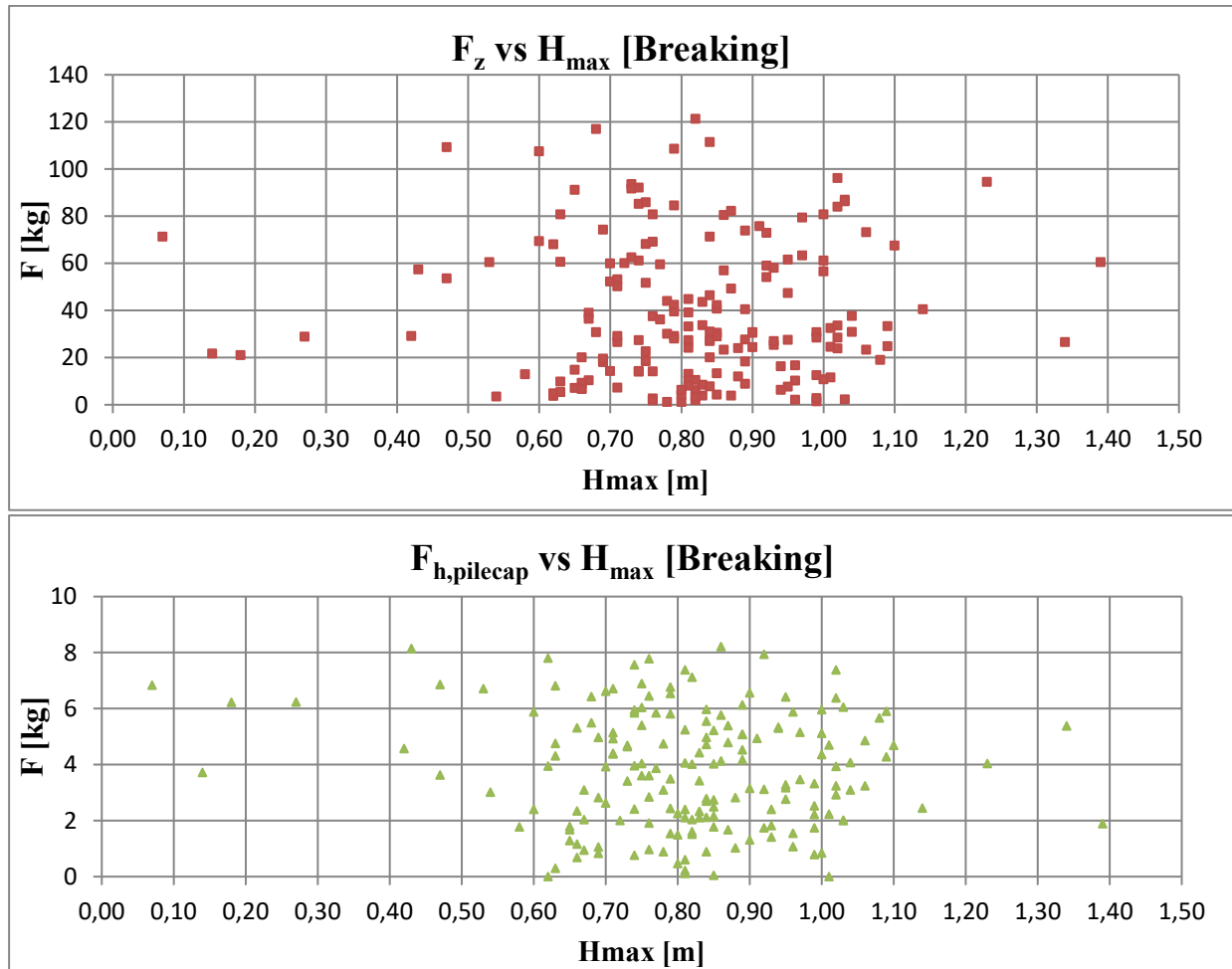


Fig. 32 – Dispersion of forces and maximum wave height for breaking waves (model scale)

It's clear that all the loads, regardless of the direction of the impact, are not strictly dependent from the maximum wave height in case of breaking waves. In this preliminary evaluation is used the maximum wave height instead of the significant wave height. This choice is made because is preferred to use a measured value, such as the maximum wave height, instead of a theoretical target value such as the significant wave height and moreover, rigid structures like the Pont del Petroli pier are designed taking into account the maximum wave height.

Further examples of this preliminary analysis are provided in the Appendix 3.

Comparison between analytical features of the flow and characteristics of the flow

The aim of the present paragraph is to find a more precise description of the breaking condition for the sea waves that occurred during the storm Gloria that have affected the Pont del Petroli pier. The papers used for this paragraph are the aforementioned Rattanapitikon and Shibayama (2006) and Goda (2010).

The first essay proposed in here is the one realized by Goda (2010) that gives a relationship between the regular breaking wave height H_b and breaking depth h_b .

$$H_b = 0.17 * L_0 * \left\{ 1 - \exp\left(-1.5 * \frac{\pi h_b}{L_0} \left(1 + 15 * \tan(\theta)^{\frac{4}{3}}\right)\right)\right\}$$

Where we set the longitude of waves in deep water L_0 , the water depth at breaking of regular waves h_b and the slope of the bottom $\tan(\theta) = 1/13 = 0.0769$.

Here have been used as L_0 the target value of the longitude of waves in a range between 149 – 178m (prototype scale), h_b has been considered the water depth at breaking of regular waves calculated with the aforementioned method of Rattanapitikon and Shibayama (2006) that have a range between 8 – 12.6m.

In the next figure is compared the maximum wave height of those test with a maximum surface elevation lower than the clearance of the structure. So the main hypothesis is that the waves breaks before the impact with the structure of the model of Pont del Petroli pier. If the measured values of maximum wave height are similar to the theoretical values of breaking wave height proposed by Goda (2010) we could think that the parameter η_{\max}/cl could be suitable for the reaching of another point of view about the physical phenomenon of breaking waves and their relative impacts on the structure.

What we can see from the Fig.33 here below is that there is some dispersion around the values of maximum wave height, in spite of the range of values of breaking wave height that is quite short. However, the most of the dots that represents the tests that satisfy the new condition $\eta_{\max} < c_l$ are in the part of the figure with less dispersion. Furthermore, the limits of this region with less dispersion are similar for both axis. This comply with what we expected because in breaking conditions the maximum wave height is a limit condition before the breaking.

Thus we can think that the method suggested by Goda (2010) could be used for the analysis of breaking waves and the design of waves and the analysis of their relative loads on the structure of Pont del Petroli. Anyway, it's desirable to realize additional tests that can prove or not these assertions.

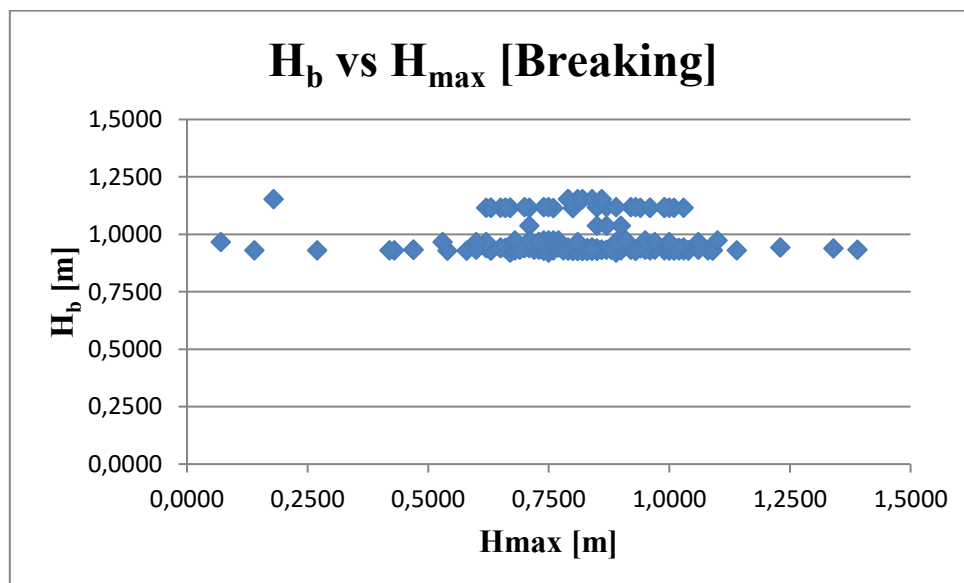


Fig. 33 – Breaking criteria according to Goda (2010) vs measured maximum wave height for breaking waves (model scale)

The second essay that has been carried out by Rattanapitikon and Shibayama (2006) proposes as breaking condition the definition of the depth of water that produces the breaking of the sea wave. This is function of the slope of the bottom and of the wave height and the longitude of the wave in deep water.

$$h_b = (3.86m^2 - 1.98m + 0.88)H_0 \left(\frac{H_0}{L_0}\right)^{-0.16}$$

Where **m** represents the bottom slope and in our case is equal to $m = 1/13 = 0.0769$, **H₀** is the wave height in deep water, **L₀** is the longitude of the wave in deep water.

In our case has been taken as **H₀** the value of the target value of the maximum wave height that here has a range of values (in prototype scale) between 6.4m and 10.9m, and instead of the **L₀** has been taken the longitude of the maximum wave that has a range of values (in prototype scale) between 149m - 178m.

In Fig.35 we see a great dispersion of the breaking wave water depth in function of the water depth used in the tests, thus are obtained results markedly different from the ones obtained with Goda (2010). This is explained thanks to the different kind of focused waves used during the tests that can break before or even after the toe of the platform. Therefore, this variability and the related dispersion of the breaking wave water depth **h_b** is justified by the variability in the characteristics of the focused waves. However, the dispersion that occurs in this case doesn't allow us to use this method for the purposes presented in this thesis work.

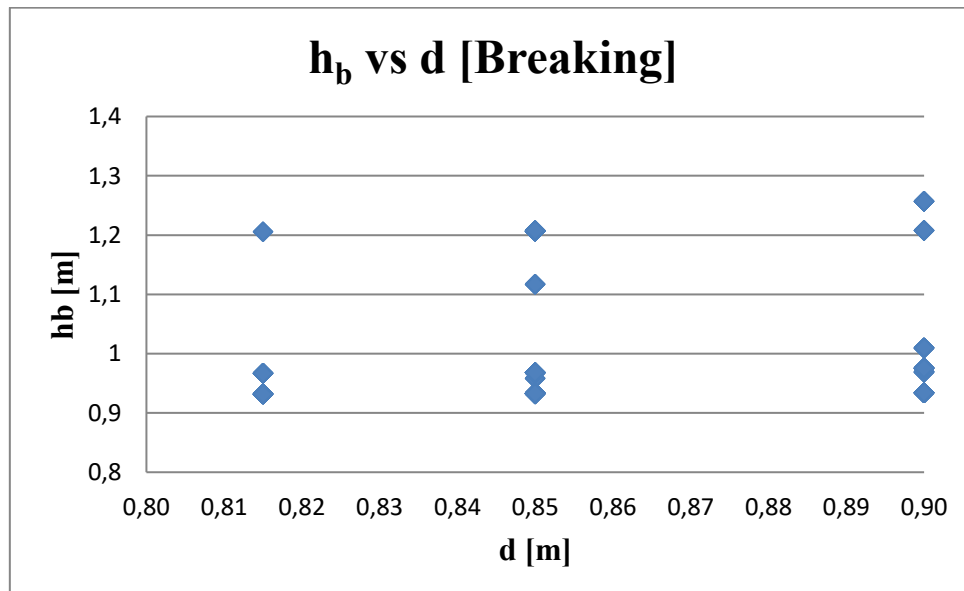


Fig. 34 – Breaking condition of water depth (Rattanapitikon & Shibayama., 2006) vs water depth at the platform for breaking waves (model scale).

Non-breaking waves

Relationship between loads on the structure and maximum wave height

The same reasoning has been made for the tests classified as breaking waves ($\eta_{\max} < cl$) are made now for non-breaking waves ($\eta_{\max} > cl$).

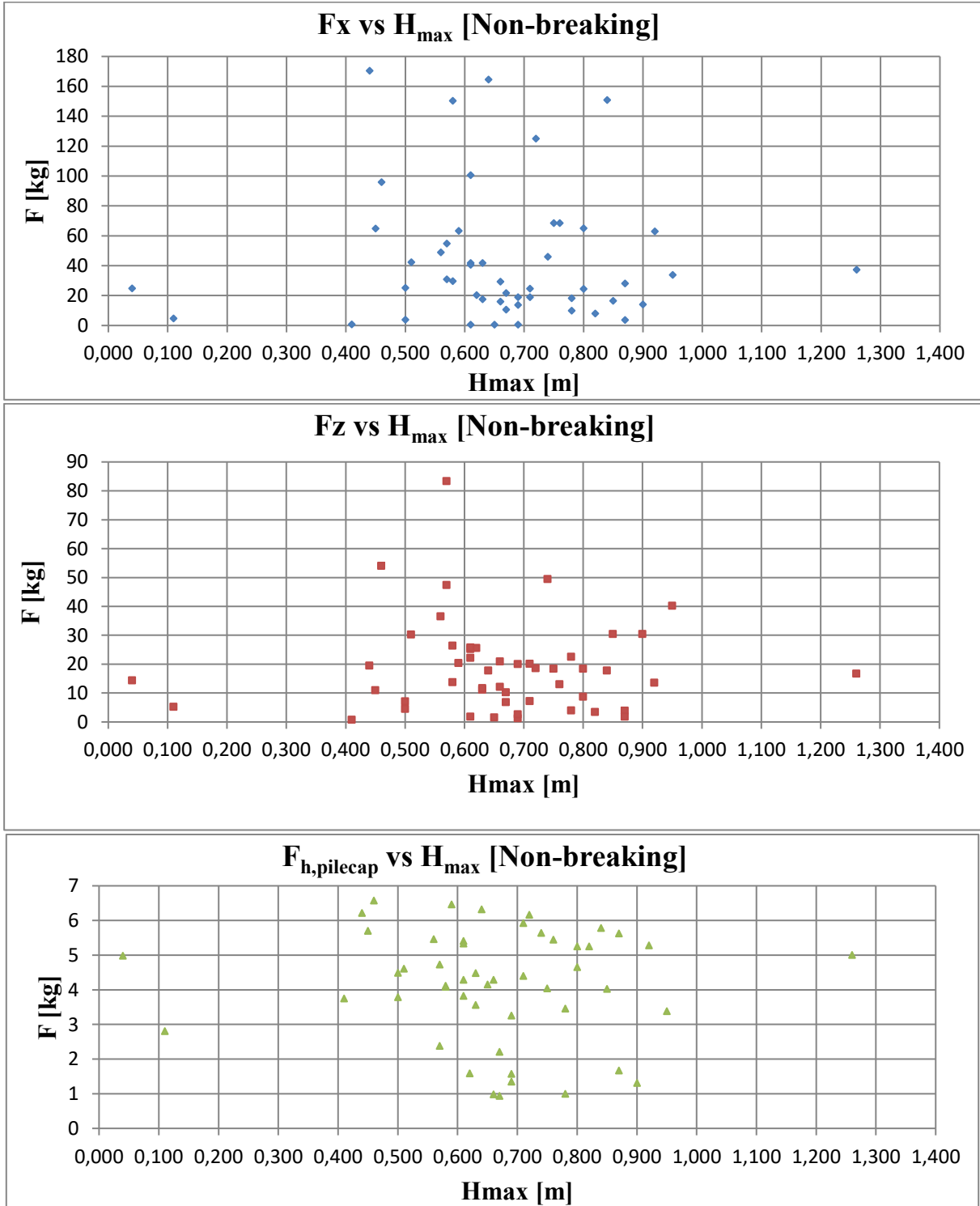


Fig. 35 - Dispersion of forces and maximum wave height for non-breaking waves (model scale).

The dispersion of the values of forces is really high if they are compared with the values of the maximum wave height. Therefore, even for those tests that have been classified as “non-breaking waves” there is not any correlation between the direction and the magnitude of the loads caused by the impact of the sea waves and the maximum wave height of the focused wave that have caused the impact.

6. Final results and range of values of non-dimensional parameters

In the present final chapter are used the formulations expressed by Gaeta et al. (2012) and Cuomo et al. (2007) in order to determine a possible expression that can determine and forecast the loads on the Pont del Petroli pier knowing the characteristics of the waves.

The formulations suggested are used for the advantage of taking into account non-dimensional parameters and this allows to make considerations that goes beyond the effective hydraulic and geometric condition of the structure and the design sea waves. The first operation is to take the forces measured in laboratory and then are calculated the relative non-dimensional forces.

The non-dimensional horizontal force in the scaled model is calculated as follows:

$$F_{h,platform}^* = \frac{F_{x,platform}}{\rho_w * g * H_{max} * A[m^2]}$$

Where are defined the density of water $\rho_w = 1000 \text{ kg/m}^3$; the acceleration of gravity $g = 9.81 \text{ m/s}^2$; the maximum wave height H_{max} , that is preferred to the significant wave height because in this case the significant wave height is a theoretical design value, the maximum wave height is measured at the toe of the structure with the resistive sensor WG8; the area of the front of the platform that is a trapezoidal area of 0.0216 m^2 in the scaled model.

The non-dimensional vertical force in the scaled model is calculated as follows:

$$F_{v,platform}^* = \frac{F_{z,platform}}{\rho_w * g * H_s * A[m^2]}$$

Where the physical constants such as the water density and the acceleration of gravity are the same used for the horizontal forces; the maximum wave heights H_{max} are measured at the toe of the structure with the resistive sensor WG8; the area of the platform is a rectangular area of 0.6581 m^2 in the scaled model.

These non-dimensional forces are compared with the non-dimensional parameters proposed by the authors of the chosen essays and then are made considerations about the method of investigation of the maximum forces and how these methods are compatible with the data set of forces measured in the CIEM flume.

The range of values of these parameters (in prototype scale) are shown in the next table.

Parameter	Range of values
H_{\max} [m]	6.2 – 10.5
η_{\max} [m]	3.1 – 7.7
Cl [m]	4.15 – 5.00
$F_{h,\text{platform}}$ [kN]	5 - 2160
$F_{v,\text{platform}}$ [kN]	7 - 1210
$F_{h,\text{pilecap}}$ [kN]	0 - 82

Tab. 6 - Range of values of the analyzed parameters (measured values scaled to prototype scale).

The following paragraphs will be divided into three categories: breaking waves, non-breaking waves and a group that takes into account both categories. The breaking criteria used are two different from the one proposed in the previous chapter and these are the criteria proposed by McCowan (1894) and Miche (1944). Further explanations are given in the following points.

6.1 All-in-one group

The first group gathers all the tests without distinguishing in breaking or non-breaking waves. Here are made general comparisons among the data set of forces and the aforementioned methods. The first expression analyzed is the one proposed by Cuomo et al. (2007) that consists of a linear regression of the data set of the forces and then the formulation suggested by Gaeta et al. (2012) that indicates a linear shape of the maximum forces in function of its non-dimensional parameter.

Cuomo et al. (2007)

The expression proposed in the paper of Cuomo et al. [2007, Wave-in-deck loads on exposed jetties] is the following.

$$F^* = \frac{F}{\rho_w * g * H_s * A[m^2]} = a * \left(\frac{\eta_{max} - c_l}{d} \right) + b$$

Where non-dimensional forces are drawn around a regression line that has a slope **a** and an independent term **b**. The forces are considered a function of the non-dimensional parameter that is the ratio of the difference between the maximum surface elevation and clearance divided by the depth of water at the toe of the structure. It is worth mentioning that the maximum surface elevation is referred to the mean sea level and the clearance is the distance of the platform from the mean sea level.

In this work the analysis is stopped to the non-dimensional analysis. However, the next step for the design of the forces, based on the non-dimensional parameter, is to bring back the forces to dimensional values. In formula is given:

$$F = F^* * (\rho_w * g * H_s * A[m^2]) = \left[a * \left(\frac{\eta_{max} - c_l}{d} \right) + b \right] * (\rho_w * g * H_s * A[m^2])$$

As mentioned before the expression of forces is based on the significant wave height H_s but in this case the maximum wave height H_{max} will be taken into account instead of the significant wave height because the first one is a measured value in spite of the second one that is a theoretical design value.

The results that come by this analysis are given as follows.

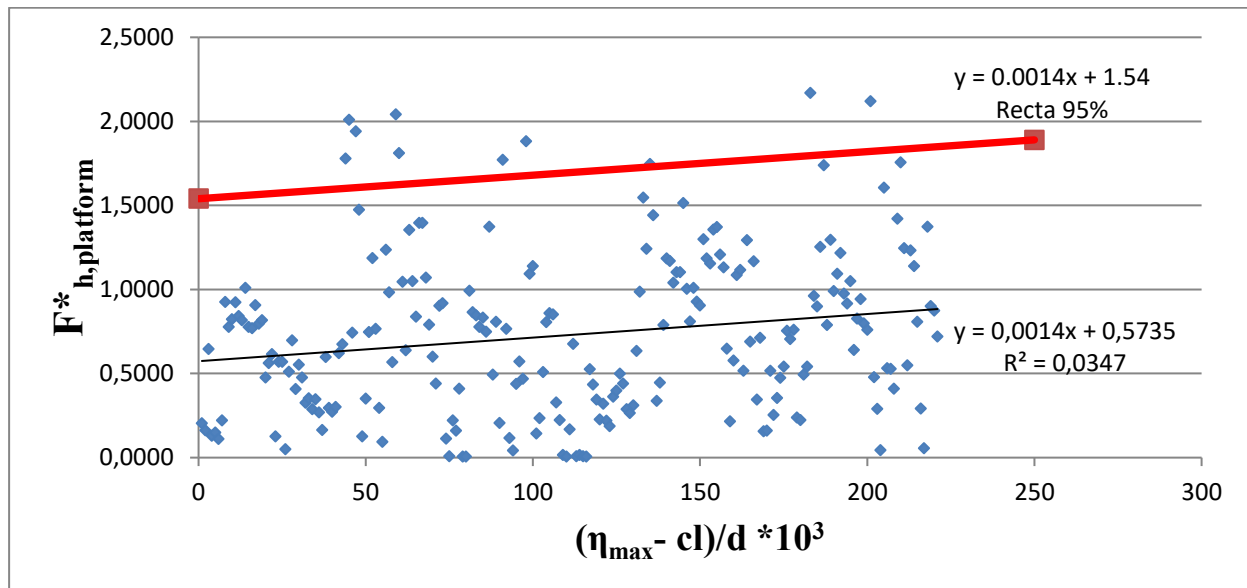


Fig. 36 – Maximum horizontal forces and relative application of Cuomo et al. (2007).

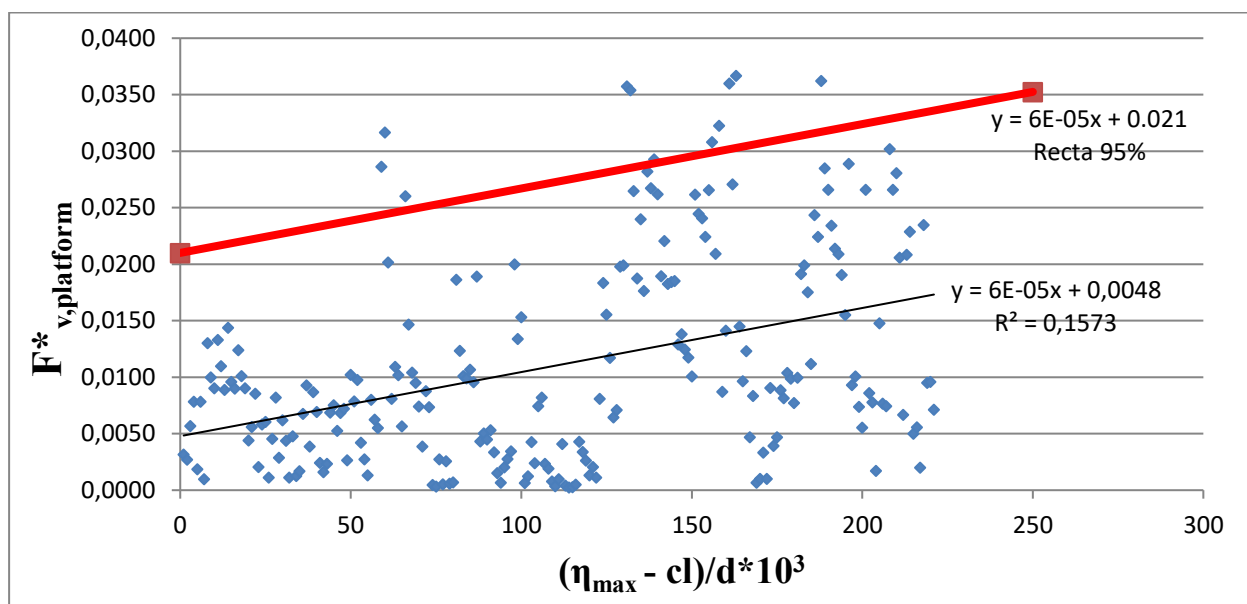


Fig. 37 – Maximum vertical forces and relative application of Cuomo et al. (2007).

It is clear that there is a great dispersion of values of non-dimensional forces around the regression line (in black) for both horizontal and vertical loads. This is due to the data setting that is not as good as the settings that Cuomo et al. have in their essay. They have fewer points and fits lines for certain subsets of points. Furthermore, Cuomo et al. only have non-breaking regular waves and a fixed horizontal bottom, in spite of our principal boundary conditions that are sloped sandy bottom and waves that in the most of the cases are breaking waves.

Besides, in Cuomo et al. (2007) is done a selection of tests and are made more regression lines for each subset of tests. This leads to a lower dispersion around the line but this means to realize more lines and so are needed more parameters a and b for each situation.

Therefore, following the methodology of Gaeta et al (2012), a proposal is to generate a red line (for both horizontal and vertical loads) that contains the 95% of the tests below it and that red line has the same slope of the regression line and an independent term. This is made in order to define a more conservative line and it doesn't have the r-squared factor.

The equation of the line named 95%-line for horizontal non-dimensional forces is:

$$y_{h,95\%} = 1.4 * 10^{-3} \left(\frac{\eta_{max} - cl}{d} \right) + 1.54$$

The equation of the line named 95%-line for vertical non-dimensional forces is then:

$$y_{v,95\%} = 6 * 10^{-5} \left(\frac{\eta_{max} - cl}{d} \right) + 0.021$$

Gaeta et al., 2012

The expression suggested by Gaeta et al. (2012) is shown here below.

$$F^*_{max} = \frac{F_{max}}{\rho g H_s A} = 5 * \theta = 5 * \frac{\eta_{max} - c}{\eta_{max}}$$

They suggest an experimental linear relationship between the maximum non-dimensional forces and their non-dimensional parameter theta. This is the quotient of the difference between the maximum surface elevation and the clearance divided by the maximum surface elevation.

Knowing the significant wave condition, it is possible to determine the maximum loads caused by the impact of them on the structure. These will be determined through the following formula.

$$F_{max} = F^* * \rho g H_s A = \left[5 * \frac{\eta_{max} - c}{\eta_{max}} \right] * \rho g H_s A$$

As mentioned for the expression proposed by Cuomo et al. (2007), the hydraulic characteristics of the flow keep the same. The area of the front of the platform is a trapezoidal area of 0.0216 m² in the scaled model and the area of the platform is a rectangular area of 0.6581 m² in the scaled model.

Here is preferred to use the maximum wave height instead of the significant wave height because the first is a real value measured at the toe of the structure, the second wave height is a theoretical design value.

The results obtained with the method proposed by Gaeta et al. (2012) with the data set of forces measured in the CIEM flume are here represented.

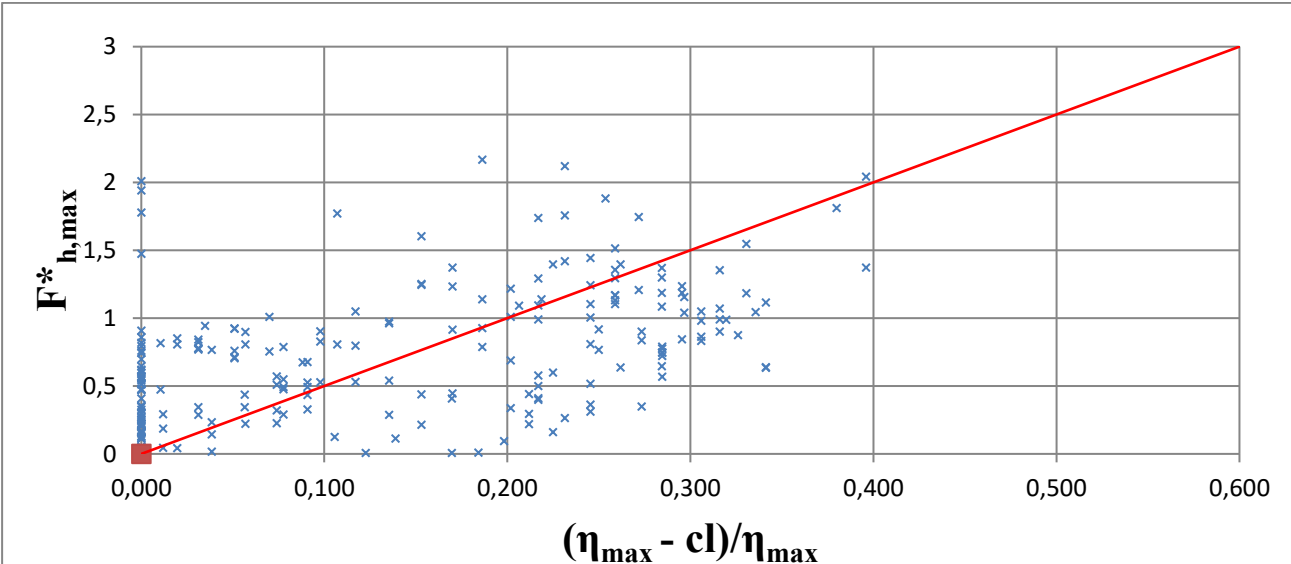


Fig. 38 – Maximum horizontal forces and relative application of Gaeta et al. (2012)

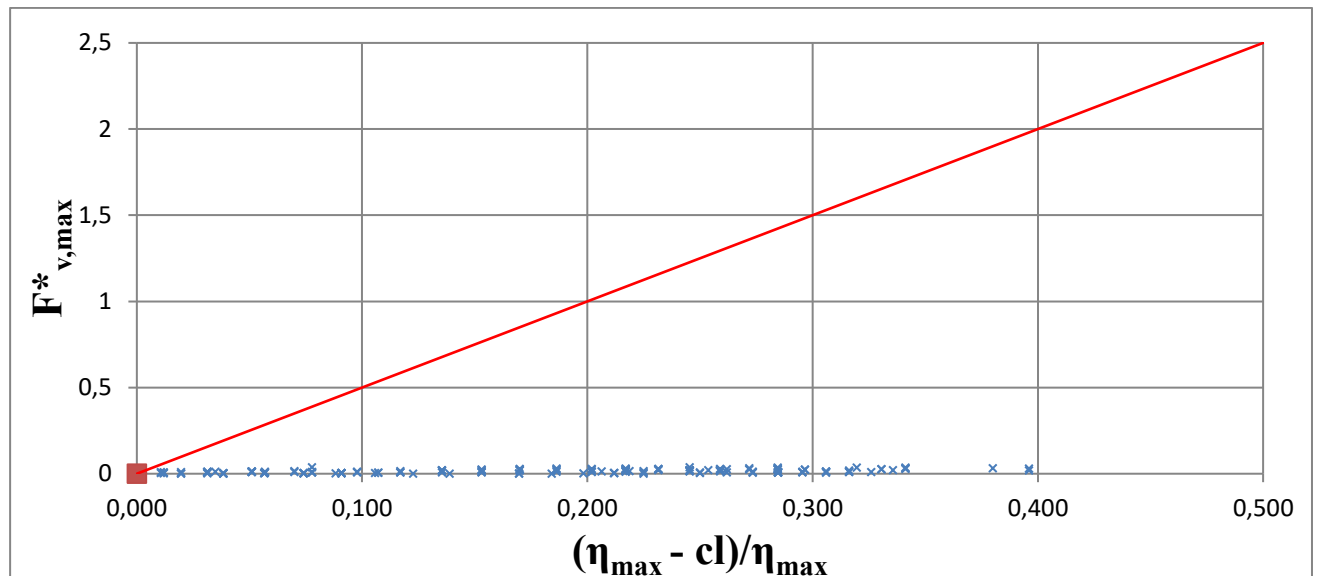


Fig. 39 - Maximum vertical forces and relative application of Gaeta et al. (2012).

In Fig.39 there are some values in horizontal forces that are above the red line of the maximum forces. So a possible solution is to divide the tests in smaller groups in order to find, eventually, a criteria for a better application of this method to our experimental results. Further considerations about this point are leaded in the following paragraphs, where the whole group of tests is divided in two sub-groups: breaking wave impacts and non-breaking wave impacts.

Regarding the vertical forces (see Fig.40), the line of maximum vertical forces proposed by Gaeta et al. (2012) is much higher than the non-dimensional vertical forces obtained in the tests. This is due to the area on which are applied the vertical loads, the area of the platform is 30 times the area of the front of the platform. Moreover, the differences could be due to the fact that also Gaeta et al. (2012) doesn't consider breaking waves.

The advantage of the present method is about how the line is built, in condition of no wave what is expected is that there are not impulsive loads due to the wave so the forces are null. This is taken into account in the formulation proposed by Gaeta et al. (2012) but not in the expression suggested by Cuomo et al. (2007). The method proposed by Cuomo et al. (2007) doesn't fix at all with our values of non-dimensional forces.

Condition of breaking

In order to find some possible details that could explain the relationships that link the magnitude and the direction of the loads caused by irregular waves and their characteristics such as the maximum wave height or the water depth, here is taken into account also the condition of breaking of the waves.

In the following paragraphs are used two breaking conditions. The first is the one proposed by McCowan, J. [1894, On the highest waves of a permanent type] that fixes a limit on the ratio between the maximum wave height and the water depth. A value of this ratio higher than 0.78 implies a limit condition for the wave that leads to its rupture.

$$\frac{H_{max}}{d} \geq 0.78$$

The second breaking criteria used is the one proposed by Miche [1944, Mouvements ondulatoires de lamer en profondeur ou d'écroissante]. He set a breaking condition based on the steepness of the wave. According to this essay, a steepness of the wave higher than 1/7 should be considered as a breaking condition of the wave.

$$\frac{H_{max}}{L} \geq \frac{1}{7}$$

The combination of both limit conditions will give the tests which lead to the breaking of the irregular wave. In this way is possible to define a more realistic representation of the reality, where a sea wave can break for exceeding the steepness limit and/or the water depth limit.

The total number of tests realized in the CIEM flume is 221 tests. 192 tests of 221 have exceeded at least one breaking condition. 29 of them have not exceeded none of the aforementioned limit states, so they are considered non-breaking waves.

6.2 Breaking waves impact

In this paragraph are applied the considerations made previously to the group of breaking waves composed by 192 tests.

Cuomo et al., 2007

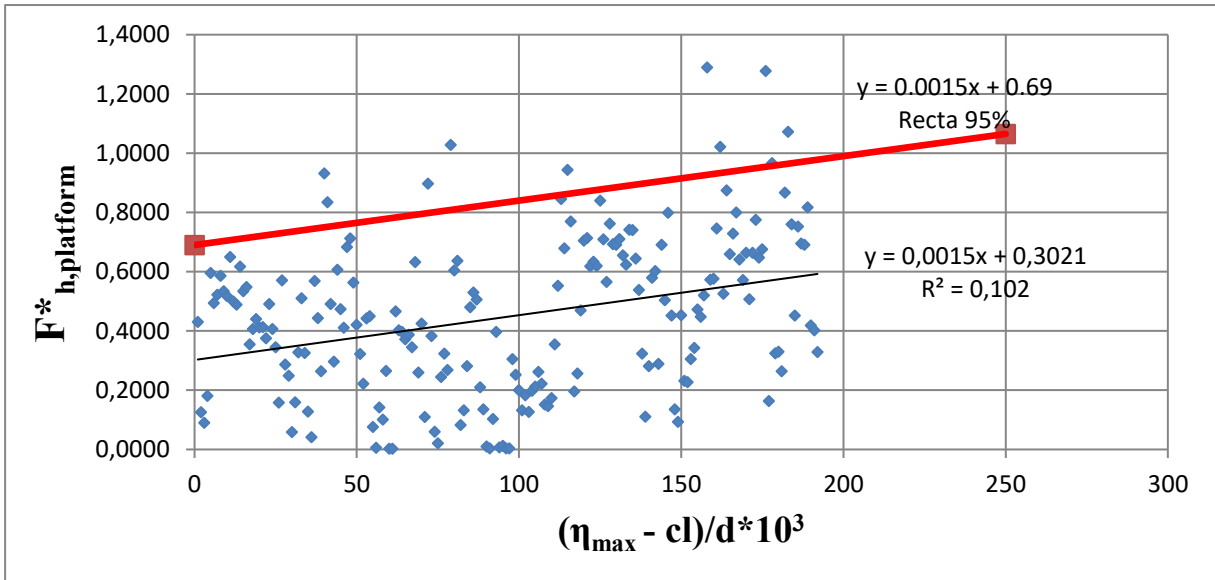


Fig. 40 – Maximum horizontal forces and relative application of Cuomo et al. (2007) (breaking condition).

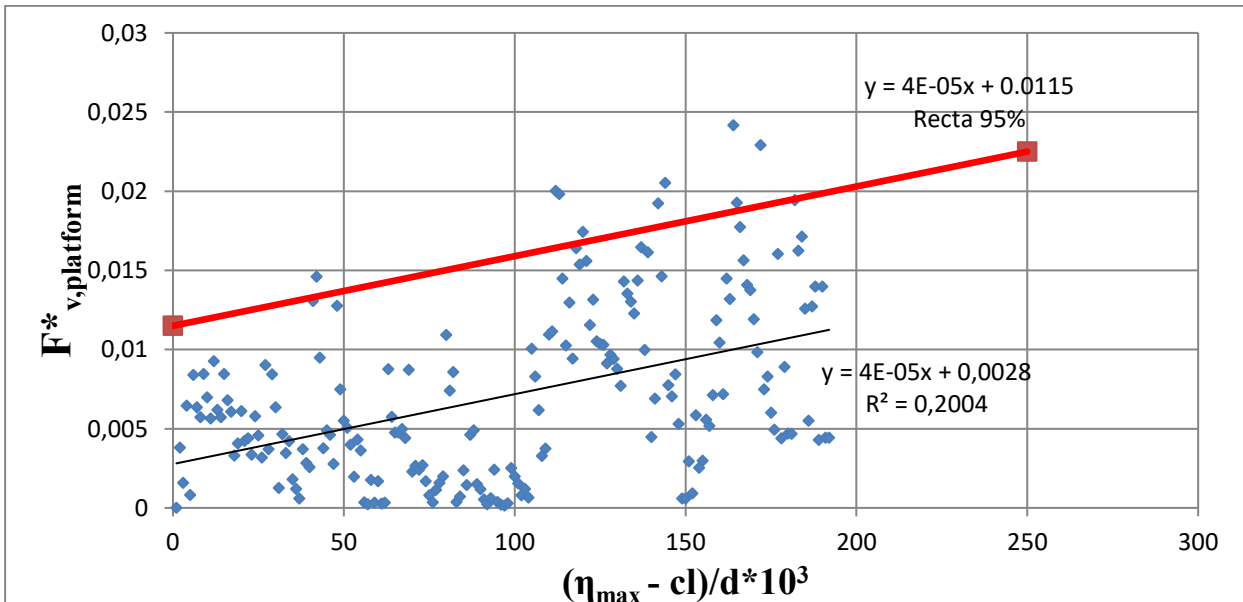


Fig. 41 – Maximum vertical forces and relative application of Cuomo et al. (2007) (breaking condition).

What is clear from Fig.40 and 41 is that there is still a high dispersion around the regression line for both horizontal and vertical dimensionless forces.

This is due to the fact that the regression lines realized by Cuomo et al. (2007) were thought for more subsets composed by a minor quantity of points. Moreover, as mentioned before, Cuomo et al. (2007) only have no-breaking regular waves and a fixed flat bottom. These differences with the conditions fixed for this work could be the reason of the unrelated results obtained with the same method.

Therefore, the proposal is to generate a conservative line, for both horizontal and vertical loads, that has the same slope of the regression line and an independent term. This line has the meaning of that element parallel to the regression line that contains the 95% of the tests below it. This is made in order to define a more conservative criteria for the application of Cuomo et al. (2007).

The equation of the line named 95%-line for horizontal non-dimensional forces is:

$$y_{h,95\%} = 1.5 * 10^{-3} \left(\frac{\eta_{max} - cl}{d} \right) + 0.69$$

The equation of the line named 95%-line for vertical non-dimensional forces is then:

$$y_{v,95\%} = 4 * 10^{-5} \left(\frac{\eta_{max} - cl}{d} \right) + 0.0115$$

Gaeta et al., 2012

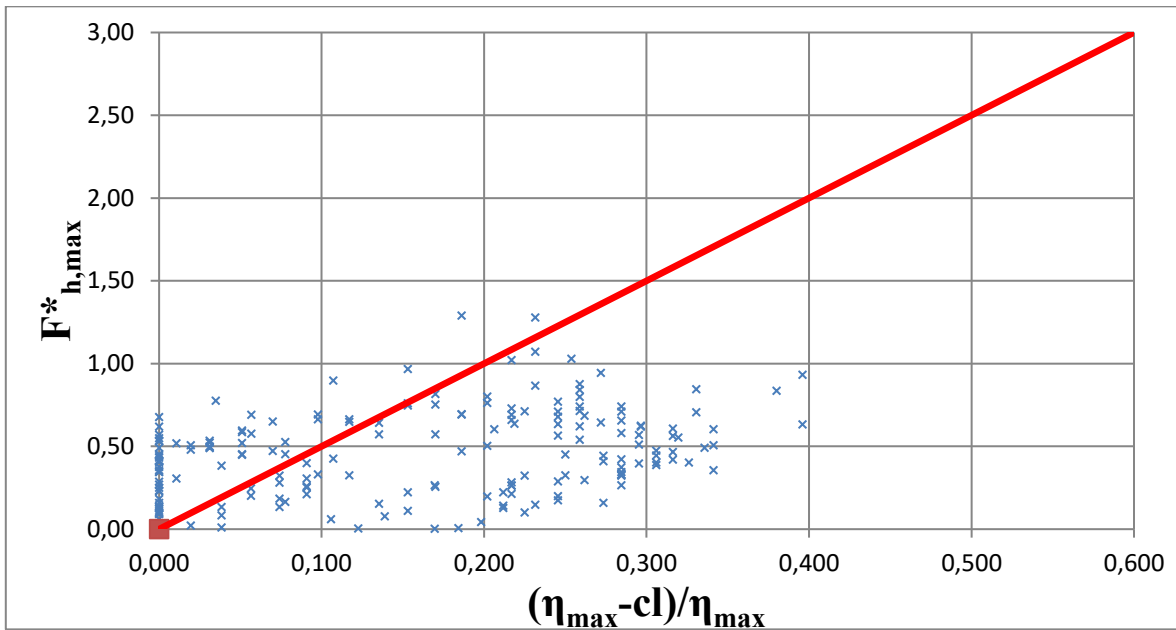


Fig. 42 – Maximum horizontal forces and relative application of Gaeta et al. (2012) (breaking condition).

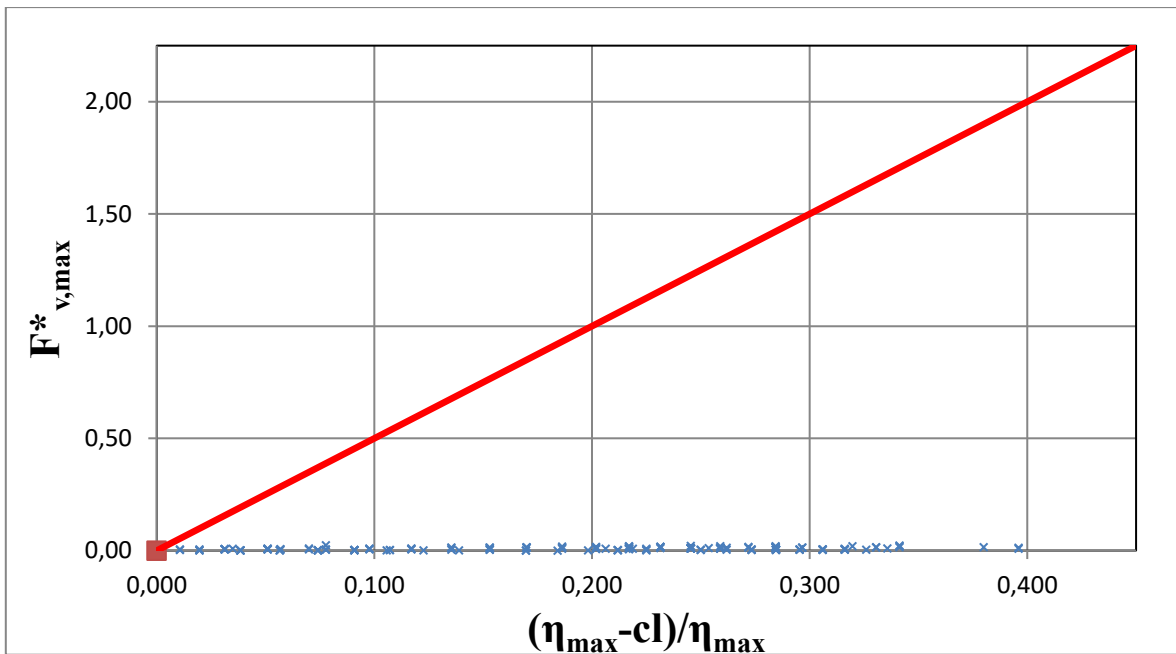


Fig. 43 - Maximum vertical forces and relative application of Gaeta et al. (2012) (breaking condition).

The method proposed by Gaeta doesn't fit with all the values of non-dimensional horizontal forces. There are some values in horizontal forces that are above the red line of the maximum forces. On the other hand, this analysis could be applicable to vertical forces but the limit prediction of maximum forces is too much conservative.

6.3 Non-breaking waves impact

In the present paragraph are made the aforementioned comparisons among the tests results of wave loads and surface elevation with the method proposed by Gaeta et al. (2012) and Cuomo et al. (2007). In this case are taken into account those 29 tests that resulted in non-breaking conditions. So for those waves that accomplish both the following limit condition:

$$\begin{cases} \frac{H_{max}}{d} < 0.78 \\ \frac{H_{max}}{L} < \frac{1}{7} \end{cases}$$

Cuomo et al., 2007

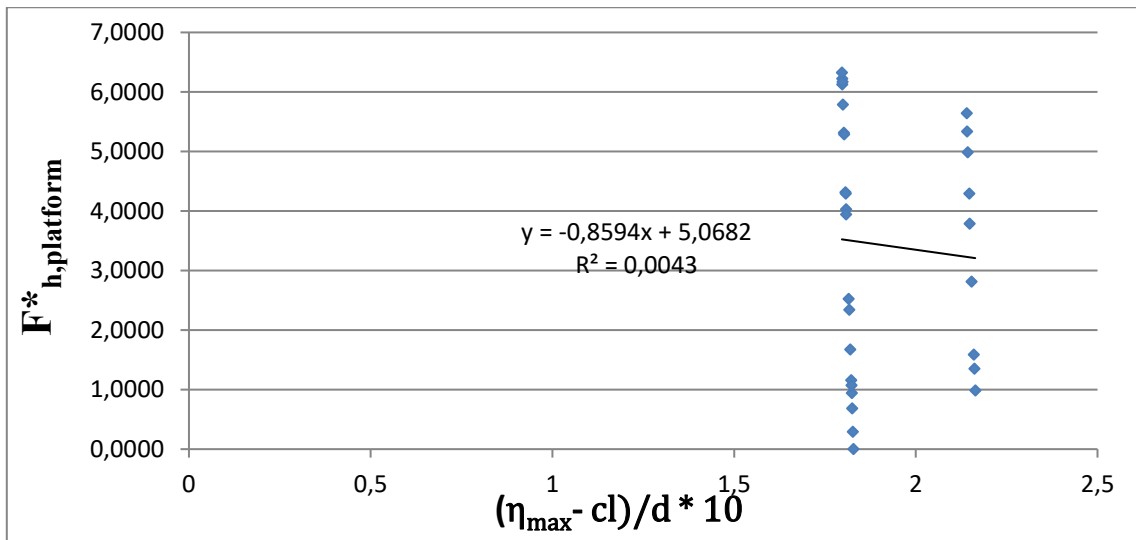


Fig. 44 – Horizontal forces of non-breaking wave impacts according to Cuomo et al. (2007).

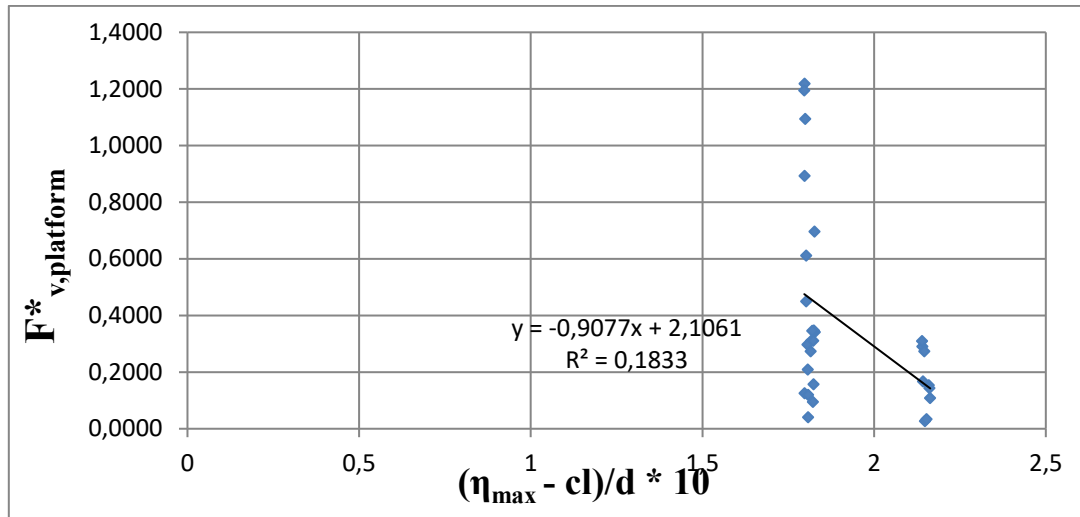


Fig. 45 – Vertical forces of non-breaking wave impacts according to Cuomo et al. (2007).

Even for non-breaking waves there is some of dispersion around the regression line for both horizontal and vertical dimensionless forces. In this case there is not realized a 95% - safety band parallel to the regression line because the tests that are collected in the sub-group of non-breaking wave impacts is composed of only 29. Its 95% is made of only 2 tests, so in this case the 95%-line is not representative of the subset of non-breaking waves.

It is interesting to notice that the impact loads caused by non-breaking waves are much higher than the forces caused by breaking waves. This result is reasonable for the fact that the non-breaking waves haven't lost yet some part of their energy due to the breaking. So this energy is saved and then conveyed to the impact on the structure.

Gaeta et al., 2012

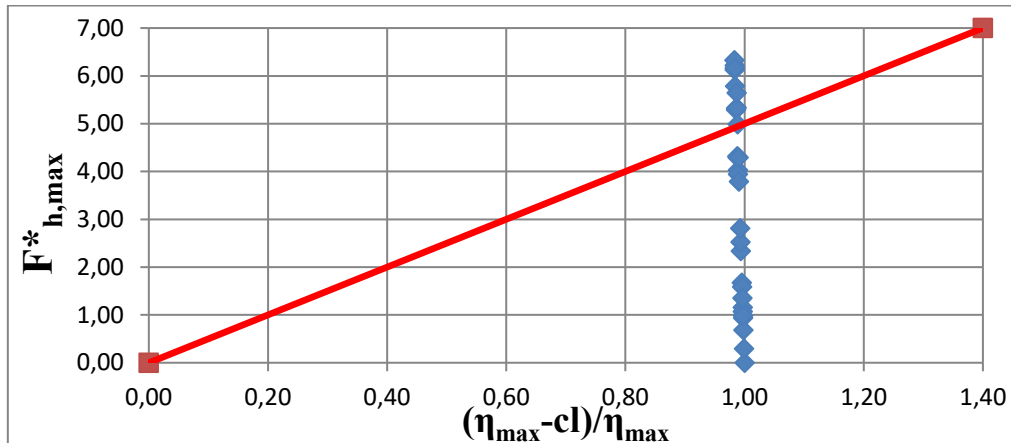


Fig. 46 – Non-dimensional horizontal forces of non-breaking wave impacts according to Gaeta et al. (2012).

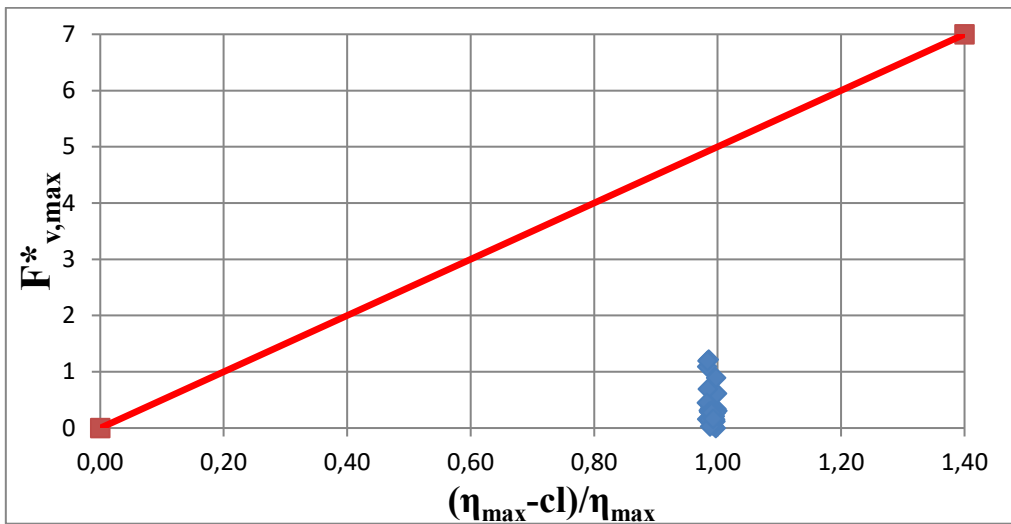


Fig. 47 – Non-dimensional maximum vertical forces of non-breaking wave impacts according to Gaeta et al. (2012).

The method proposed by Gaeta fix good with vertical non-dimensional forces but there are still some non-dimensional horizontal forces measurements that are above the red line of maximum forces. It’s interesting to notice that in this case vertical forces are below the line of maximum forces but now the limit condition suggested by Gaeta et al. (2012) starts to have more compatibility with the forces measured in laboratory. This is an expected results because in this case the wave conditions are the same because here are treated irregular non-breaking waves as in the aforementioned study.

6.4 New setting: η_{\max}/cl – Breaking waves

In this new chapter there is presented a new setting for both the methods proposed by Cuomo and Gaeta. Instead of $(\eta-cl)/d$ suggested by Cuomo et al. (2007) and $(\eta-cl)/\eta$ presented by Gaeta et a. (2012), it has been proposed η/cl . This has been done because η/cl is still a physical representative setting and it has always a positive value. In the following figures has been set a border with the central value of $\eta/cl = 1$ that separates the tests in two groups. These two groups divide the impacts in direct impacts ($\eta/cl \geq 1$) and in impacts that suffered a previous breaking of the extreme wave ($\eta/cl < 1$). Moreover, this new setting is fixed in order to find a new behavior of the results of measured forces obtained.

The breaking condition are the two proposed by McCowan (1894) and Miche (1944) and they are combined with the new breaking parameter used for the preliminary comparison, in which all the tests that have a ratio $\eta/cl \geq 1$ is considered non-breaking at the moment of the impact, on the other hand, those tests that led to a ratio $\eta/cl < 1$ are considered breaking waves at the moment of the impact with the structure. This could be useful for making analysis about the strength of the new non-dimensional parameter.

In particular, there could be 4 possible cases in breaking according to the new setting. The case history is:

- the wave doesn't break but there is a direct impact on the structure: $\eta_{\max} \geq cl$ + Direct impact
- the wave could break on the top of the platform: $\eta_{\max} \geq cl$ + Breaking wave
- the wave surface elevation is smaller than the clearance: $\eta_{\max} < cl$ + No impact
- the wave surface elevation is smaller than the clearance caused by a previous breaking phenomenon. Then the breaking wave rebound on itself hitting the platform from below: $\eta_{\max} < cl$ + Vertical impact

After made these clarifications about the new setting, then are applied the same methods used in the previous chapters but with η/cl as new non-dimensional parameter.

Cuomo et al., 2007

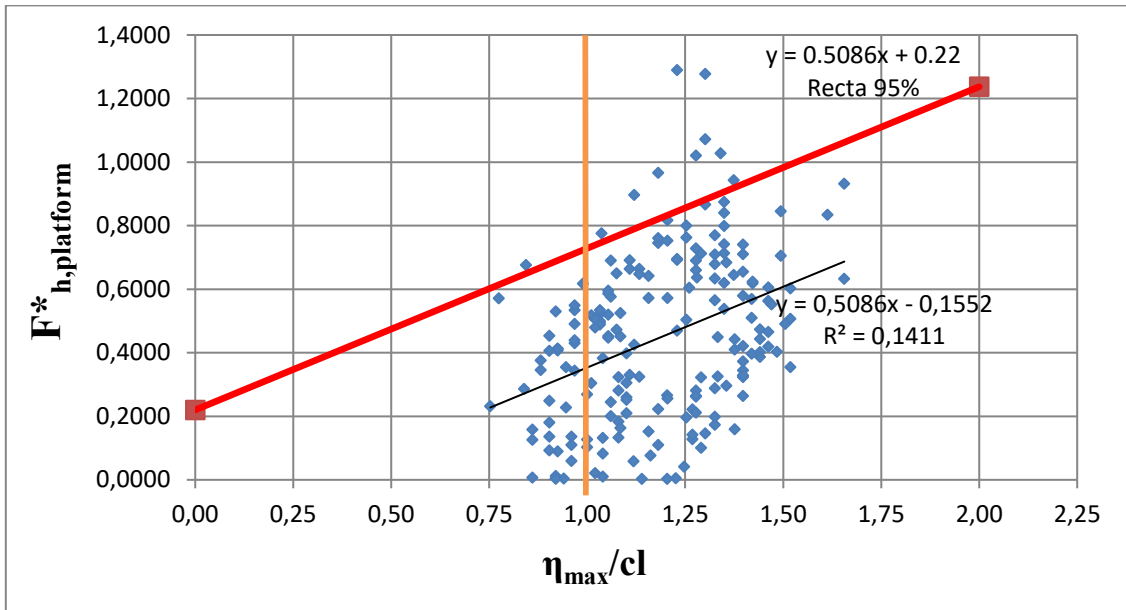


Fig. 48 – Application of Cuomo et al. (2007) to horizontal forces for breaking waves with the new setting.

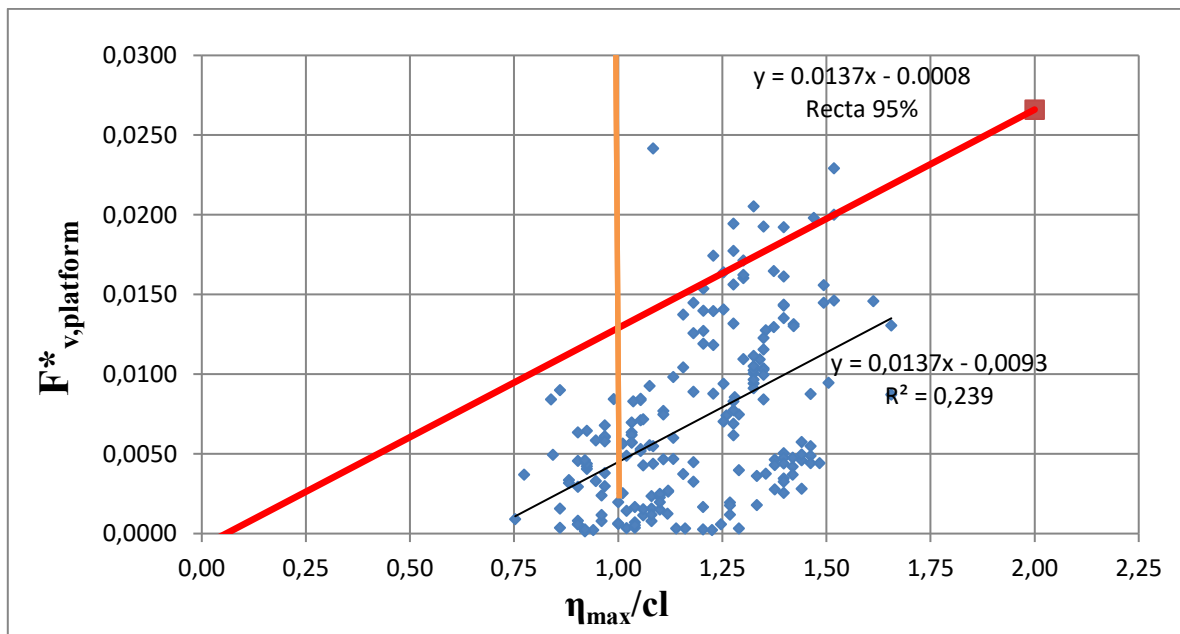


Fig. 49 - Application of Cuomo et al. (2007) to vertical forces for breaking waves with the new setting.

Here is made the same thing proposed in the previous paragraphs. It has been realized a regression line and a 95%-line as conservative limit. Even with the new setting η_{max}/cl there is still an high dispersion. This is reasonable because the differences between the boundary

conditions of our tests and the boundary conditions in the essay of Cuomo are kind of important like the fixed flat bottom and the flow of regular non-breaking waves.

The equation of the line named 95%-line for horizontal non-dimensional forces is:

$$y_{h,95\%} = 0.5086 \left(\frac{\eta_{max} - cl}{d} \right) + 0.22$$

The equation of the line named 95%-line for vertical non-dimensional forces is then:

$$y_{v,95\%} = 0.0137 \left(\frac{\eta_{max} - cl}{d} \right) + 8 * 10^{-4}$$

Gaeta et al., 2012

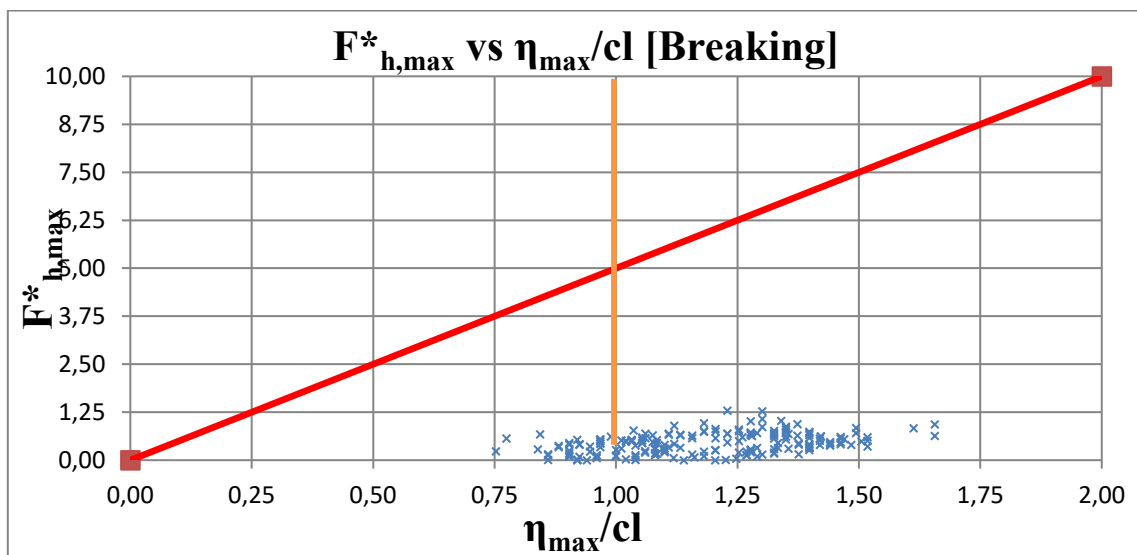


Fig. 50 – Non-dimensional horizontal maximum forces according to Gaeta et al. (2012) for breaking waves with the new setting.

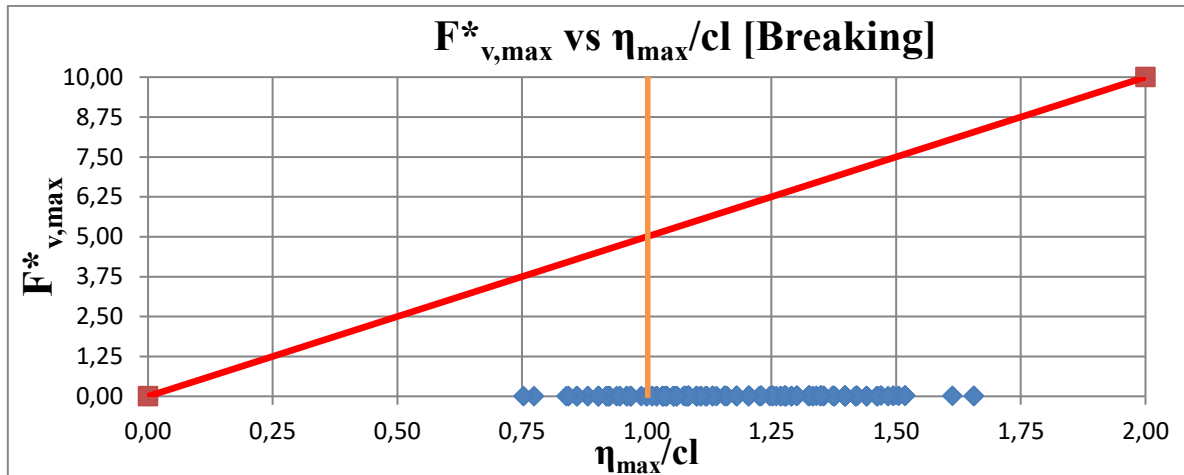


Fig. 51 - Non-dimensional vertical maximum forces according to Gaeta et al. (2012) for breaking waves with the new setting.

In spite of the results obtained in the previous paragraphs, all the tests are below the red line that represents the maximum forces for those specific conditions of wave height and clearance of the structure. On the other hand, further considerations are needed in order to determine if the line of maximum force (which equation is 5θ) is still the best one for the new setting η_{max}/cl and for our dataset of measured forces.

6.5 New setting: η_{max}/cl – Non-breaking waves

Cuomo et al., 2007

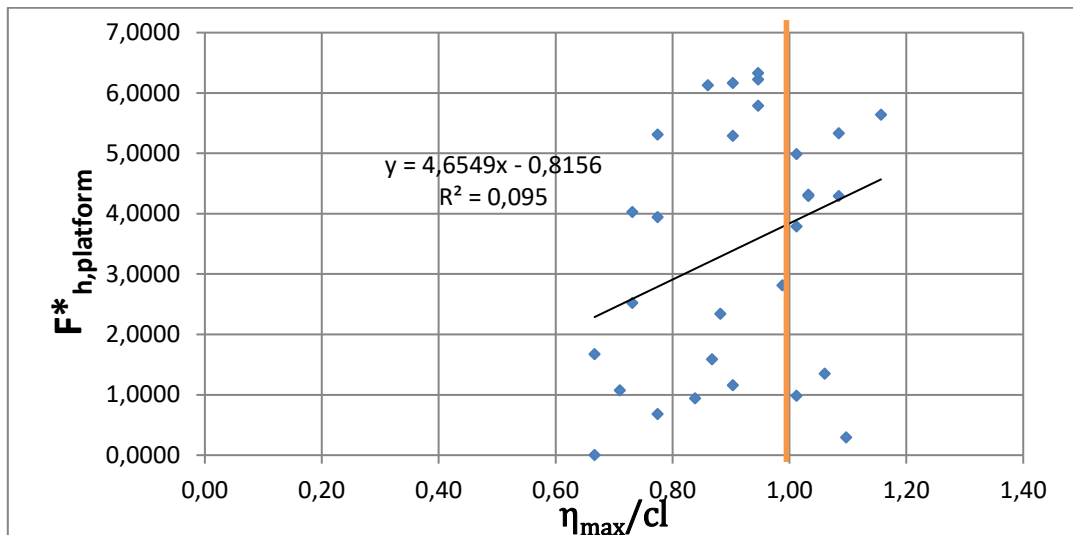


Fig. 52 - Application of Cuomo et al. (2007) to horizontal forces for non-breaking waves with the new setting.

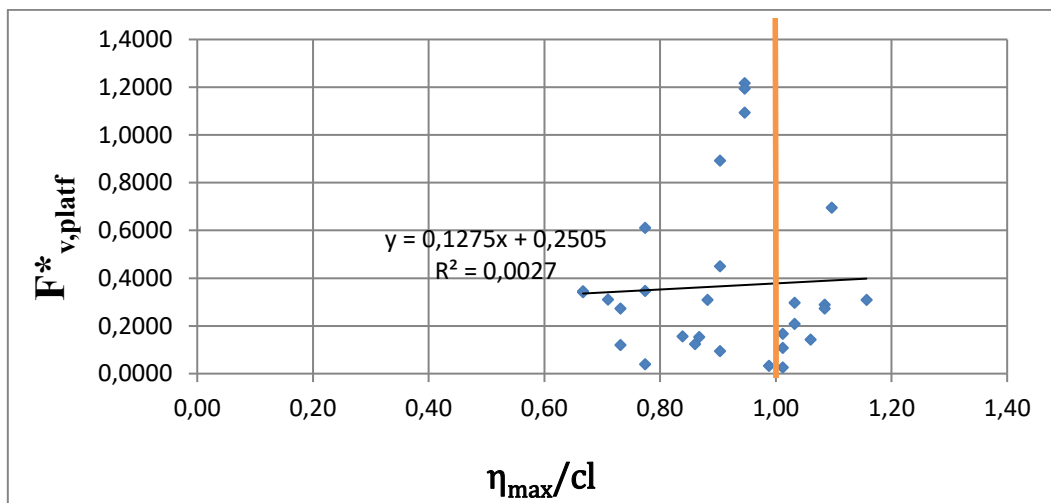


Fig. 53 - Application of Cuomo et al. (2007) to vertical forces for non-breaking waves with the new setting.

As mentioned above, the essay of Cuomo et al. (2007) and its method present some dispersion using the data gathered with our tests. At this point it is clear that the method proposed by Cuomo et al. (2007) is not suitable for the problem put in analysis in this thesis work.

Gaeta et al., 2012

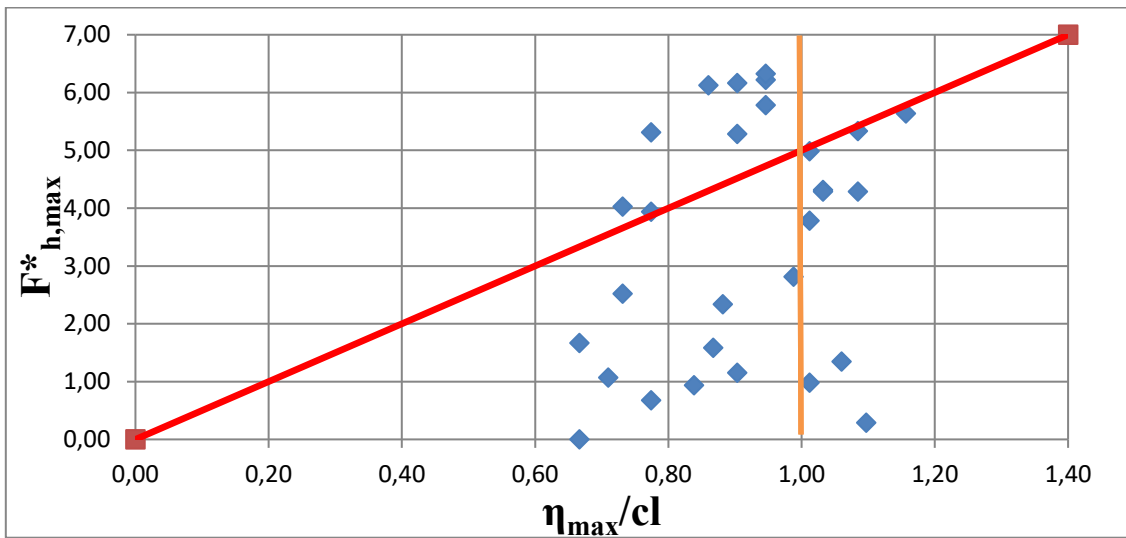


Fig. 54 - Non-dimensional horizontal maximum forces according to Gaeta et al. (2012) for non-breaking waves with the new setting.

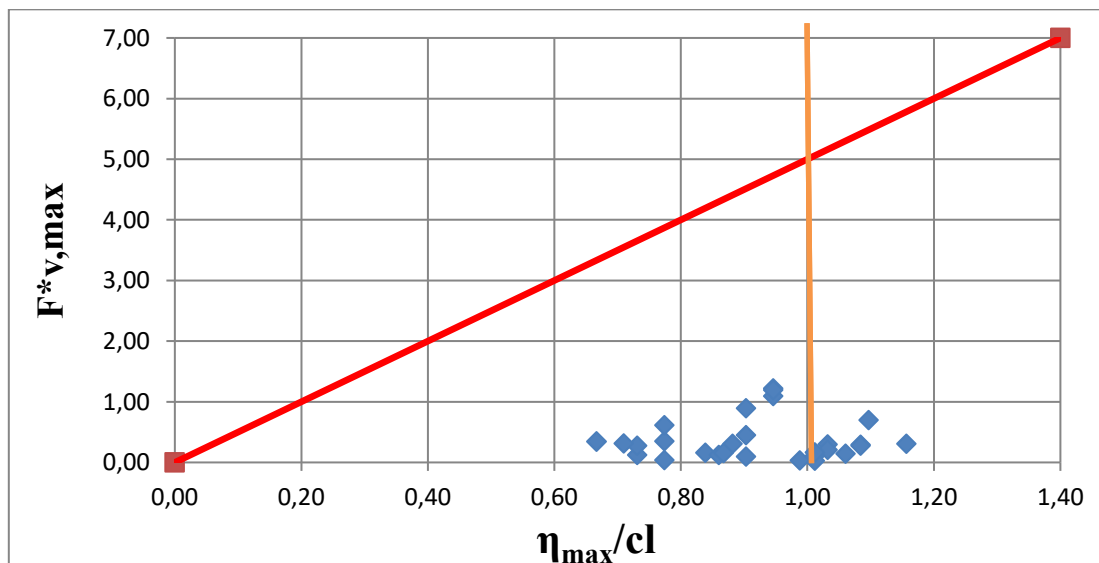


Fig. 55 - Non-dimensional vertical maximum forces according to Gaeta et al. (2012) for non-breaking waves with the new setting.

All non-dimensional forces are below the line of maximum forces. For horizontal forces there are still some tests above the line of maximum force, but in this case the limit condition suggested by Gaeta et al. (2012) is more suitable for vertical loads of irregular non-breaking waves.

7. Final discussion and conclusions

Experimental tests have been conducted to analyze the impact of extreme waves on the Pont del Petroli pier, in Badalona (Spain). The results obtained in the preliminary visual validation allows us to think that the waves realized in the CIEM flume with the theory of focused waves on the scaled model are very similar in many cases. For sake of brevity are shown only two of these cases. Anyway, the method of creating focused waves can be considered suitable for the objective of this thesis work and so also for the production of irregular waves that can reach in some cases the breaking condition.

The maximum wave heights reached during the tests were of 11.1 m (in prototype scale). This is the equivalent height of a three-storey building. Furthermore, during the physical analysis there were extreme waves that overtopped the platform of the pier for a height of 3m. These results are reasonable that would have been occurred during the storm Gloria on the coast of Badalona and this was proved in the preliminary visual analysis were a relevant number of impacts realized in the experimental campaign presented strong similarities with the few available data taken by photographs or video and the time series plot of the significant wave height of Puertos del Estado shown previously.

Therefore, what resulted by the physical model campaign is that the forces acting on the pier platform caused by extreme waves, similar to the ones shown in this thesis work, reached maximum horizontal forces of 2160 kN (in real scale). The maximum recorded vertical force on the platform exceeded 1210 kN. On the first pilecap (seawards) were measured a maximum horizontal force of 80 kN, much less than the values obtained for the platform. This is due to the strong turbulence of the waves that reached the pilecap, the phenomenon of turbulence wastes a great part of the energy that won't be spent in the impact with the structure. In order to make a scale comparison of the horizontal loads in the reality, 2160 kN of impulsive load is the equivalent force produced by a car accident that involves a medium truck with a weight of 50 kN that was traveling at 75km/h of speed. But these loads are applied to the Pont del Petroli pier all night long with a rate of an impact every 11.2 s (average period of waves in prototype scale). For sure this is an approximation (a kind of conservative approximation) of the reality but we can assure that the damage provoked by the

impact of these extreme waves for sure can cause the failure and the collapse of a structure as the Pont del Petroli pier.

About the breaking conditions there are still some issues opened, such as the distance of breaking from the structure that could produce the highest vertical force on the platform, the relationship between the breaking of the sea wave and their relative loss of energy and what is the best combination of breaking condition that leads to a maximization of the design forces to apply to the model of the Pont del Petroli pier in order to define the best design wave conditions.

Furthermore, it is not clear the effective relation that occurs between the magnitude and the direction of forces with the design characteristic of the sea waves. As shown in the chapter 6 of preliminary considerations and in the Appendix 3, there is not any relationship between all the characteristics proposed in this thesis work. The chosen one has been the maximum wave height, the maximum surface elevation, the period of the focused wave, the water depth at the toe of the platform and the wave steepness. A different power or a combination of these wave characteristic could bring new interesting results.

The main results obtained in the final analytical comparison is that the method proposed by Cuomo et al. (2007) is not suitable for the aim of this thesis work that consists in find an expression that can define impulsive loads due to the impact of irregular waves on an exposed pier as the Pont del Petroli pier, which collapse is the objective of this work. This final result is confirmed in all the cases and in all the conditions posed in here. The formulation proposed by Cuomo et al. (2007), combined with the phenomenon of breaking (or non-breaking) waves doesn't give a new key to understanding of the problem. Anyway, these results confirm the doubts exposed at the beginning of the presentation of the applicability of this expression to our problem. The differences in the model set up are enough to provoke a different behavior of the impact of the waves on the structure. The effect of the slope of the bottom and the use of extreme breaking waves instead of regular non-breaking waves are quite important for the dispersion of the points around the regression line and the design of forces.

On contrary, the similarity between the model set up of Gaeta et al. (2012) and the model set up realized in the CIEM flume is higher and this leads to some effect on the final results of the analytical comparison. However, the suitability of their formulation of maximum forces is

not a trivial issue. There are some tests that leads to horizontal forces that exceed the limit condition of maximum forces. On the other hand, the limit of maximum forces is too much conservative in case of breaking waves and this makes the linear expression proposed by Gaeta et al. (2012) not suitable in most of the cases. The best results are obtained for the comparison with non-breaking waves but this is only a small part of the whole group of extreme waves that could impact to the pier of Pont del Petroli.

Thus is desirable to produce new formulations and further analysis of the loads caused by the impacts of irregular waves, on exposed jetties as the Pont del Petroli pier, with sloped bottom and how the breaking of the extreme waves can affect the structural response of the jetty.

Regarding to the new setting η_{\max}/cl , it is high the variability of behavior that are assumed by the sea waves. Anyway, this is a proposal for a new key of understanding of phenomena of the impact of extreme waves similar to those that collided on the Pont del Petroli pier during the storm Gloria. However, it is recommendable to find and tests new parameters that could give a new interpretation of the aforementioned phenomena related to the impact of extreme waves on exposed piers. Also a combination of more parameters or a multilinear analysis could bring interesting results.

The results obtained and the visual analysis made in this thesis work are an important beginning of further investigations because the available data are really few and this work offers some first results that will help us understand why the structure of Pont del Petroli pier collapsed, how this happened and also it gives new information that allows to redirect further analysis about the loads caused by extreme waves impacts produced by storms, similar to the storm Gloria, that clashed on exposed structure such as the Pont del Petroli pier.

8. Bibliography

- Ajuntament de Badalona, «*Badalona destina 325.00 euros a la reparació del pont del Petroli afectat pel temporal*», 2017
- Ajuntament de Badalona. «*Pont del petroli*», 2012
- Altomare C., Tafuni A., Domínguez J.M., Crespo A.J.C., Gironella X., Sospedra J. (2020) *SPH Simulations of Real Sea Waves Impacting a Large-Scale Structure*, Journal of Marine Science and Engineering 2020, 8, 826.
- Buckley, W. H., R. D. Pierce, J. B. Peters and M. J. Davis, 1984, *Use of the half-cycle analysis method to compare measured wave height and simulated Gaussian data having the same variance spectrum*, Ocean Engineering, **11**, 423–445
- Cuomo G., Tirindelli M., Allsop W. (2007). *Wave-in-deck loads on exposed jetties*. Coast. Eng. 54, 657-679
- El Punt Avui, «*El fons marí es degrada a la meitat dels llocs de control*». 12-04-2014.
- Gaeta M.G., Martinelli L., Lamberti A., (2012). *Uplift forces on wave exposed jetties: scale comparison and effect of venting*.
- Goda, Y., (1986), *Effect of wave tilting on zero-crossing wave heights and periods*, Coastal Engineering in Japan, **29**, 79–90
- Goda, Y., (2010), *Reanalysis of regular and random breaking wave statistics*, Coastal Engineering Journal, Vol.52, No.1 (2010) 71-106
- Hughes and Thornton (2016), “Estimation of time-varying discharge and cumulative volume in individual overtopping waves”, Coastal Engineering 117, 191 - 204
- Iversen, H. W. [1951] “Laboratory study of breakers,” Gravity Waves, Proc. NBS Semicentennial Symp., June 1951, NBS Circular 521, pp. 9–32.
- Kortenhaus, Andreas, Streicher, Maximilian, Gruwez, Vincent, Altomare, Corrado, Hofland, Bas, Chen, Xuexue, Klein Breteler, Mark. (2019). *WALOWA (Wave Loads on Walls) - Large-scale Experiments in the Delta Flume on Overtopping Wave Loads on Vertical Walls [Data set]*. Zenodo. <http://doi.org/10.5281/zenodo.2843140>
- Martínez, Lluís; Membrives, Marta «*Badalona reobre el pont del petroli, convertit ja en un símbol per a la ciutat*». El Punt Avui, 09-06-2014 [Consulta: 12 novembre 2012].

- McCowan, J. (1894). *On the highest waves of a permanent type*, Philosophical Magazine, Edinburgh 38, 5th Series, pp. 351-358.
- Miche, R. (1944), “*Mouvements ondulatoires de lamer en profondeur ou d’ecroissante*”, Annles de Ponts et Chaussées 19, 370–406.
- Shaffer (1996), “Second-order wavemaker theory for irregular waves”, Ocean Engineering Vol.23, 47 - 88
- Orszaghova et al. (2014), “Importance of second-order wave generation for focused wave group run-up and overtopping”, Coastal Engineering 94, 63 - 79
- Whittaker et al. (2018), “Extreme coastal responses using focused wave groups: Overtopping and horizontal forces exerted on an inclined seawall”, Coastal Engineering Vol.140, 292 - 305
- Servei Metereològic de Catalunya, <http://meteo.cat> , 19-23 January 2020
- thelocal.es , *What’s happening with deadly Storm Gloria in Spain*, 22 January 2020
- Whittaker C. et al., (2017). *Optimisation of focused wave group runup on a plane beach*. Coast. Eng. 121, 44–55.
- Whittaker et al. (2016), “*The average shape of large waves in coastal zones*” , Coastal Engineering 114

Appendices

Appendix 1 - Instruments characteristics

RESISTANCE WAVE GAUGES

Description

The resistance type wave gauges used in the CIEM operate on the principle of measuring the current flowing in an immersed probe which consists of a pair of parallel stainless-steel wires (the absence of other support reduces the interaction between the measuring device and the incoming/reflected waves). The current flowing between the probe wires is proportional to the depth of immersion and this current is converted into an output voltage proportional to the instantaneous depth of immersion. The output circuitry is suitable for driving both a chart recorder and a data logger.

Each wave probe needs a wave probe monitor with the energising and sensing circuits for the operation. Each monitor contains the circuits required to compensate for the resistance of the cable that is connected to the probe. Without this, the output of the wave probe monitor would be non-linear. In order to avoid polarization effects at the probe surface, a high frequency square wave voltage is used to energise the probe. The oscillator that produces this square wave may be set to one of six different frequencies. This allows probes to be used close together without causing any interference.



The current in each probe is detected by measuring the voltage drop across two resistors. Because the measured voltage is alternating, the signal is fed to a precision rectifier to produce a DC voltage proportional to the wave height. This signal feeds a small centre-zero

balance indicator and a BNC socket on the front of the panel. The signal is also fed to a pre-set gain stage that may be set for a gain of between 0.5 and 10. Controls on the front of each wave probe module enable the output signal to be set to zero for any given initial depth of probe immersion. This, together with the gain adjustment, produces a full-scale output of $\pm 10V$ for all waves.

Application range

The steel wires lengths allow detect any wave height up to 2m.

Calibration

The transformation function (from voltage to depth) is calibrated due the possible changes in the water conductivity (temperature and salinity concentration effects). An overall calibration from wave height to output voltage can be performed by measuring the change in output voltage, raising or lowering the mean water level of the flume.

Data acquisitions

The laboratory works with a global data acquisition system. The data acquisition component supports the following hardware manufacturers: Data Translations boards which is supported by the Open-Layer interface. National Instruments boards supported by NI-DAQmx 8.6

The component supports data acquisition on several boards at the same time as long as they are from the same manufacturer. The component supports controlling of external equipment through digital and analogical outputs which can be triggered on a specified time or by an input channel. Component supports high throughput using hardware trigger which leads to little CPU utilization for even high sampling frequencies (>1 kHz).

Specifications

Output Signals:	front of monitors $\pm 10V$ via BNC socket rear of case $\pm 10V$ via 25 way D socket
Gain	0.5, 0.75, 1.0, 1.5, 2.55, 3.75, 6.0, 10.0
Excitation frequency	4.6 kHz to 11.6 kHz
Filter band width	-3dB at 20Hz
Supply voltage	220 or 110V $\pm 10\%$ 40-60Hz
Active length	2000 mm
Diameter	1.5 mm

ACOUSTIC WAVE GAUGES

Two different kinds of AWG have been used on the performed experiments large range and medium range. Here both are presented.

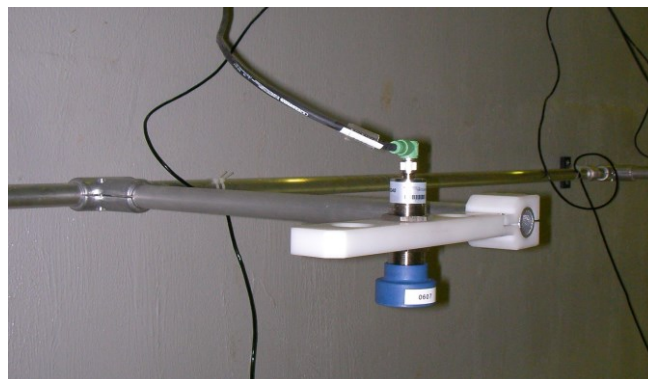
Long Range

Description

The ULS-40D is an Acoustic sensor that emit ultrasound pulses that reflect on the measurement object and is received back as an echo.

Application range

From 0.18 m up to 3.5 m



Calibration

Calibration is need for every device to correlate the output voltage signal to distances.

Data acquisitions

The ultrasound measurement system outputs a voltage proportional to distance of between 0 and 10 V. A calibration straight line, previously done, is applied to the output voltage to transform the intensity signal to the proportional distance.

Specifications

Accuracy	Up to +/- 1 mm (under stable environmental conditions)
Resolution	from 0.18 m to 3.5 m
Measurement frequency	from 20 to 75 Hz
Voltage output	BNC socket: 0 – 10V
Beam angle	<3°
Power supply	230 VAC, 250 mA
Temperature range	-20 / +70 °C

Medium Range

Description

The mic+130 from Microsonic is an Acoustic sensor that emit ultrasound pulses that reflect on the measurement object and is received back as an echo.

Application range

From 0.20 m up to 1.7 m

Calibration

Calibration is need for every device to correlate the output voltage signal to distances.



Data acquisitions

The ultrasound measurement system outputs a voltage proportional to distance of between 0 and 10 V. A calibration straight line, previously done, is applied to the output voltage to transform the intensity signal to the proportional distance.

Specifications

Resolution, sampling rate	up to 0.18 mm
Resolution	from 0.2 m to 1.7 m
Transducer frequency	200 kHz
Voltage output	BNC socket: 0 – 10V
Power supply	230 VAC, 250 mA
Temperature range	-25 / +70 °C

PORE PRESSURE SENSORS (PPT)



Description

Provided by STS the ATM/N pressure sensors have the next characteristics

Application range

Up to 100 or 400 mb (1 and 4 m of water respectively)

Calibration

They are calibrated by using a calibration pipe.

Data acquisitions

The signal intensity output is related, taking into account the calibration curve of each probe, to water height.

Specifications

Accuracy	< 0.5			
Thermal shift	0.....70°C	-25...85°C	0.....70°C	-25...85°C
Span	0.06	0.08	0.015	0.02

LOAD CELLS (LC)

The load cells employed to measure the forces exerted by the waves on the pier elements comprise four S-type load cells (TEDEA Model 616) and three beam type load cells (model Z6FC3).

S-type load cells

Description

TEDEA, Model 616 compression-tension load cells



Application range

Up to 300 Kg

Calibration

They are calibrated with the software CatManEasy v3.4.2 by applying different weights. Eigen-frequency of the load cells is characterized by hammer-test once they are mounted on the structure.

Data acquisitions

A calibration function is applied to the output voltage to transform the intensity signal to the proportional weight. Sampling frequency is 2400 Hz.

Specifications

Accuracy	≈ 0.03%*rated capacity
Temperature range	-10 to +45 °C
Weight	0.58 kg
Construction	Stainless Steel

Beam-type load cells

Description

Model Z6FC3.



Application range

50-500 Kg

Calibration

They are calibrated with the software CatManEasy v3.4.2 by applying different weights. Eigen-frequency of the load cells is characterized by hammer-test once they are mounted on the structure.

Data acquisitions

A calibration function is applied to the output voltage to transform the intensity signal to the proportional weight. Sampling frequency is 2400 Hz.

Specifications

Accuracy	$\approx 0.05\%$ *rated capacity
Temperature range	-10 to +40 °C
Weight	0.50 kg
Construction	Stainless Steel

PRESSURE SENSORS (PS)

Description

Model P8AP, 2 mV/V strain gage sensor. Working for static and dynamic pressure.



Application range

10-500 bar

Data acquisitions

Sampling frequency is 2400 Hz.

Specifications

Nominal rate sensitivity	$2\pm 2\%$ mV/V
Control volume	0.3-2 mm ³
Temperature effect on the zero signal relative to the actual value	
per 10 K	± 0.3
Weight	250 g

ECHO SOUNDER

Description

UltraLab UWS echo sounder is used for highly spatial and temporal resolved measurements of distances in fluids. It works with an ultrasonic impulse runtime procedure and the 1MHz, highly sensitive transducer with a very narrow beam enables the resolution of smallest targets or changings of the measurement object. Due to its high resolution, it can resolve small scale contours in a measuring range from 2 cm up to 15m. The small size of the sensor enables even the use in very small-scale applications or at applications with challenging placement or mounting requirements.



Application range

From 2 cm to 15 m in water.

Data acquisitions

The measured distance is directly shown on a four digit display and the proportional analogue 0-10V output voltage at a BNC socket allows the integration into external data acquisition.

Specifications

Measuring rate	Max. 10 Hz
Resolution	1% of the measuring range
Temperature range	-20 to +70 °C
Output	BNC-Socket, 0-10 V analogue with zoom-function

Appendix 2 - Organization and structure of data files

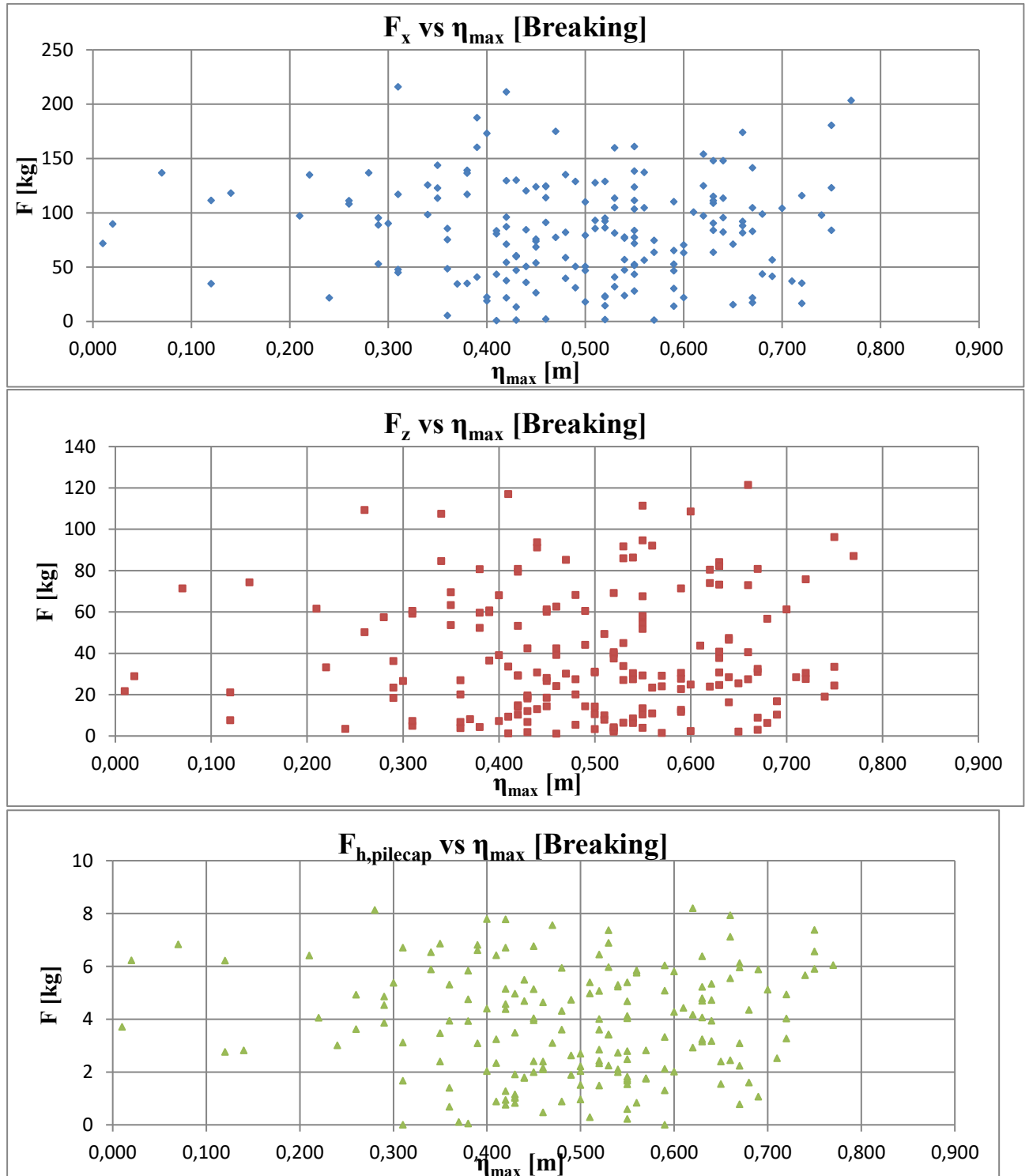
All data files are stored in a local hard drive at UPC. To access and receive the data, contact Dr. Corrado Altomare (email: corrado.altomare@upc.edu). The data is structured as followed:

- Directory “**DATA**” comprises:
 1. File "03_RESULTS.txt": file with information on the maximum target and measured wave characteristics for each test case;
 2. File "04_PEAKEs.txt": file containing all results of force peaks for each test case
 3. **Test directories** with water surface elevation time series (raw data), categorized per date (**DATE=GGMAA**), containing the data acquired during each test case. Each directory includes several test cases. Each test case name is coded employing the DATE followed by “_##_conv.txt”, being **TESTID= GGMAA_##**.
 - Subdirectory **Perfils**: it contains an Excel file with the results of the beach profile measurements and corresponding measurement dates.
 - Subdirectory **LC_PS**, located inside the folder TESTID and containing the files of LCs and PSs measurements (raw data).
 - file **TESTID.TSX**: metadata for LC and PS data;
 - file **TESTID.asc**: LCs and PSs measurements (raw data).
 4. Directory **_RESULTS** containing a subfolder for each test case. The subfolder name is coded as follows: “**Case_TESTID**” and contains the post-processed data for water surface elevation and forces, in particular:
 - File “ETA.mat”: MatLab data file with post-processed signals from WGs, AWGs and PPTs and sensor locations.
 - File “F.mat”: MatLab data file with the resultant and filtered time series of forces (4 columns: Time, Total Horizontal Force on the Platform, Total Vertical Force on the Platform, Horizontal Force on the Pile Cap);
 - Figures (both in .fig and .tiff format) from the analysis of water surface elevation signal.
 5. Directory **Media**: it contains several subfolders with videos of the tests. They are organized per date and test number.

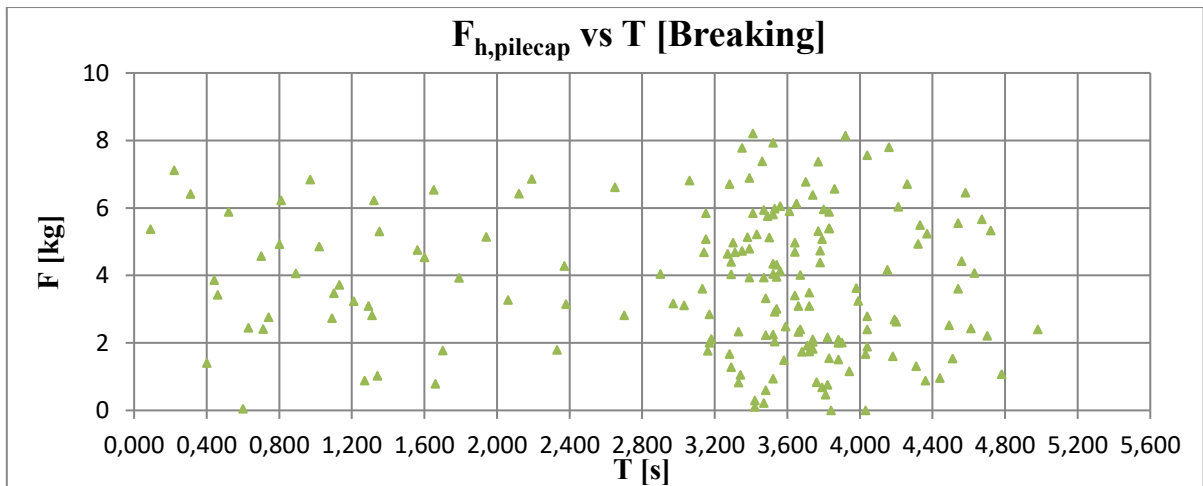
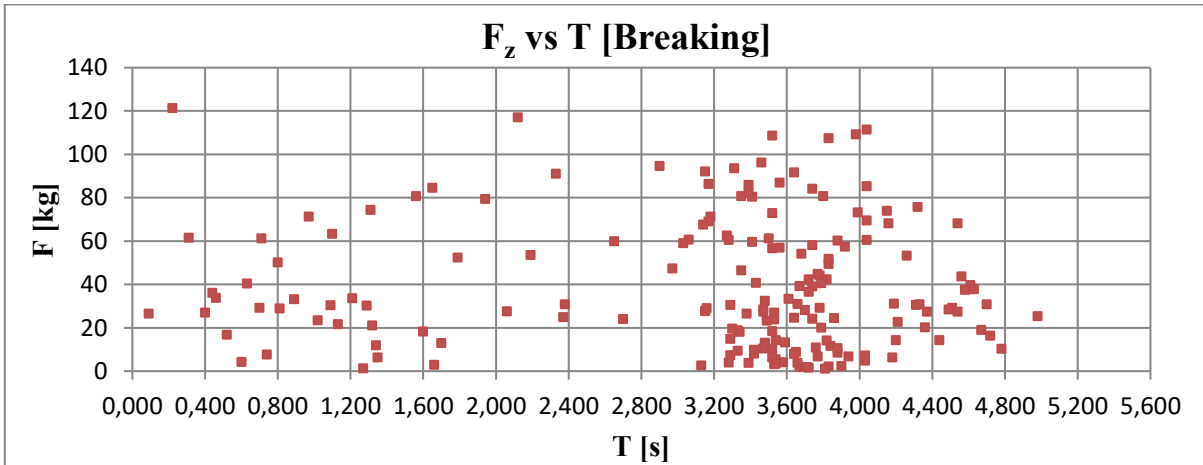
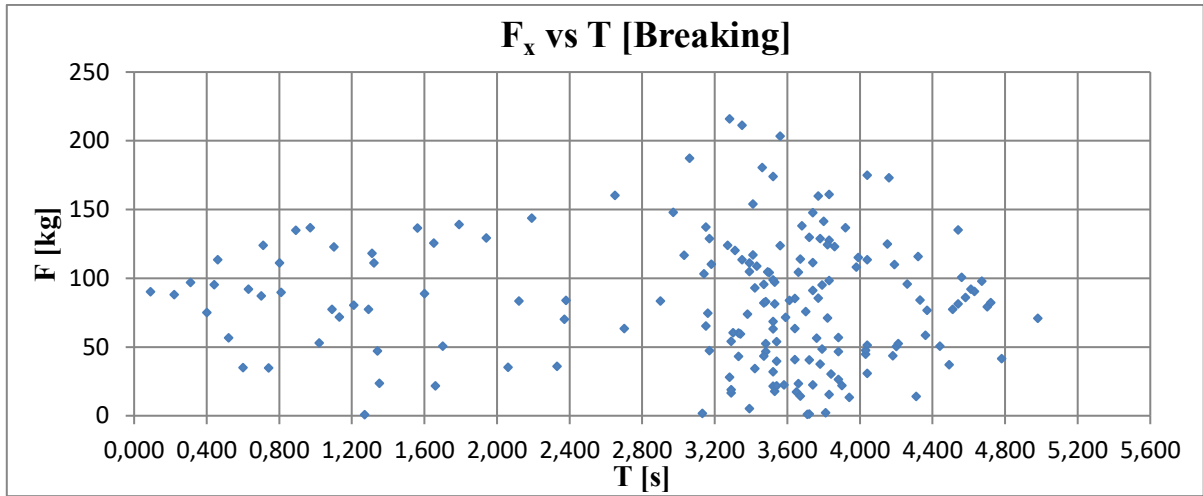
Appendix 3 – Further preliminary comparisons about the dependence of the loads from some basic characteristics

Breaking waves

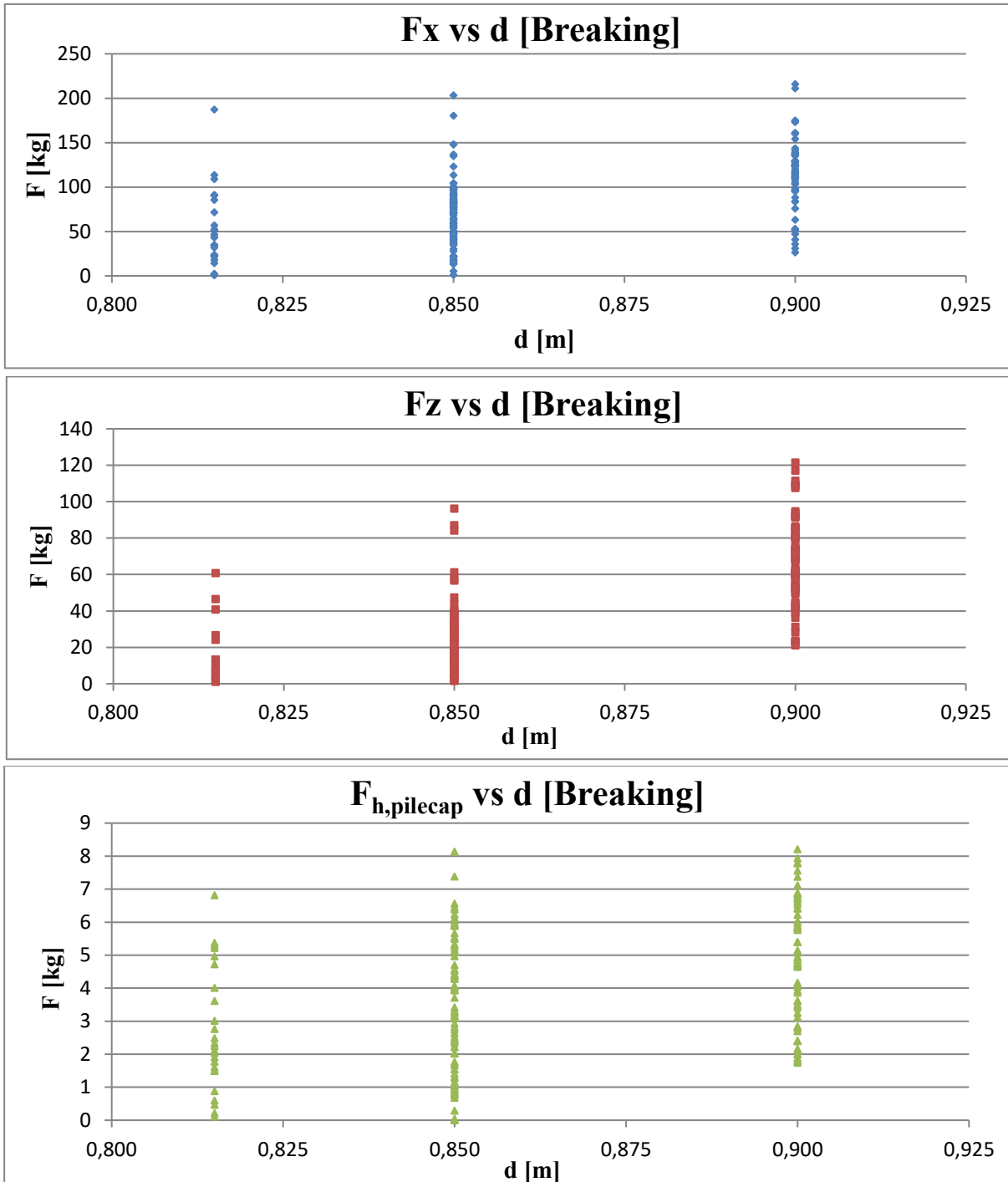
Relationship between loads on the structure and surface elevation



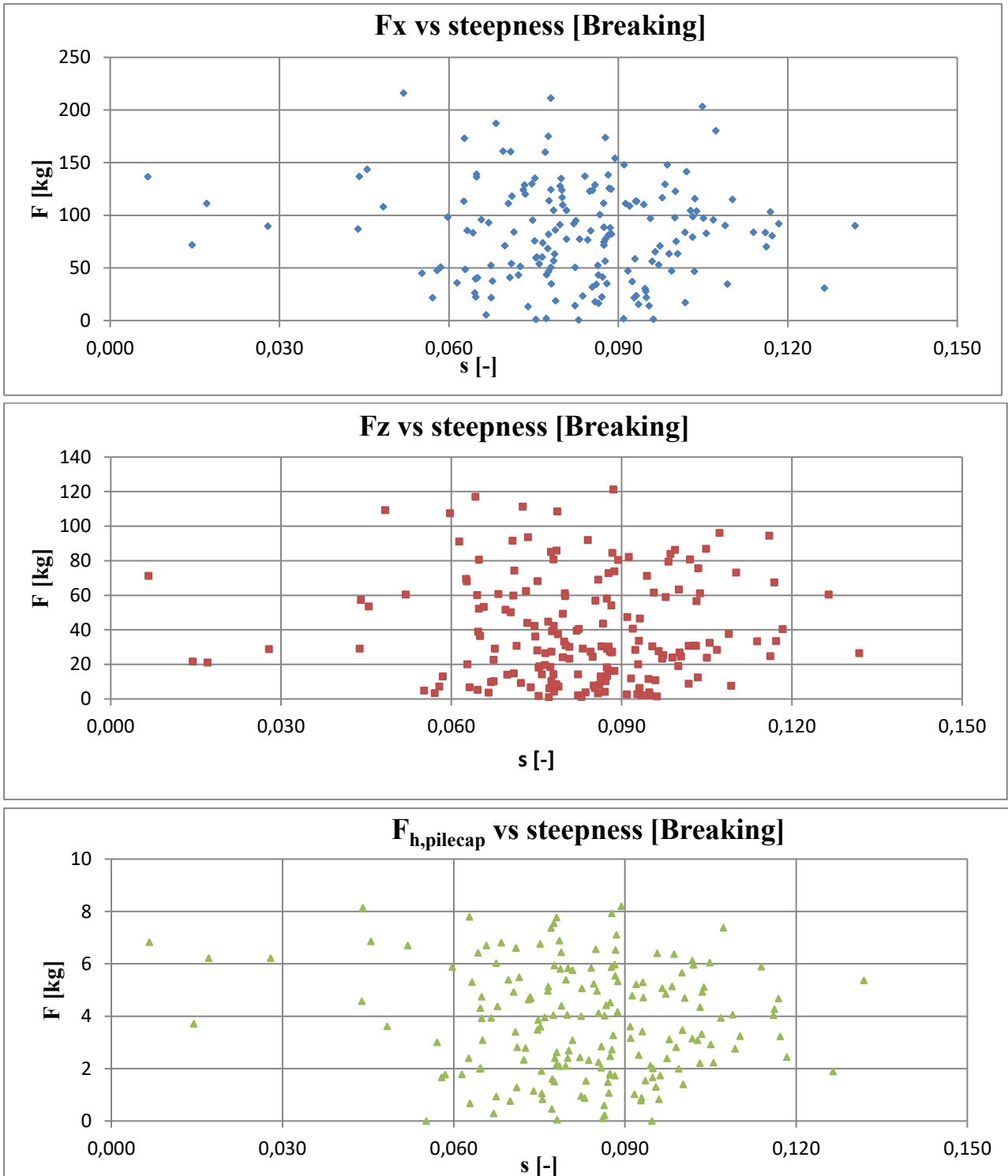
Relationship between loads on the structure and wave period



Relationship between loads on the structure and water depth at the toe of the platform

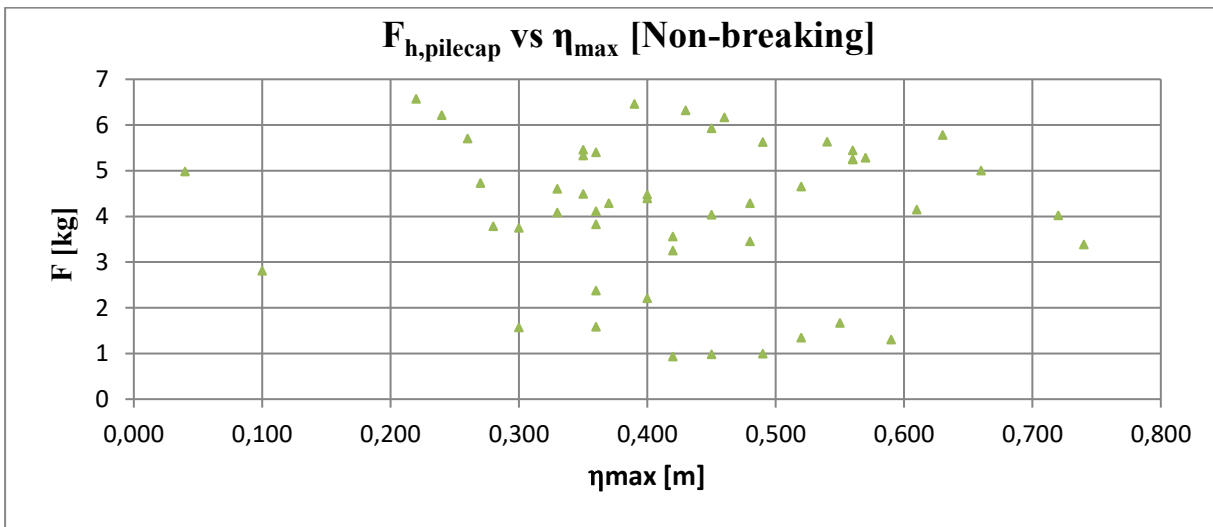
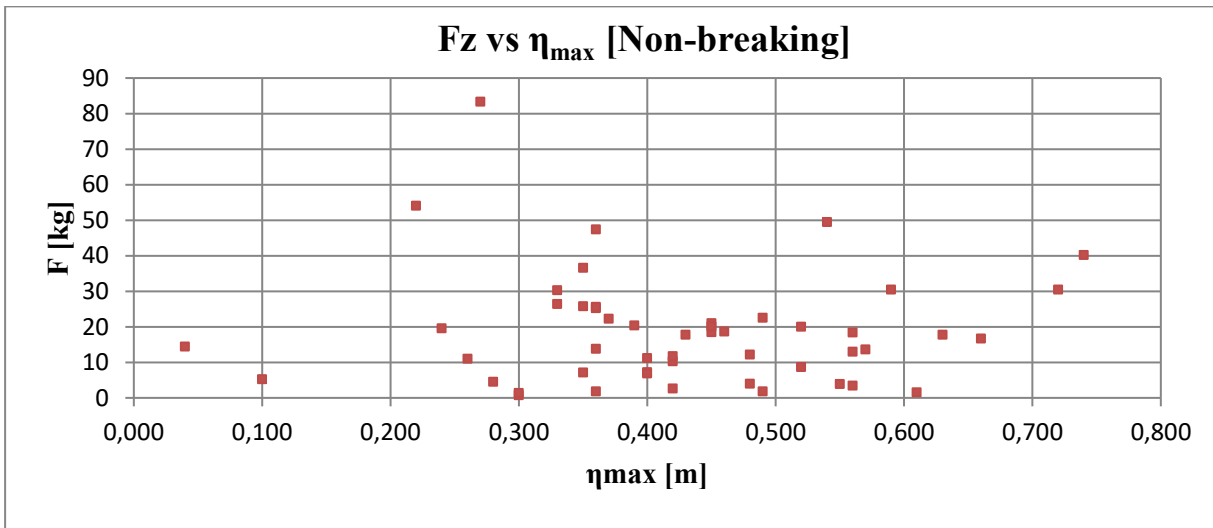
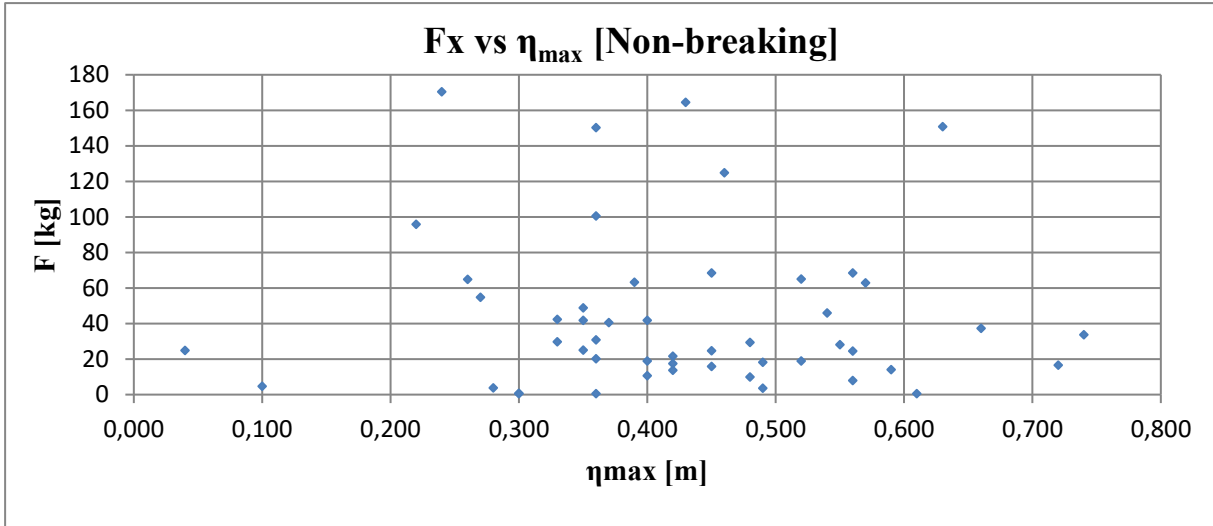


Relationship between loads on the structure and wave steepness

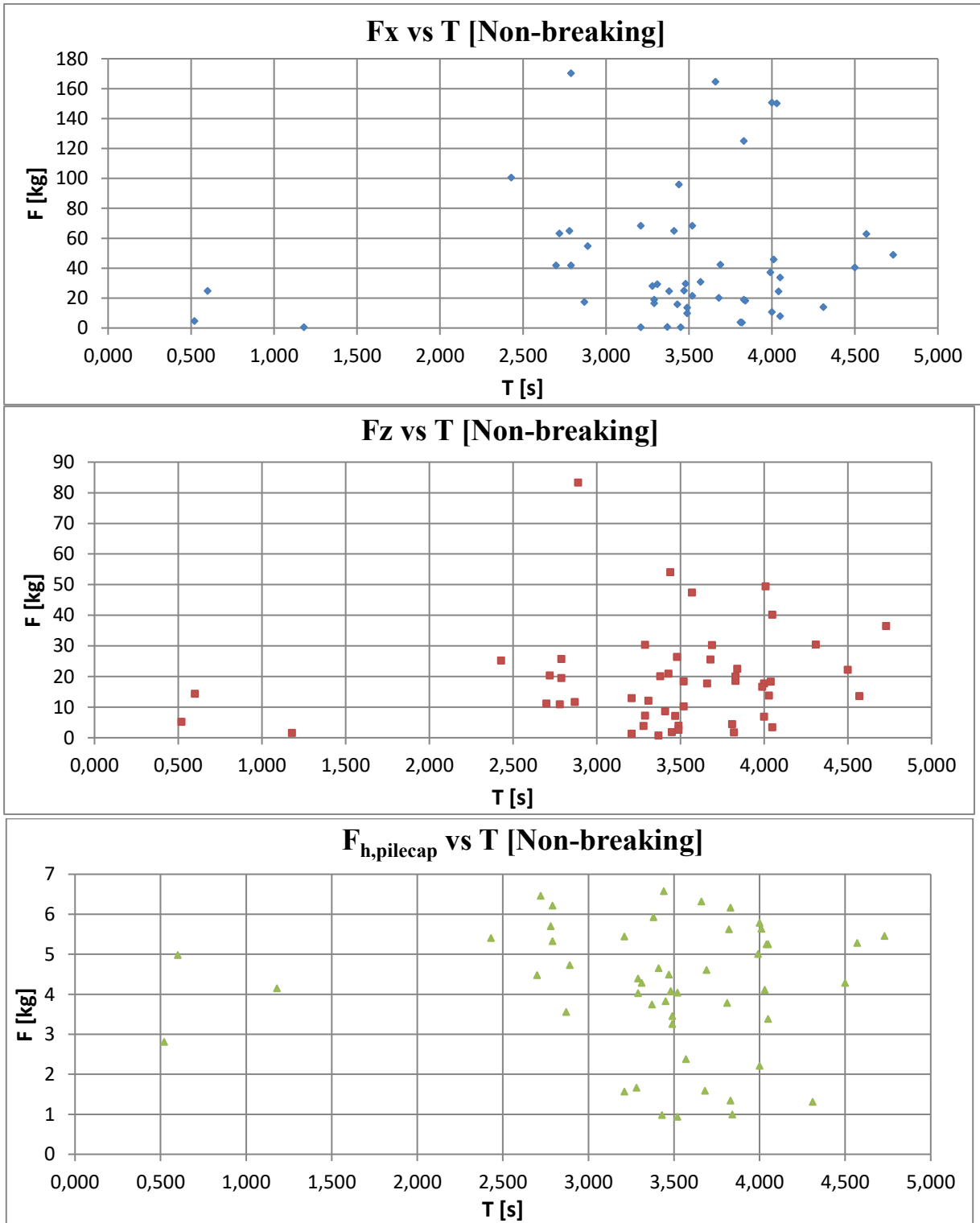


Non-breaking waves

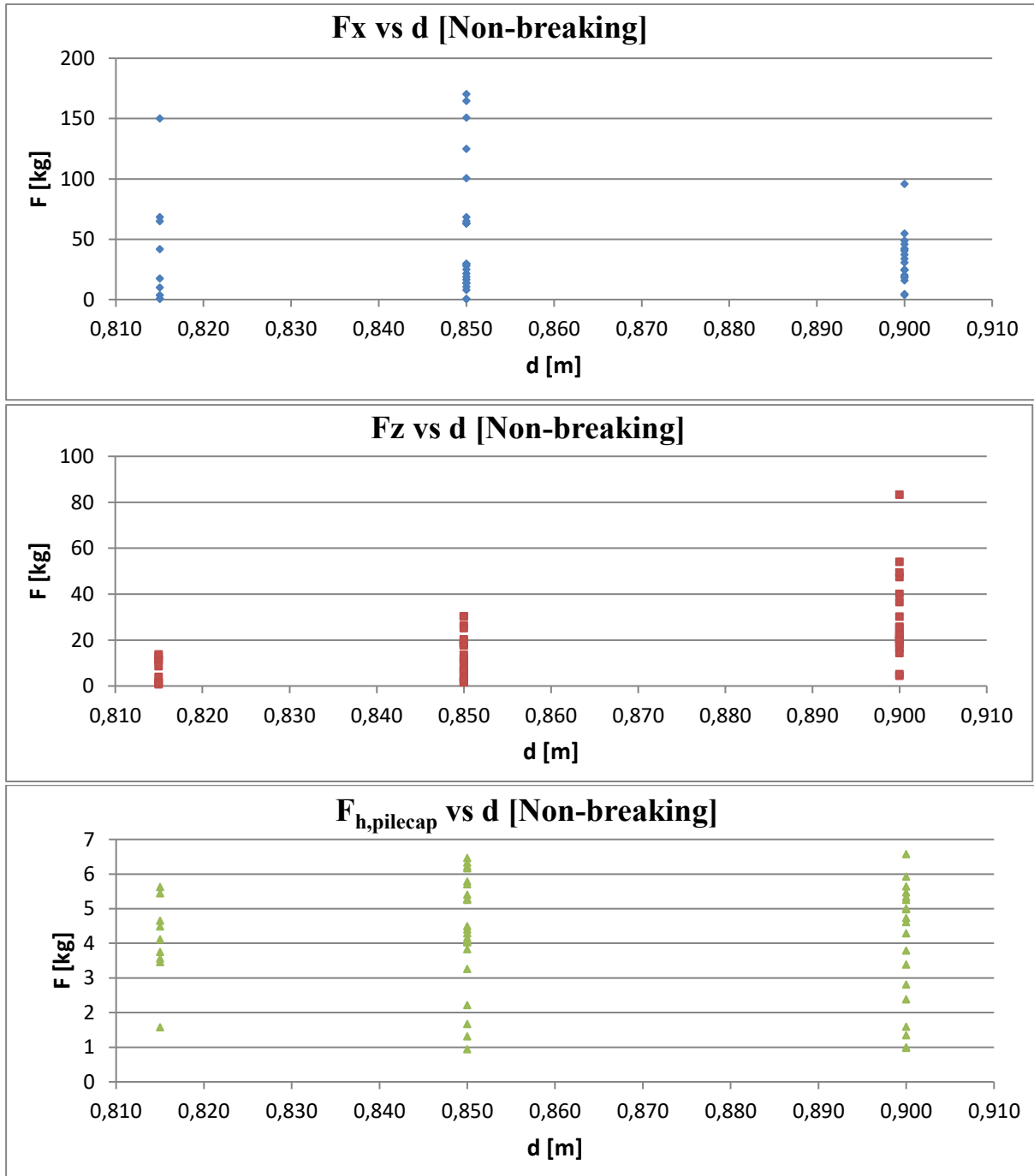
Relationship between loads on the structure and surface elevation



Relationship between loads on the structure and wave period



Relationship between loads on the structure and water depth at the toe of the platform



Relationship between loads on the structure and wave steepness

